Low Temperature Oxidation of Ethylene by Silica-Supported Platinum Catalysts

(シリカ担持白金触媒によるエチレンの低温酸化)

Shazia Sharmin Satter

Hokkaido University

2018

Table of Content

Chapter 1: General Introduction

1.1 General Background: Heterogeneous Catalysts to Ethylene Oxidation – Friend or Foe?

"Catalysis", a term derived from two Greek words in the 1800's by Berzelius[1] to describe an unknown force promoting chemical reactions without the "catalyst" being consumed – this power turned out to be the most mysterious and magic-wand character in the chemical history. Heterogeneous catalysis, the use of solid catalysts to avoid separation issues has given rise to mega chemical industries operating at enormous scales. After the commercialization of *Haber-Bosch* process,[2,3] the first major breakthrough in industrial catalysis, the rise of the role of heterogeneous catalysts in the lives of people were unstoppable. This image of heterogeneous catalysts is not entirely true and the catalysts directly affect our daily lives even though we hardly notice them. One such example is the use of catalytic converters present in all modern cars that is an excellent example of heterogeneous catalysis under our noses.[4] The ability of catalysts to crack long-chain hydrocarbons to short chain ones was critical for the emerging automobile industry. Their uses in the processing of crude oils to fuels and other petrochemical products had a huge impact on the lifestyle of people during the 1900's. Then came the use of these solid catalysts and the use of renewable feedstocks in chemical synthesis which is a core theme behind the principles of Green Chemistry.[5] The world is pretty hard to imagine without heterogeneous catalysis in this 21st century. Environmental and economic concerns increase the needs for better catalysts every day.

Besides all these concerns, another challenge which the society is facing is "food loss". It has turned out to be a major problem all over the world. In developing countries 40% of losses occur at post-harvest and processing levels while in developed countries more than 40% of losses happen at retail and consumer levels.[6] Highest wastage rates are coming from fruits and vegetables due to their decrease in freshness within a short period of time. This is caused by the release of a maturation hormone from fruits and vegetables, ethylene.[7,8] Continuous removal of this particular plant ripening hormone is required to keep these fruits and vegetables fresh for a long time. It is believed that heterogeneous catalysis is able to mitigate food spoilage hence playing a more intimate role in our lives. This application has the potential ability to solve 'food crisis', which is predicated to be a major issue as the population increases rapidly. In this thesis, the author has aimed at development and modification of the heterogeneous catalysts for targeting an efficient and environmentally benign oxidation reaction of the plant hormone, ethylene and provides an insight into such reactions over solid catalysts.

1.2 Mesoporous Silica

1.2.1 An Overview

Nature has been building nanoporous materials for ages. Many living organisms produce nanoporous siliceous structures. For example, plants produce phytoliths, sponges produce spicules and diatoms produce cell walls made-up of silica.[9] In reality, it is difficult to make porous materials naturally since "*the overwhelming tendency for solids to minimize void space within their structures*" is inherent. However, Albert Einstein said "*In the middle of difficulty lies opportunity*". This task was considered a breakthrough in 1992, made possible

by the scientists of Mobil Oil Corporation (USA), when they first successfully synthesized MCM (Mobil Composition of Matters)-41/48 through surfactant-mediated self-assembly method[10,11] although the similar material was first discovered in 1990 by researchers in Japan.[12] This surfactant assisted templating pathway or soft templating strategy opened a new class of materials named as mesoporous materials. Generally, a porous material is defined as a continuous and solid network material filled through voids. In the case of nanoporous materials the pore or voids are of the order of around 1–100 nm. A material can be recognized as porous if its internal voids can be filled with gas. Pores are classified into two types: open pores which connect to the outside of the material and closed pores which are isolated from the outside. Porosity provides materials with lower density and higher surface area compared to dense materials. For most industrial applications including separation, catalysis and bioreactors open pores can play a crucial role.

According to IUPAC convention, depending upon size of the pore, the porous materials are of three types: mesoporous, microporous and macroporous materials. *Meso*, the Greek prefix, meaning "in between", has been adopted by IUPAC to define porous materials having dimension of pores in between micropore and macropore i.e. typically between 2 and 50 nm.[13] Owing to their high surface areas and large pore volumes they are used technically as adsorbents, ion-exchangers, catalysts, catalyst supports and in many other related applications.[14,15] Such materials can be ordered or disordered in nature. Ordered mesoporous materials such as MCM-41/48, Santa Barbara Amorphous, (SBA-15) have uniform and regular arrangements of pore (or channel) widths whereas atomic arrangements are not ordered.[10] Due to the noncommercial availability of the long-chain surfactants used in the preparation and the need for swelling agents that can often lead to the complete extinction of pore ordering, the use of MCM-41 has been limited.[16]

Alternatively, non-ionic triblock copolymers, ($EO_nPO_mEO_n$) with large polyethyleneoxide (EO)n and polypropyleneoxide (PO)m blocks have recently emerged as cheap and valuable supramolecular templates for mesostructured materials possessing long range order.[17] In particular, Zhao *et al.*[18,19] demonstrated the synthesis of a family of highly ordered mesoporous silica structures, i.e., SBA-15, with pore dimensions between 20 and 300 Å using commercially available alkyl PEO oligomeric surfactants in acid media without the use of swelling agents besides the report of SBA-1 (cubic),[20] SBA-11 (cubic),[21] SBA-12 (3D hexagonal network),[21] SBA-14 (lamellar),[22] SBA-15 (2D hexagonal)[18,21] and SBA-16 (cubic cage-structured).[21,22] However, SBA-15 consisting of thermally stable thick walls and ordered hexagonal mesopores which overcame the weak hydrothermal stability encountered by M41S materials[22] received a lot of attention due to its desirable features. Besides having an ordered hexagonal array and uniform mesopores (5-9 nm), SBA-15 also has channels interconnected by pore systems, preferably, micropores or secondary mesopores[22-27] which might play a role in adsorption and diffusion processes of gases compared to that of MCM-41. All these characteristics made SBA-15 extremely useful in applications such as drug delivery system,[28] separation of biochemicals,[29] adsorption of biomolecules,[30] use in HPLC[31] and used as a promising support in the field of catalysis.[32]

1.2.2 Synthesis Pathway and Mechanism of Formation of Mesoporous Materials

Structure directing agents (SDA) or templates play a decisive role in the synthesis of mesoporous silica.[33] Surfactants or non-ionic triblock copolymers can be employed as SDAs consisting typically of a hydrophobic (non-polar) tail and hydrophilic (polar) head as shown in Figure 1.1(A) (general figure for a surfactant molecule). Stabilization of such amphiphilic surfactants occurs by arranging themselves at the surface of water where the head interacts

with water and the tail is held above surface as shown in Figure 1.1(B). At a particular concentration, critical micelle concentration (CMC), when the surface becomes loaded with surfactants, they self-aggregate encapsulating the hydrophobic part in the cluster form and hydrophilic part being exposed to the solvent[34] (Figure 1.1(C)) hence forming micelle. Far above the CMC value, with increase in concentration, micelle self-assembles to form a 3D spherical or 2D rod like array (Figure 1.1(D)) which results in generation of pore.

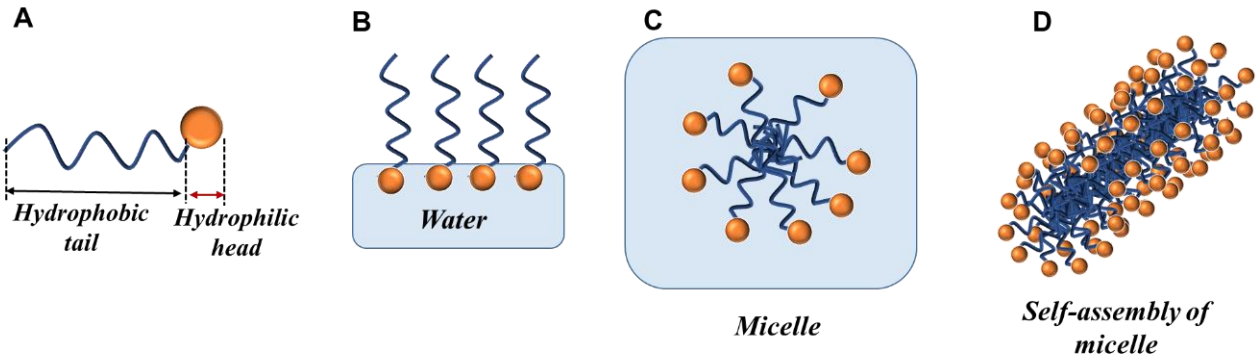

Figure 1.1. Behavior of surfactant molecule in aqueous media.

If specifically thought of synthesis mechanism of SBA-15, similar phenomenon occurs using the SDA, non-ionic poly(ethylene oxide)-block-poly(propylene oxide)-block-poly(ethylene oxide) block co-polymer (P123) comprising of hydrophilic (PEO) and hydrophobic (PPO) by $(S°H^+)(X^+ I^-)$ pathway.[22] Association of water molecules with the hydrophilic polyethylene oxide (PEO) in a non-ionic surfactant (S°) through hydrogen bonding occurs. Acidic media (HX) is used to improve solubilization, where hydronium (H_3O^+) ions associate with the ethylene oxide instead of the water molecules, resulting in long-range columbic interactions.[22] Furthermore, the charge density of cation and the rate of hydrolysis of tetraorthosilicate (TEOS) increase at the interface of template of surfactant due

to lowering of pH below isoelectric point of silica (IEP ~ 2) which results in the generation of silica gels. The reaction occurs in two steps:

(1) Solubilization of P123 by the association of H_3O^+ from acidic media and EO moieties of surfactant as shown in Eq. 1

$$REO_m + yHX \xrightarrow{H_2O} REO_{m\text{-}y}\,[(EO)^*\,H_3O^+]\ldots\ldots yX^- \qquad (1)$$

(2) Hydrolysis of alkoxysilane species followed by partial oligomerization at the interface of surfactant as shown in Eq. 2

$$Si(OCH)_4 + nH_3O^+ \xrightarrow[pH<2]{Hydrolysis} Si(OC_2H_5)_{4-n}\,(OH_2^+) + nC_2H_5OH \qquad (2)$$

where R and X represent hydrophobic polypropylene oxide (PPO) and halide ions (Cl^-, Br^- and I^-).

The EO moieties of P123 associate with the silica species (cationic) via hydrogen bonding, electrostatic and van der Waals interaction through $(S^0H^+)(X^+I^-)$ pathway as shown in Step 1 of Figure 1.2. The growth of spherical micelle occurs through coordination between X^- and $Si–OH^+$ and next polymerization of silicate around SDA occurs as shown in Step 2 (Figure 1.2) followed by condensation which results in the formation of silica species around the surfactant in a composite hexagonal mesophase. The silica based solution is then washed and subjected to high temperature in order to remove the template from the pores which results in the formation of hexagonal ordered mesoporous channels. Removal of EO from the walls of SBA-15 gives rise to the micropores.[35]

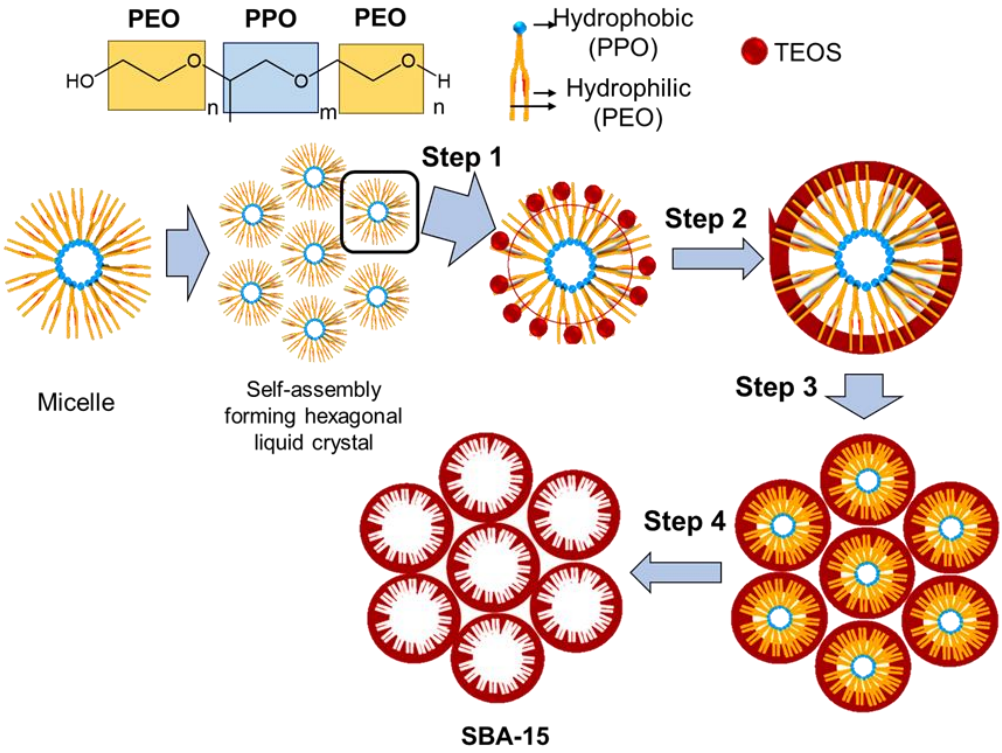

Figure 1.2. Detailed mechanism of formation of mesoporous SBA-15.

1.2.3 Surface Property and Modification of Mesoporous Silica

In 1936, Kiselev and his co-workers came up with a point of the skeleton of silica surface being covered with hydroxyl groups and hence provided with the chemical interpretation of the "structural water" on silica surface.[36] Irrespective of being aerosol or mesoporous in nature, it is worth mentioning about its significant surface chemical activity[37] due to the presence of silanol and siloxane groups. The silanol density[38] is a function of temperature and the further distinction between different types of silanol as well as the hydrophobic siloxane groups can be studied by the use of ^{29}Si NMR spectroscopy.[39–42] In addition to the presence of the different silanol groups, existence of the physically adsorbed water on the surface and structurally bound water inside of the pores of the mesoporous silica must also be taken into account.[43,44] Eventually, the presence of the silanol groups can result in the interference with

the catalytic activity[45] which has resulted in developing numerous strategies for the modification of mesoporous silica surface in order to regulate surface hydrophobicity by silylation.[42,46–48]

One of the easiest ways of surface modification besides silylation is by a simple calcination treatment.[49] SBA-15 has been recognized to have two different chemical groups on their surfaces,[50,51] hydrophobic siloxane (≡Si–O–Si≡) and hydrophilic silanol groups (≡Si–OH) as shown in Figure 1.3. Silanol groups are again divided into three types:

- Geminal - Consist of two silanol groups attached to one silicon atom.
- Isolated (or free silanols) - A surface silicon atom is linked to three O–Si and one –OH.
- Vicinal (or bridged silanols) – Two silanol groups are attached by hydrogen bridge.

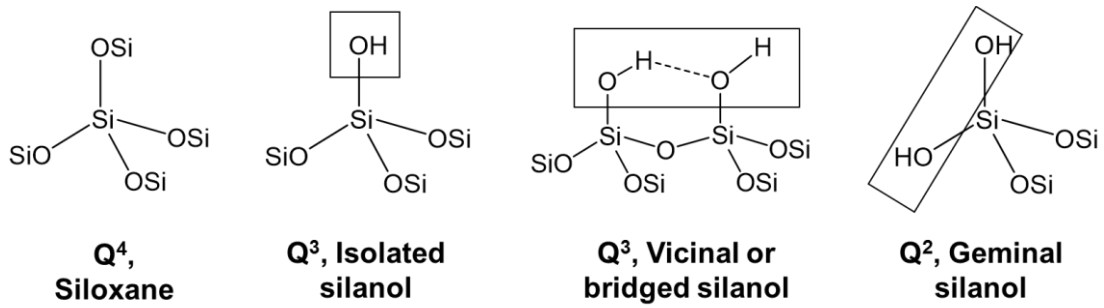

Figure 1.3. Chemical structure of silica surface.

Study of three different types of silica gel (Kieselgel 40, 60 and 100) of varying pore distribution revealed that the relative distribution of free and vicinal silanol groups depends on calcination temperature.[37] Although siloxane constitutes main part of solid matrix, it is the silanol groups which usually allows the chemical anchorage of different chemical groups.[52,53] The mesoporous silica, when subjected to high calcination temperature results in removal of the OH and H from geminal and single silanol groups subsequently giving rise to condensation reaction to form siloxane as shown in Figure 1.4.

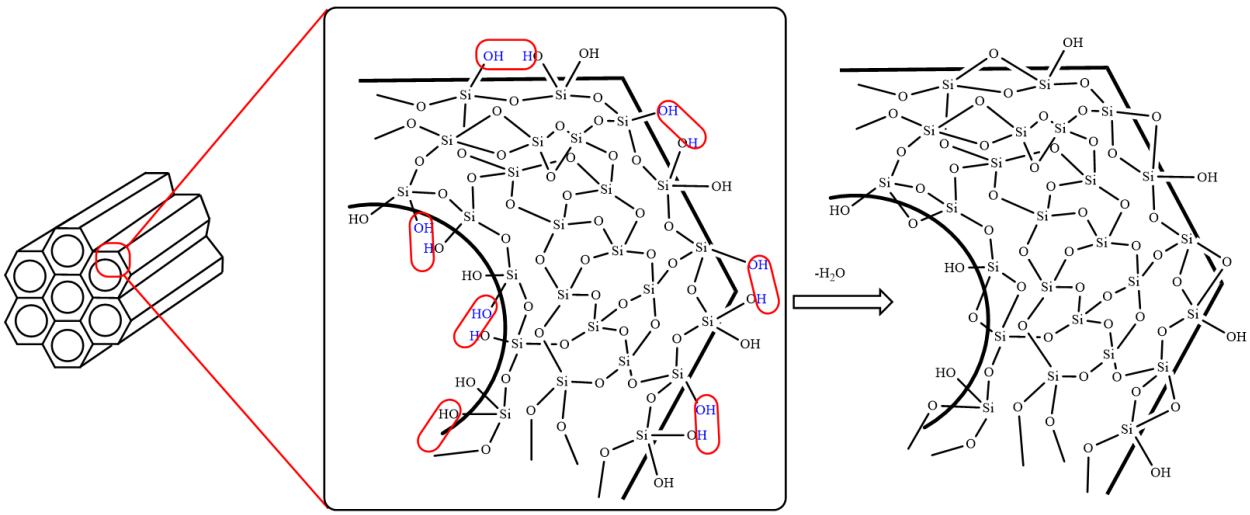

Figure 1.4. Condenstaion of silanol groups from surface of mesoporous silica on heat treatment.

This decrease in the silanol groups result in increase in hydrophobicity which can be studied using water adsorption isotherm[54,55] and ^{29}Si NMR spectroscopy.[39]

1.3 Platinum Nanoparticle Supported Mesoporous Silica

Platinum – a noble metal has the power to influence the course of chemical events though catalysis. After its discovery since 1820s, when Dobereiner invented a small 'tinderbox',[56] Pt has been widely used for reactions in complete oxidations,[57–59] selective oxidations,[60–62] dehydrogenations[63] and hydrogenations.[64] Preparation of small metallic Pt nanoparticles (NPs) results in high catalytic activity due to quantum confinement arising from change in density and band gap of electronic energy level and high surface to bulk atom ratio.[65]

One of the most common strategies of preparing Pt catalysts is by depositing them on a support material in order to get a high dispersion. Al_2O_3[66,67] and TiO_2[68,69] are usually the

conventional choices of support materials for impregnating Pt NPs but in recent years, mesoporous silica, MCM-41 or SBA-15 have received considerable attention due to their high surface areas.[70–72] Generally, SBA-15 is inert in nature with high hydrothermal and mechanical strength than that of MCM-41 and possesses hexagonal mesopores. Various methodologies are opted for the preparation of Pt/SBA- 15, including wetness impregnation (WI),[72] deposition–precipitation (DP),[73] colloids immobilization (CI)[74] and nanoparticle encapsulation (NE). Other methodologies also include the direct incorporation of Pt into pores of SBA-15 by solid-state grinding method,[75] graft hybrid[76] and vacuum calcination.[77] However, due to the simplicity of the method, adding Pt precursor salt to SBA-15 dispersed in water and then drying and reduction in presence of hydrogen makes it the most widely used method.

CO oxidation is the widely performed reaction in the field of heterogeneous catalysis, where Pt/SBA-15 has been employed as a possible catalyst for such reaction.[77] The availability of large number of low coordination sites facilitated CO adsorption and induced strong reactivity towards its oxidation. Oxidation of methanol[78] and aromatic hydrocarbon such as toluene[79] has also been studied using Pt/SBA-15. Another very important reaction is the oxidation of volatile organic compounds, VOCs such as PAHs (Polycyclic aromatic hydrocarbons).[80] Use of Pt/SBA-15 in this oxidation reaction showed much better catalytic activity and selectivity compared to that of γ-Al_2O_3 due to the mesopore characteristic of SBA-15. The high surface area gave rise to better dispersion of Pt NPs and smaller particle size resulting in high catalytic activity.

1.4 Oxidation of Ethylene

1.4.1 Ethylene – Small Molecule with a Big Impact

Ethylene, a natural ripening hormone of plants which affects the growth, development and storage life of fruits, vegetables and crops[81] was first noticed in 1864, when it was traced that gaseous material leaking from street lighting was modifying plant growth.[82] Even at extremely low concentration, it can result in faster deterioration of the fresh products during shipping and storage. Most of the food loss occurs during postharvesting storage and transporting of the fruits and vegetables. The fruits and vegetables release ethylene in trace amount even at a low temperature, which decreases the freshness and results in decay. Usually, ethylene is released from plants and vegetables all the time following a particular chemical pathway. Among lots of potential compounds available in plants to be converted to ethylene, methionine (MET) is suggested to be the most possible starting material.[83] As shown in Figure 1.5, MET is first activated by ATP to form *S*-adenosylmethionine (SAM) (step 1)[84] which is used as a substrate to produce 1-aminocyclopropane-1-carboxylic acid (ACC) with the aid of ACC synthase (ACS). This is the rate-limiting step in the ethylene biosynthesis pathway and releases 5′-methylthioadenosine (MTA), which is recycled back to methionine via the so-called "Yang cycle." In the presence of O_2, ACC is degraded by ACC oxidase (ACO) to produce ethylene, CO_2 and cyanide.

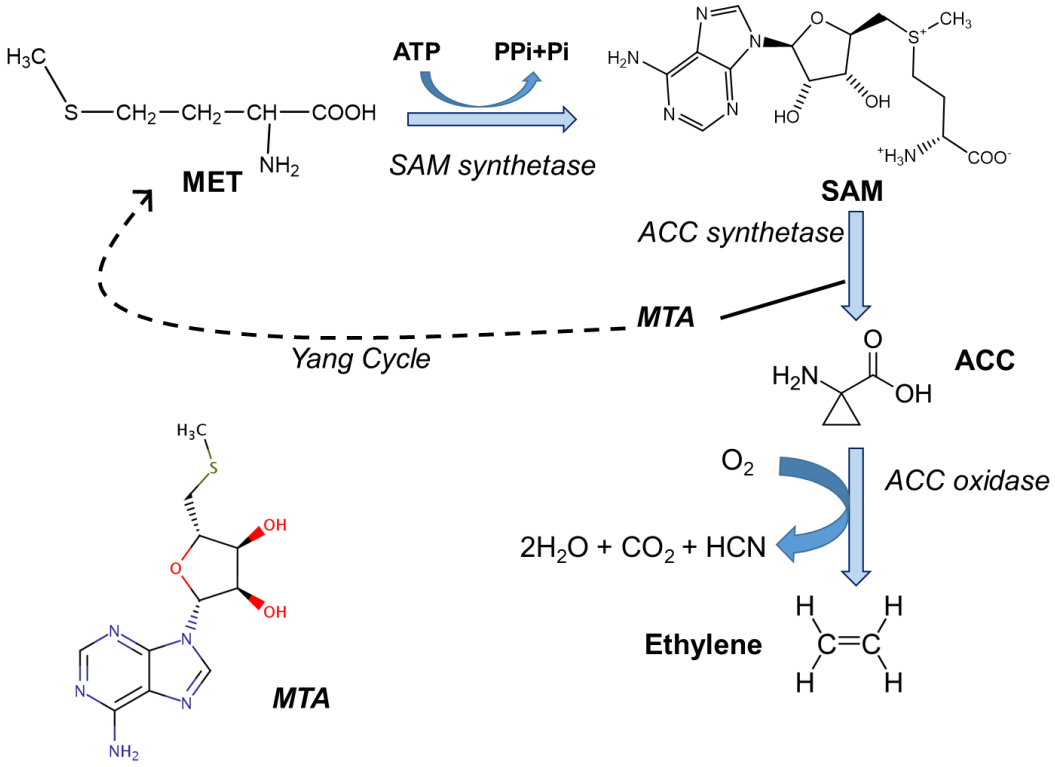

Figure 1.5. Ethylene biosynthesis pathway.

The ability to control ripening as well as freshness is extremely important in order to avoid losses during postharvest, transit and storage. Therefore, the control of the ambient ethylene concentration is the key to prolonging the shelf-life of many horticultural products, fruits and vegetables. Over the years, many strategies have been developed for protecting the postharvest supplies as well as fruits and vegetables from the detrimental effect of ethylene.

One of the most basic ways of decreasing the biosynthesis of ethylene[85] is storing fruits at lower temperature to reduce fruit respiration which will result in reduction of ATP break. This falls under the CTHH (controlled temperature and high humidity) technology which has been already employed for preservation of certain vegetables before.[86,87] However, even at low temperatures, trace amount of ethylene is produced, which results in the decrease of shelf life of fruits and vegetables.

Silver treatment was used in a number of studies as an inhibitor of ethylene formation which showed a decrease in ripening processes of banana slices[88] and also showed an effect on abscission time of leaves.[89] However, silver ions have a toxic effect on organisms. This limited their usage for inhibition of ethylene in fruits.

Use of oxidizing agents such as O_3 and $KMnO_4$ have been one of the most widely used methodologies for removal of ethylene. Though O_3 can be used to remove ethylene from atmosphere, it can be harmful for fruits and vegetables limiting in use in commercial area.[90] $KMnO_4$, the most commonly used oxidizing agent to convert ethylene to CO_2 and water, where early studies have shown bananas keeping green and firm when kept in a sealed bag with $KMnO_4$ and $Ca(OH)_2$ for 16 days.[91] However drawbacks of both the oxidizing agents are the high toxicity and non-renewability. Physical adsorption with activated carbons[92] and zeolites[93] are also insufficient for ethylene removal, due to non-selective adsorption and limited adsorption capacity.

Photocatalysis, one of the emerging and promising sciences have been used in ethylene removal. Use of TiO_2 P25 has been reported for ethylene photodegradation under UV light.[94–96] The reactivity shown by a sol-gel prepared Pt/TiO_2 photocatalyst was greatly enhanced compared to that obtained for bare TiO_2.[96] In such cases, usually, O^* or OH^* radicals are generated which attack the ethylene molecule, producing intermediate of $C_2H_4OH^*$ or $C_2H_4O^*$ thus resulting in the formation of CO_2 and H_2O. Other photocatalysts such as Pt homogeneously decorated over porous TiO_2 sheet[97] and Pt supported on defective tungsten bronze type $KSr_2Nb_5O_{15}$[98] with high stability have been successfully utilized for ethylene oxidation. Both the catalysts showed high activity under ultra-violet (UV) and visible light irradiation. In the case of photocatalytic removal of ethylene, the constant use of the UV light turned out to be a drawback for such methodology, where the absence of any kind of light

will result in no oxidation reaction. The use of solid catalysts came to light in the last few years.

1.4.2 Heterogeneous Catalysis Making Way through Ethylene Oxidation

C–C bond activation is one of the most fundamental topics in chemistry. In particular, selective C–C cleavage of hydrocarbons is of great importance in heterogeneous catalysis. One of the earliest reported reaction is the gas phase, homogeneous oxidation reaction of ethylene at a temperature ranging from 300-600 °C[99] which produced a number of products such as ethylene oxide, formaldehyde, formic acid, CO and CO_2. Use of Ag plate later resulted in the formation of ethylene oxide, CO_2 and water[100] and further studies using Ag was carried out for partial oxidation of ethylene.[101,102] Although ethylene oxidation is a thermodynamically favored process, catalysts are required to activate it at room or low temperature.

Au, one of the most widely used noble metal, was deposited on Al_2O_3 or metal oxides and used for ethylene oxidation, as a target for removing ethylene evolved from fruits and vegetables.[103] However, the reaction was carried out at a temperature higher than 100 °C. Followed by this work, Hao *et al.* reported three consecutive works based on oxidation of trace ethylene, where Au/Co_3O_4 was found to be most efficient for removal of the gas.[104–106] In one of their first findings they showed effect of concentration of ethylene on Au/Co_3O_4 at different temperatures, with not much success. They synthesized Au/mesoporous Co_3O_4 and Au/Co_3O_4 nanorods which showed 76% and 93.7% of 50 ppm of ethylene conversion, respectively at 0 °C. However, they did not account for the time required for the conversion of ethylene, CO_2 formation and also reaction mechanism. Hence the lack of information and the synthesis of specialized Co_3O_4 made these catalysts difficult to be utilized commercially.

Catalysts like porous copper manganese oxides[107] and cobalt oxide supported mesoporous carbon[108] were also studied at potential catalysts for oxidation of ethylene (high concentration, 1%), but high temperatures were necessary for those reactions. They might be attractive for the removal of other volatile organic compounds unlike ethylene. The kinetics of ethylene oxidation using cobalt oxide supported mesoporous carbon was studied in detail, revealing the order of reaction with respect to ethylene is determined to be 0.44 with an activation energy of 79.2 kJ/mol.[108] Baranova *et al.* studied the effect of size of Pt on carbon on ethylene oxidation at a range of temperatures, 25-220 °C and concluded that Pt nanoparticles in size of 1.5 ± 0.5 nm exhibit much higher catalytic activity.[109] An increase in activation energy from 61.1 to 142.1 kJ/mol was also suggested as the average particle size of Pt increase from 1.5 to 6.3 nm. A $Pt/Ce_{0:64}Zr_{0:16}Bi_{0:20}O_{1:90}/\gamma\text{-}Al_2O_3$ catalyst showed complete oxidation of ethylene below 100 °C unlike Pt/Al_2O_3 decomposed ethylene at a higher temperature.[110] Pt supported transition metal oxide (TMO) also emerged as a potential catalyst for such ethylene oxidation reaction. TMOs have a large amount of surface/edge sites, which bring out unique catalytic activity. Pt/MnO_2 nanosheets were employed in the oxidation of 20 ppm of ethylene which showed around 28% ethylene conversion at 25 °C, it but was successful removing ethylene completely at 50 °C for 12 hours.[111] These studies suggest that Pt/MnO_2 nanosheet show poor activity in oxidizing trace ethylene at high temperatures.

After the reports of all these solid catalysts, the use of mesoporous materials emerged highly as the use of support material for ethylene oxidation. A different attempt was opted to immobilize Pt (5 wt%) NPs in confined spaces of mesoporous silica, SBA-15,[112] by introducing Pt precursor to the confined spaces of template and silica walls by grinding. In this case, the mesoporous silica is synthesized[19] and after the hydrothermal treatment, it was filtered and dried. The Pt precursor is grinded with this silica followed by calcination to

remove the template and is denoted as Pt/SBA-15(AS). The confined nanospace controls the size of Pt. Although a different approach for synthesizing the catalyst was conducted, high amount of Pt loading is required to oxidize concentrated ethylene gas (0.32 %) at 40 °C as shown in Figure 1.6. However, it cannot be used for practical application due to high temperature and concentration.

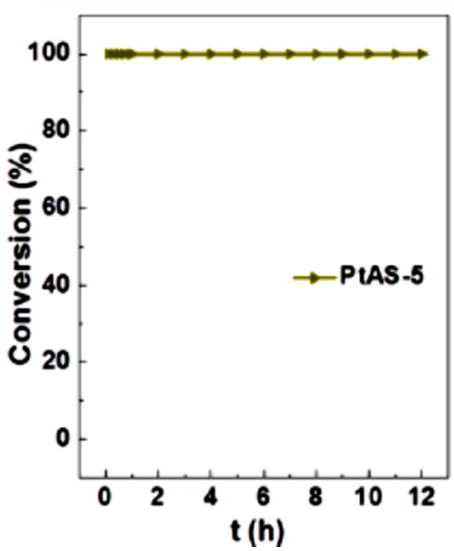

Figure 1.6. Conversion of ethylene (0.32 %) over 5 % Pt/SBA-15(AS) at 40 °C.[112] Reaction Condition: Pt/SBA-15 (Pt 5 wt%, 0.2 g), C_2H_4 0.32 %, O_2 20%, N_2 balance.

In a very recent work, potential catalysts, microporous Ag/zeolite (ZSM-5, Beta, Y and Mordenite) for ethylene oxidation were reported from a Chinese research group.[113] Among the catalysts, Ag/ZSM-5 and Ag/Beta were found to exhibit high activity in trace ethylene (100 ppm) gas in the presence of O_2 (21%) at 25 °C under both dry and humid conditions. They concluded that Brønsted acid sites are catalytically active sites for ethylene oxidation and water vapor in atmosphere blocks these sites, resulting in deactivation of catalyst. Following this work, Hao *et al.* reported two more cases, where they studied the effect of water on Ag/ZSM-5[114] and employed Pt supported fluorine modified ZSM-5[115] during ethylene oxidation. The Pt/F-ZSM showed complete conversion of ethylene (100 ppm) to

CO_2 for more than 600 minutes compared to that of Pt/ZSM-5 since the enhanced surface Brønsted acidity by F ions improves catalytic acivity.[115] However, Ag/ZSM-5 shows longer time for ethylene conversion (720 minutes) activity when compared to that of Pt/F-ZSM-5, provided, the reaction conditions are same as shown in Table 1.1. In another investigation, they showed the effect of SiO_2/Al_2O_3 ratio of ZSM-5 on catalytic activity.[115] It was observed that ethylene oxidation at 25 °C was greatly influenced by Ag/ZSM-(38) with SiO_2/Al_2O_3 ratio of 38. This catalyst can keep complete ethylene conversion for 405 min which is less compared to the Ag/ZSM showing conversion for 720 minutes (Table 1.1).

Table 1.1. Comparison of catalytic activity of various catalysts during ethylene oxidation at temperature range of 0 to 25 °C.

Catalyst	C_2H_4 Concentration (ppm)	Reaction Temperature (°C)	Time (min)	Conversion (%)	CO_2 Yield (%)	Ref.
Au/mesoporous Co_3O_4	50	0	N.D.[a]	73	N.D.[a]	106
Au/Co_3O_4 nanorods	50	0	N.D.[a]	93.7	N.D.[a]	105
Ag/ZSM-5	100	25	720	100	N.D.[a]	113
Pt/F-ZSM	100	25	460	100	N.D.[a]	115
Ag/ZSM-5(38)	100	25	405	100	N.D.[a]	114
Pt/MCM-41	50	25	720	100	N.D.[a]	71
		0	> 60	100		

[a]N.D. Not determined

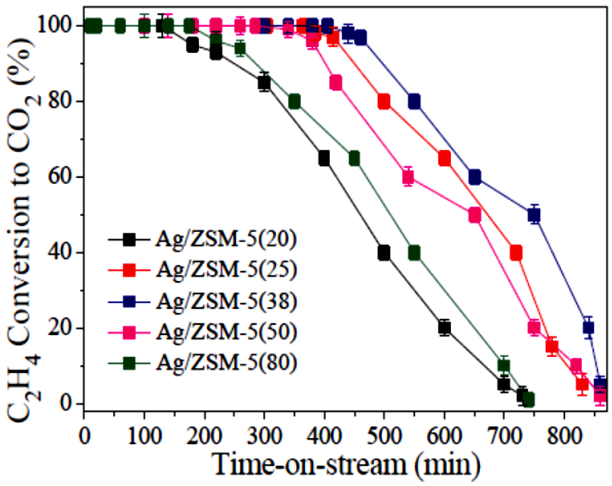

Figure 1.7. Reaction tests for ethylene oxidation to CO_2 with time-on-stream over Ag/ZSM-5 catalysts at 25 °C.

Further experiments showed that H_2O molecules block active acid sites and decrease the original catalytic activity. Despite high initial activity, ethylene conversion of Ag/ZSM-5(38) decreases down to almost zero as shown in Figure 1.7 instead of reaching a steady state, which indicates that the water formation during ethylene oxidation completely deactivate the catalyst.

Although they showed the activity in terms of conversion of ethylene to CO_2, it gives a vague idea about formation of CO_2 during the oxidation reactions. They also proposed a mechanism for Ag/ZSM-5 where the Brønsted acid sites activate the adsorbed ethylene which are attacked by surface active oxygen species promoted by Ag resulting in formation of HCHO followed by carbonic acid. In case of Pt/ZSM-5, ethylene was activated by Brønsted acid sites and Pt activated the oxygen. However, both the proposed mechanisms were based on lack of FTIR data where the bands of the proposed intermediates was not identified elaborately.

A study of Pt/mesoporous silica, next found its way for ethylene oxidation. Fukuoka *et al.* showed a systematic study of various supported metal catalysts for the oxidation of ethylene (0.32%) in the presence of oxygen (20%) and identified a mesoporous silica-supported Pt catalyst that affords the highest activity over a wide range of reaction temperatures (25-100 °C) among various catalysts that consisted of a variety of combinations of metals (Pt, Au, Ag and Pd) and supports (SiO_2, Al_2O_3, TiO_2 and ZrO_2).[71] The Pt (1 wt%) supported mesoporous silica showed complete conversion of 50 ppm of ethylene for 720 minutes at 25 °C and for more than 60 minutes at 0 °C. This is by far the highest time reported for complete conversion of ethylene using such low concentration of ethylene, loading of metal and also for the lowest temperature, 0°C. However, despite the decrease in initial activity, the original activity of the catalyst was easily recovered after heat treatment of the spent catalyst under dry conditions proving its durability. Nonetheless, the ability of this heterogeneous catalyst to remove ethylene and evolve CO_2 at 0 °C has led to it now being used practically for ethylene decomposition in refrigerators.[116] A mechanistic study using Fourier-transform infrared spectroscopy at 50 °C suggested that ethylene was converted to CO_2 and H_2O via formaldehyde and CO as possible intermediates.

1.5 Objective of the Work

Maintaining the freshness of fruits and vegetables is extremely important at low temperature as already described above. Heterogeneous catalysts have attracted a great deal of attention in the field of ethylene oxidation due to its easy handling, high activity and reusability. All these made it possible for one of the catalysts to be used commercially in refrigerators. In this area, most of the researchers focused more on the catalyst preparation and characterization but less on the detailed catalytic study with no information on CO_2 yield.

Even if some catalysts showed high activity, such as Ag/ZSM-5(38) the water formation resulted in instant decrease in catalytic activity.[115] Interestingly, it was found that Pt/mesoporous silica can maintain good catalytic activity at both 25 °C and 0 °C for ethylene oxidation irrespective of stabilization of carbon species and formation of water formation.

Hence, one of the objectives of this work is to study the detailed reaction of ethylene oxidation over Pt/SBA-15 at 0 °C. Owing to the description in the previous work, stating the formation of carbon compounds as intermediates,[71] simple heat treatment was carried out for the spent catalyst in order to achieve the carbon balance.

Next, the author focused on changing the hydrophobicity of meosporous silica. Increasing the activity of catalysts for such low temperature reaction is still considered to be a challenge and the effect of water molecules as catalyst poison makes in more difficult. Hence the effect of hydrophobicity was studied which developed a better, hydrophobic mesoporous silica supported Pt catalyst. This successfully showed high activity of the catalyst at 0 °C.

The third target was to study the surface species produced during the course of ethylene oxidation using in-situ FTIR spectroscopy. This enabled us to detect the intermediates formed during the reaction and hence conclude how heat treatment resulted in reusability of the catalyst.

1.6 Outlines of the Thesis

The importance of removal of ethylene in the current world situation is described. Synthesis mechanism of the mesoporous support material and impregnation of Pt following various methods are described in detail. Subsequently, conventional methodologies followed by the use of heterogeneous catalysts used in ethylene oxidation is discussed.

Mesoporous silica supported Pt nanoparticles were synthesized and characterized in detail using different techniques. The heterogeneous catalyst was employed for ethylene oxidation at 0 °C showing reusability and the simple heating of the spent catalyst resulted in desorption of stabilized carbon compounds on catalyst surface as CO_2. Effect of different kinds of silica support effect was also discussed.

Effect of water adsorption to catalyst bed during ethylene oxidation was studied which revealed decrease in catalytic activity. Change in hydrophobicity of the mesoporous silica support was brought about by simple calcination treatment and Pt nanoparticles were impregnated in the hydrophobic mesopores. The catalysts were characterized in detail, employed for low temperature ethylene oxidation and compared to the catalytic activity of Pt supported aerosol support calcined at various temperatures. Hence, effect of water adsorption to the hydrophobic catalyst bed was also studied. A relationship between the hydrophobicity and desorption of water from Pt incorporated in hydrophobic mesopores was established.

The oxidation reaction was carried out at varying temperature for varying space velocities in order to reveal the activation energy of the reaction. CO oxidation was carried out and effect of water was studied. Detailed FTIR study was carried out for ethylene oxidation at 0 and 30 °C using flow and batch type system respectively to reveal the surface species produced during the course of reaction.

The results represented here is an outline for designing catalysts and provides a detailed and basic insight to the oxidation of ethylene.

References

(1) Berzelius, J. J. Årsberättelsen Om Framsteg i Fysik Och Kemi. *R. Swedish Acad. Sci*. **1835**.

(2) Davis, B. H. Handbook of Heterogeneous Catalysis. In *Wiley-VCH*; Ertl, G.; Knözinger, H.; Weitkamp, J. **1997**, 13.

(3) Haber, F. The Synthesis of Ammonia from Its Elements. *Nobel Lect.* **1920**.

(4) Taylor, K. C. Automobile Catalytic Converters. *Stud Surf Sci Catal*. **1987**, *30*, 97–116.

(5) Anastas, P.; Warner, J. Green Chemistry: Theory and Practice; *Oxford University Press*, New York, **1998**.

(6) Kumar, D.; Kalita, P. Reducing Postharvest Losses during Storage of Grain. *Foods* **2017**, *6*, 1–22.

(7) Abeles, F. B.; Morgan, P. W.; Saltveit, M. E. Ethylene in Plant Biology, 2nd ed. *Academic Press*, San Diego, California, **1992**.

(8) Gane, R. Production of Ethylene by Some Ripening Fruits. *Nature*. **1934**, *134*, 1008–1008.

(9) Brzezinski, M. A. Mining the Diatom Genome for the Mechanism of Biosilicification. *Proc. Natl. Acad. Sci. U. S. A.* **2008**, *105*, 1391–1392.

(10) Kresge, C. T.; Leonowicz, M. E.; Roth, W. J.; Vartuli, J. C.; Beck, J. S. Ordered Mesoporous Molecular Sieves Synthesized by a Liquid-Crystal Template Mechanism. *Nature*. **1992**, *359*, 710–712.

(11) Beck, J. S.; Vartuli, J. C.; Roth, W. J.; Leonowicz, M. E.; Kresge, C. T.; Schmitt, K. D.; Chu, C. T. W.; Olson, D. H.; Sheppard, E. W.; McCullen, S. B.; Higgins, J. B.; Schlenker, J. L. A New Family of Mesoporous Molecular Sieves Prepared with Liquid Crystal Templates. *J. Am. Chem. Soc.* **1992**, *114*, 10834–10843.

(12) Tsuneo, Y.; Toshio, S.; Kazuyuki, K.; Chuzo, K.; The Preparation of Alkyltriinethylaininonium–Kaneinite Complexes and Their Conversion to Microporous Materials. *Bull. Chem. Soc. Jpn*. **1990**, *63*, 988-992.

(13) Behrens, P.; Stucky, G. D. Ordered Molecular Arrays as Templates: A New Approach to the Synthesis of Mesoporous Materials. *Angew. Chem. Int. Ed*. **1993**, *32*, 696–699.

(14) Davis, M. E.; Lobo, R. F. Zeolite and Molecular Sieve Synthesis. *Chem. Mater*. **1992**, *4*, 756–768.

(15) Mal, N. K.; Bhaumik, A.; Kumar, R.; Ramaswamy, A. V. Sn-ZSM-12, a New, Large Pore MTW Type Tin-Silicate Molecular Sieve: Synthesis, Characterization and Catalytic Properties in Oxidation Reactions. *Catal. Lett.* **1995**, *33*, 387–394.

(16) Huo, Q.; Margolese, D. I.; Ciesla, U.; Demuth, D. G.; Feng, P.; Gier, T. E.; Sieger, P.; Firouzi, A.; Chmelka, B. F.; Schüth, F.; Stucky, G. D. Organization of Organic Molecules with Inorganic Molecular Species into Nanocomposite Biphase Arrays. *Chem. Mater*. **1994**, *6*, 1176–1191.

(17) Bagshaw, S. A.; Prouzet, E.; Pinnavaia, T. J. Templating of Mesoporous Molecular Sieves by Nonionic Polyethylene Oxide Surfactants. *Science* **1995**, *269*, 1242–1244.

(18) Zhao, D.; Feng, J.; Huo, Q.; Melosh, N.; Fredrickson, G. H.; Chmelka, B. F.; Stucky, G. D. Tri Block Copolymer Synthesis of Mesoporous Silica with Periodic 50 to 300 Angstrom Pores. *Science* **1998**, *279*, 548–552.

(19) Zhao, D.; Sun, J.; Li, Q.; Stucky, G. D. Morphological Control of Highly Ordered Mesoporous Silica SBA-15. *Chem. Mater*. **2000**, *12*, 275–279.

(20) Kim, M. J.; Ryoo, R. Synthesis and Pore Size Control of Cubic Mesoporous Silica SBA-1. *Chem. Mater*. **1999**, *11*, 487–491.

(21) Kim, J. M.; Stucky, G. D. Synthesis of Highly Ordered Mesoporous Silica Materials Using Sodium Silicate and Amphiphilic Block Copolymers. *Chem. Commun*. **2000**, *13*, 1159–1160.

(22) Zhao, D.; Huo, Q.; Feng, J.; Chmelka, B. F.; Stucky, G. D. Nonionic Triblock and Star Diblock Copolymer and Oligomeric Sufactant Syntheses of Highly Ordered,

Hydrothermally Stable, Mesoporous Silica Structures. *J. Am. Chem. Soc*. **1998**, *120*, 6024–6036.

(23) Ravikovitch, P. I.; Neimark, A. V. Characterization of Micro- and Mesoporosity in SBA-15 Materials from Adsorption Data by the NLDFT Method. *J. Phys. Chem. B* **2001**, *105*, 6817–6823.

(24) Kruk, M.; Jaroniec, M.; Ko, C. H.; Ryoo, R. Characterization of the Porous Structure of SBA-15. *Chem. Mater*. **2000**, *12*, 1961–1968.

(25) Yang, C. M.; Zibrowius, B.; Schmidt, W.; Schüth, F. Stepwise Removal of the Copolymer Template from Mesopores and Micropores in SBA-15. *Chem. Mater*. **2004**, *16*, 2918–2925.

(26) Lukens, W. W.; Schmidt-Winkel, P.; Zhao, D.; Feng, J.; Stucky, G. D. Evaluating Pore Sizes in Mesoporous Materials: A Simplified Standard Adsorption Method and a Simplified Broekhoff-de Boer Method. *Langmuir* **1999**, *15*, 5403–5409.

(27) Ryoo, R.; Ko, C. H.; Kruk, M.; Antochshuk, V.; Jaroniec, M. Block-Copolymer-Templated Ordered Mesoporous Silica: Array of Uniform Mesopores or Mesopore−Micropore Network? *J. Phys. Chem. B* **2000**, *104*, 11465–11471.

(28) Moritz, M.; Laniecki, M. Application of SBA-15 Mesoporous Material as the Carrier for Drug Formulation Systems. Papaverine Hydrochloride Adsorption and Release Study. *Powder Technol.* **2012**, *230*, 106–111.

(29) Hartmann, M.; Vinu, A.; Chandrasekar, G. Adsorption of Vitamin E on Mesoporous Carbon Molecular Sieves. *Chem. Mater.* **2005**, *17*, 829–833.

(30) Dos Santos, S. M. L.; Nogueira, K. A. B.; De Souza Gama, M.; Lima, J. D. F.; Da Silva Júnior, I. J.; De Azevedo, D. C. S. Synthesis and Characterization of Ordered Mesoporous Silica (SBA-15 and SBA-16) for Adsorption of Biomolecules. *Microporous Mesoporous Mater*. **2013**, *180*, 284–292.

(31) Wan, H.; Liu, L.; Li, C.; Xue, X.; Liang, X. Facile Synthesis of Mesoporous SBA-15 Silica Spheres and Its Application for High-Performance Liquid Chromatography. *J. Colloid Interface Sci.* **2009**, *337*, 420–426.

(32) Kim, J.; Ichikuni, N.; Hara, T.; Shimazu, S. Study on the Selectivity of Propane Photo-Oxidation Reaction on SBA-15 Supported Mo Oxide Catalyst. *Catal. Today* **2016**, *265*, 90–94.

(33) Cheng, C.; Luan, Z.; Klinowski, J. The Role of Surfactant Micelles in the Synthesis of the Mesoporous Molecular Sieve MCM-41. *Langmuir* **2000**, *11*, 2815–2819.

(34) Alexandridis, P.; Olsson, U.; Lindman, B. A Record Nine Different Phases (Four Cubic, Two Hexagonal, and One Lamellar Lyotropic Liquid Crystalline and Two Micellar Solutions) in a Ternary Isothermal System of an Amphiphilic Block Copolymer and Selective Solvents (Water and Oil). *Langmuir* **1998**, *14*, 2627–2638.

(35) Sayari, A.; Han, B. H.; Yang, Y. Simple Synthesis Route to Monodispersed SBA-15 Silica Rods. *J. Am. Chem. Soc.* **2004**, *126*, 14348–14349.

(36) Kiselev, A. V. No Title. *Kolloidn. Zh.* **1936**, *2*, 17.

(37) Van Der Voort, P.; Gillis-D'Hamers, I.; Vrancken, K. C.; Vansant, E. F. Effect of Porosity on the Distribution and Reactivity of Hydroxyl Groups on the Surface of Silica Gel. *J. Chem. Soc. Faraday Trans.* **1991**, *87*, 3899–3905.

(38) Zhuravlev, L. T. Concentration of Hydroxyl Groups on the Surface of Amorphous Silicas. *Langmuir* **1987**, *3*, 316–318.

(39) Léonardelli, S.; Facchini, L.; Fretigny, C.; Tougne, P.; Legrand, A. P. Silicon-29 Nuclear Magnetic Resonance Study. *J. Am. Chem. Soc.* **1992**, *114*, 6412–6418.

(40) Tuel, A.; Hommel, H.; Legrand, A. P. A 29Si NMR Study of the Silanol Population at the Surface of Derivatized Silica. *Langmuir* **1990**, *6*, 770–775.

(41) Luhmer, M.; D'Espinose, J. B.; Hommel, H.; Legrand, A. P. High-Resolution 29Si Solid-State NMR Study of Silicon Functionality Distribution on the Surface of Silicas. *Magn. Reson. Imaging* **1996**, *14*, 911–913.

(42) Zhao, X. S.; Lu, G. Q. Modification of MCM-41 by Surface Silylation with Trimethylchlorosilane and Adsorption Study. *J. Phys. Chem. B* **1998**, *102*, 1556–1561.

(43) Hertl, W.; Hair, M. L. Adsorption of Water on Silica. *Nature* **1969**, *223*, 1150–1151.

(44) Zhuravlev, L. T. The Surface Chemistry of Amorphous Silica. Zhuravlev Model. *Colloids Surfaces A Physicochem. Eng. Asp*. **2000**, *173*, 1–38.

(45) Ruddy, D. A.; Tilley, T. D. Highly Selective Olefin Epoxidation with Aqueous H_2O_2 over Surface-Modified TaSBA15 Prepared via the TMP Method. *Chem. Commun*. **2007**, *0*, 3350-3352.

(46) Zhao, X. S.; Lu, G. Q.; Whittaker, A. K.; Millar, G. J.; Zhu, H. Y. Comprehensive Study of Surface Chemistry of MCM-41 Using Si-29 CP/MAS NMR, FTIR, Pyridine-TPD, and TGA. *J. Phys. Chem. B* **1997**, *101*, 6525–6531.

(47) Kimura, T.; Saeki, S.; Sugahara, Y.; Kuroda, K. Organic Modification of FSM-Type Mesoporous Silicas Derived from Kanemite by Silylation. *Langmuir* **1999**, *15*, 2794–2798.

(48) Hara, K.; Akahane, S.; Wiench, J. W.; Burgin, B. R.; Ishito, N.; Lin, V. S. Y.; Fukuoka, A.; Pruski, M. Selective and Efficient Silylation of Mesoporous Silica: A Quantitative Assessment of Synthetic Strategies by Solid-State NMR. *J. Phys. Chem. C* **2012**, *116*, 7083–7090.

(49) Ojeda-López, R.; Pérez-Hermosillo, I. J.; Marcos Esparza-Schulz, J.; Cervantes-Uribe, A.; Domínguez-Ortiz, A. SBA-15 Materials: Calcination Temperature Influence on Textural Properties and Total Silanol Ratio. *Adsorption* **2015**, *21*, 659–669.

(50) Legrand, A. P. The Surface Properties of Silicas. *Wiley* **1998**, 470.

(51) Vansant, E. F.; Voort, P. Van Der; Vrancken, K. C. Characterization and Chemical Modification of the Silica Surface. *Elsevier* **1995**.

(52) Liu, Y.; Lee, J.Y.; Hong, L. Functionalized SiO_2 in Poly (Ethylene Oxide)-Based Polymer Electrolytes. *J. Power Sources* **2002**, *109*, 507–514.

(53) Wang, X. L.; Mei, A.; Li, M.; Lin, Y.; Nan, C. W. Effect of Silane-Functionalized Mesoporous Silica SBA-15 on Performance of PEO-Based Composite Polymer Electrolytes. *Solid State Ion.* **2006**, *177*, 1287–1291.

(54) Inagaki, S.; Fukushima, Y. Adsorption of Water Vapor and Hydrophobicity of Ordered Mesoporous Silica, FSM-16. *Microporous Mesoporous Mater*. **1998**, *21*, 667–672.

(55) Matsumoto, A.; Sasaki, T.; Nishimiya, N.; Tsutsumi, K. Evaluation of the Hydrophobic Properties of Mesoporous FSM-16 by Means of Adsorption Calorimetry. *Langmuir* **2001**, *17*, 47–51.

(56) Thomas, J. M.; Thomas, W. J. Principles and Practice of Heterogeneous Catalysis. *Wiley-VCH* **1997**, 70.

(57) McClure, S. M.; Goodman, D. W. New Insights into Catalytic CO Oxidation on Pt-Group Metals at Elevated Pressures. *Chem. Phys. Lett*. **2009**, *469*, 1–13.

(58) Mergler, Y. J.; Van Aalst, A.; Van Delft, J.; Nieuwenhuys, B. E. CO Oxidation over Promoted Pt Catalysts. *Appl. Catal. B Environ*. **1996**, *10*, 245–261.

(59) Doherty, R. P.; Krafft, J. M.; Méthivier, C.; Casale, S.; Remita, H.; Louis, C.; Thomas, C. On the Promoting Effect of Au on CO Oxidation Kinetics of Au-Pt Bimetallic Nanoparticles Supported on SiO_2: An Electronic Effect? *J. Catal.* **2012**, *287*, 102–113.

(60) Xu, J.; Xu, X. C.; Ouyang, L.; Yang X.-J.; Mao, W.; Su, J.; Han, Y.-F. Mechanistic Study of Preferential CO Oxidation on a Pt/NaY Zeolite Catalyst. *J. Catal.* **2012**, *287*, 114–123.

(61) Tsuji, A.; Rao, K. T. V.; Nishimura, S.; Takagaki, A.; Ebitani, K. Selective Oxidation of Glycerol by Using a Hydrotalcite-Supported Platinum Catalyst under Atmospheric Oxygen Pressure in Water. *ChemSusChem* **2011**, *4*, 542–548.

(62) Igarashi, H.; Uchida, H.; Suzuki, M.; Sasaki, Y.; Watanabe, M. Removal of Carbon Monoxide from Hydrogen-Rich Fuels by Selective Oxidation over Platinum Catalyst Supported on Zeolite. *Appl. Catal. A Gen*. **1997**, *159*, 159–169.

(63) Xu, C.; Koel, B. E.; Newton, M. A.; Frei, N. A.; Campbell, C. T. Dehydrogenation of Methylcyclohexane on Pt(111). *J. Phys. Chem*. **1995**, *99*, 16670–16675.

(64) Anpo, M.; Aikawa, N.; Kubokawa, Y. Photocatalytic Hydrogenation of Alkynes and Alkenes with Water over Titanium Dioxide. Platinum Loading Effect on the Primary Processes. *J. Phys. Chem.* **1984**, *88*, 3998–4000.

(65) Alivisatos, A. P. Semiconductor Clusters, Quantum Nanocrystals, and Quantum Dots. *Science* **1996**, *271*, 933–937.

(66) Manasilp, A.; Gulari, E. Selective CO Oxidation over Pt/Alumina Catalysts for Fuel Cell Applications. *Appl. Catal. B Environ*. **2002**, *37*, 17–25.

(67) Ivanova, A. S.; Slavinskaya, E. M.; Gulyaev, R. V.; Zaikovskii, V. I.; Stonkus, O. A.; Danilova, I. G.; Plyasova, L. M.; Polukhina, I. A.; Boronin, A. I. Metal–support Interactions in Pt/Al_2O_3 and Pd/Al_2O_3 Catalysts for CO Oxidation. *Appl. Catal. B Environ.* **2010**, *97*, 57–71.

(68) Kim, S. S.; Lee, H. H.; Hong, S. C. The Effect of the Morphological Characteristics of TiO_2 supports on the Reverse Water-Gas Shift Reaction over Pt/TiO_2 catalysts. *Appl. Catal. B Environ.* **2012**, *119*, 100–108.

(69) Zhai,W.; Xue, S.; Zhu, A.; Luo, Y.; Tian, Y. Plasmon-Driven Selective Oxidation of Aromatic Alcohols to Aldehydes in Water with Recyclable Pt/TiO_2 Nanocomposites. *ChemCatChem* **2011**, *3*, 127–130.

(70) Long, R.; Yang, R. T. Pt /MCM-41 Catalyst for Selective Catalytic Reduction of Nitric Oxide with Hydrocarbons in the Presence of Excess Oxygen. *Catal. Lett.* **1998**, *52*, 91–96.

(71) Jiang, C.; Hara, K.; Fukuoka, A. Low-Temperature Oxidation of Ethylene over Platinum Nanoparticles Supported on Mesoporous Silica. *Angew. Chem. Int. Ed*. **2013**, *52*, 6265–6268.

(72) Fukuoka, A.; Kimura, J.; Oshio, T.; Sakamoto, Y.; Ichikawa, M. Preferential Oxidation of Carbon Monoxide Catalyzed by Platinum Nanoparticles in Mesoporous Silica. *J. Am. Chem. Soc.* **2007**, *129*, 10120–10125.

(73) Chytil, S.; Glomm, W. R.; Blekkan, E. A. Characterization of Pt/SBA-15 Prepared by the Deposition-Precipitation Method. *Catal. Today* **2009**, *147*, 217–223.

(74) Huang, W.; Kuhn, J. N.; Tsung, C. K.; Zhang, Y.; Habas, S. E.; Yang, P.; Somorjai, G. A. Dendrimer Templated Synthesis of One Nanometer Rh and Pt Particles Supported on Mesoporous Silica: Catalytic Activity for Ethylene and Pyrrole Hydrogenation. *Nano Lett*. **2008**, *8*, 2027–2034.

(75) Yin, Y.; Yang, Z. F.; Wen, Z. H.; Yuan, A. H.; Liu, X. Q.; Zhang, Z. Z.; Zhou, H. Modification of as Synthesized SBA-15 with Pt Nanoparticles: Nanoconfinement Effects Give a Boost for Hydrogen Storage at Room Temperature. *Sci. Rep*. **2017**, *7*, 1–10.

(76) Yang, C.–M.; Liu, P.–H.; Ho, Y.–F.; Chiu, C.–Y.; Chao, K.–J. Highly Dispersed Metal Nanoparticles in Functionalized SBA-15. *Chem. Mater*. **2003**, *15*, 275–280.

(77) Wu, H.-C.; Chen, T.-C.; Lai, N.-C.; Yang, C.-M.; Wu, J.-H.; Chen, Y.-C.; Lee, J.-F.; Chen, C.-S. Synthesis of Sub-Nanosized Pt Particles on Mesoporous SBA-15 Material and Its Application to the CO Oxidation Reaction. *Nanoscale* **2015**, *7*, 16848–16859.

(78) Chen, C. S.; Lai, Y. T.; Chen, T. C.; Chen, C. H.; Lee, J. F.; Hsu, C. W.; Kao, H. M. Synthesis and Characterization of Pt Nanoparticles with Different Morphologies in Mesoporous Silica SBA-15 for Methanol Oxidation Reaction. *Nanoscale* **2014**, *6*, 12644–12654.

(79) Lai, Y. T.; Chen, T. C.; Lan, Y. K.; Chen, B. S.; You, J. H.; Yang, C. M.; Lai, N. C.; Wu, J. H.; Chen, C. S. Pt/SBA-15 as a Highly Efficient Catalyst for Catalytic Toluene Oxidation. *ACS Catal*. **2014**, *4*, 3824–3836.

(80) Park, J. Il; Lee, J. K.; Miyawaki, J.; Yoon, S. H.; Mochida, I. Catalytic Oxidation of Polycyclic Aromatic Hydrocarbons (PAHs) over SBA-15 Supported Metal Catalysts. *J. Ind. Eng. Chem.* **2011**, *17*, 271–276.

(81) Saltveit, M. E. Effect of Ethylene on Quality of Fresh Fruits and Vegetables. *Postharvest Biol. Technol.* **1999**, *15*, 279–292.

(82) Girardin, J. Einfluss Des Leuchtgases Auf Die Promenaden Und Strassenbaume. *Jahresb. Agrik.* **1864**, *7*, 199–200.

(83) Lieberman, M.; Mapson, L. W. Genesis and Biogenesis of Ethylene. *Nature* **1964**, *204*, 343–345.

(84) Adams, D. O.; Yang, S. F. Ethylene Biosynthesis: Identification of 1-Aminocyclopropane-1-Carboxylic Acid as an Intermediate in the Conversion of Methionine to Ethylene. *Proc. Natl. Acad. Sci.* **1979**, *76*, 170–174.

(85) Graham, D.; Patterson, B. D. Responses of Plants to Low, Nonfreezing Temperatures: Proteins, Metabolism, and Acclimation. *Annu. Rev. Plant Physiol.* **1982**, *33*, 347–372.

(86) Bhowmik, S. R.; Pan, J. C. Shelf Life of Mature Green Tomatoes Stored in Controlled Atmosphere and High Humidity. *J. Food Sci*. **1992**, *57*, 948–953.

(87) Ketsa, S.; Pangkool, S. The Effect of Temperature and Humidity on the Ripening of Durian Fruits. *J. Hortic. Sci*. **1995**, *70*, 827–831.

(88) Saltveit, M., Jr.; Bradford, K.; Dilley, D. Silver Ion Inhibits Ethylene Synthesis and Action in Ripening Fruits [Apples, Banana, Musa Sp., Tomatoes]. *J. Am. Soc. Hortic. Sci*. **1978**.

(89) Beyer, E. M. A Potent Inhibitor of Ethylene Action in Plants. *Plant Physiol*. **1976**, *58*, 268–271.

(90) Kader, A. A. Postharvest Technology of Horticultural Crops. University of California, Agriculture and Natural Resources: Oakland, CA, **2002**, *3311*.

(91) Scott, K. J.; McGlasson, W. B.; Roberts, E. A. Potassium Permanganate as an Ethylene Absorbent in Polyethylene Bags to Delay Ripening of Bananas during Storage. *Aust. J. Exp. Agric.* **1970**, *10*, 237–240.

(92) Ma, X.; Ouyang, F. Adsorption Properties of Biomass-Based Activated Carbon Prepared with Spent Coffee Grounds and Pomelo Skin by Phosphoric Acid Activation. *Appl. Surf. Sci.* **2013**, *268*, 566–570.

(93) Triebe, R. W.; Tezel, F. H.; Khulbe, K. C. Adsorption of Methane, Ethane and Ethylene on Molecular Sieve Zeolites. *Gas Sep. Purif.* **1996**, *10*, 81–84.

(94) Park, D.-R.; Zhang, J.; Ikeue, K.; Yamashita, H.; Anpo, M. Photocatalytic Oxidation of Ethylene to CO_2 and H_2O on Ultrafine Powdered TiO_2 Photocatalysts in the Presence of O_2 and H_2O. *J. Catal.* **1999**, *185*, 114–119.

(95) Fu, X.; Clark, L. A.; Zeltner, W. A.; Anderson, M. A. Effects of Reaction Temperature and Water Vapor Content on the Heterogeneous Photocatalytic Oxidation of Ethylene. *J. Photochem. Photobiol. A Chem.* **1996**, *97*, 181–186.

(96) Xianzhi, F. U.; Clark, L. A.; Yang, Q.; Anderson, M. A. Enhanced Photocatalytic Performance of Titania-Based Binary Metal Oxides: TiO_2/SiO_2 and TiO_2/ZrO_2. *Environ. Sci. Technol.* **1996**, *30*, 647–653.

(97) Pan, X.; Chen, X.; Yi, Z. Defective, Porous TiO_2 Nanosheets with Pt Decoration as an Efficient Photocatalyst for Ethylene Oxidation Synthesized by a C_3N_4 Templating Method. *ACS Appl. Mater. Interfaces* **2016**, *8*, 10104–10108.

(98) Zhang, W.; Pan, X.; Long, P.; Liu, X.; Long, X.; Yu, Y.; Yi, Z. Platinum Nanoparticles Supported on Defective Tungsten Bronze-Type $KSr_2Nb_5O_{15}$ as a Novel Photocatalyst for Efficient Ethylene Oxidation. *J. Mater. Chem. A* **2017**, *5*, 18998–19006.

(99) Lenher, S. The Reaction between Oxygen and Ethylene. I. *J. Am. Chem. Soc.* **1931**, 53, 3737–3751.

(100) Twigg, G. H. The Mechanism of the Catalytic Oxidation of Ethylene. I. Experiments Using a Flow System. *Proc. R. Soc. A Math. Phys. Eng. Sci*. **1946**, *188*, 92–104.

(101) Bal'zhinimaev, V. I. Ethylene Epoxidation over Silver Catalysts. *Kinet. Catal.* **1999**, *40*, 795–810.

(102) Özbek, M. O.; Van Santen, R. A. The Mechanism of Ethylene Epoxidation Catalysis. *Catal. Lett.* **2013**, *143*, 131–141.

(103) Ahn, H. G.; Choi, B. M.; Lee, D. J. Complete Oxidation of Ethylene over Supported Gold Nanoparticle Catalysts. *J Nanosci Nanotechnol* **2006**, *6*, 3599–3603.

(104) Li, J.; Ma, C.; Xu, X.; Yu, J.; Hao, Z.; Qiao, S. Efficient Elimination of Trace Ethylene over Nano-Gold Catalyst under Ambient Conditions. *Environ. Sci. Technol.* **2008**, *42*, 8947–8951.

(105) Xue, W. J.; Wang, Y. F.; Li, P.; Liu, Z. T.; Hao, Z. P.; Ma, C. Y. Morphology Effects of CO_3O_4 on the Catalytic Activity of Au/Co_3O_4 catalysts for Complete Oxidation of Trace Ethylene. *Catal. Commun*. **2011**, *12*, 1265–1268.

(106) Ma, C. Y.; Mu, Z.; Li, J. J.; Jin, Y. G.; Cheng, J.; Lu, G. Q.; Hao, Z. P.; Qiao, S. Z. Mesoporous CO_3O_4 and Au/Co_3O_4 Catalysts for Low-Temperature Oxidation of Trace Ethylene. *J. Am. Chem. Soc*. **2010**, *132*, 2608–2613.

(107) Njagi, E. C.; Genuino, H. C.; King'Ondu, C. K.; Dharmarathna, S.; Suib, S. L. Catalytic Oxidation of Ethylene at Low Temperatures Using Porous Copper Manganese Oxides. *Applied Catalysis A: General*. **2012**, *421–422*, 154–160.

(108) Li, W.; Zhang, Z.; Wang, J.; Qiao, W.; Long, D.; Ling, L. Low Temperature Catalytic Combustion of Ethylene over Cobalt Oxide Supported Mesoporous Carbon Spheres. *Chem. Eng. J.* **2016**, *293*, 243–251.

(109) Isaifan, R. J.; Ntais, S.; Baranova, E. A. Particle Size Effect on Catalytic Activity of Carbon-Supported Pt Nanoparticles for Complete Ethylene Oxidation. *Appl. Catal. A Gen*. **2013**, *464–465*, 87–94.

(110) Imanaka, N.; Masui, T.; Terada, A.; Imadzu, H. Complete Oxidation of Ethylene at Temperatures below 100 °C over a $Pt/Ce_{0.64}Zr_{0.16}$ $Bi_{0.20}$ $O_{1.90}/\gamma$-Al_2O_3 Catalyst. *Chem. Lett.* **2008**, *37*, 42–43.

(111) Wang, M.; Zhang, L.; Huang, W.; Zhou, Y.; Zhao, H.; Lv, J.; Tian, J.; Kan, X.; Shi, J. Pt/MnO_2: Facile Synthesis and Highly Efficient Catalyst for Ethylene Oxidation at Low Temperature. *RSC Adv*. **2017**, *7*, 14809–14815.

(112) Kou, Y.; Sun, L.-B. Size Regulation of Platinum Nanoparticles by Using Confined Spaces for the Low-Temperature Oxidation of Ethylene. *Inorg. Chem*. **2018**, *57*, 1645–1650.

(113) Yang, H.; Ma, C.; Zhang, X.; Li, Y.; Cheng, J.; Hao, Z. Understanding the Active Sites of Ag/Zeolites and Deactivation Mechanism of Ethylene Catalytic Oxidation at Room Temperature. *ACS Catal*. **2018**, *8*, 1248–1258.

(114) Yang, H.; Ma, C.; Li, Y.; Wang, J.; Zhang, X.; Wang, G. Synthesis, Characterization and Evaluations of the Ag/ZSM-5 for Ethylene Oxidation at Room Temperature : Investigating the Effect of Water and Deactivation. *Chem. Eng. J.* **2018**, *347*, 808–818.

(115) Yang, H.; Ma, C.; Wang, G.; Sun, Y.; Cheng, J.; Zhang, Z.; Zhang, X.; Hao, Z. Fluorine-Enhanced Pt/ZSM-5 Catalysts for Low Temperature Oxidation of Ethylene. *Catal. Sci. Technol*. **2018**, *8*, 1988–1996.

Chapter 2: Synthesis, Characterization and Introduction to Low Temperature Ethylene Oxidation over Pt/Mesoporous Silica

2.1 Introduction

Ethylene, a natural hormone produced by fruits and vegetables,[1] is physiologically active at extremely low parts-per-million level concentrations, and plays a positive role as a ripening agent under controlled conditions. However, such trace ethylene causes undesirable deterioration of fresh products in containers and refrigerators even at low temperatures, which finally results in forming food waste. Continuous and complete removal of trace ethylene at low temperatures is therefore an important issue worldwide in order to keep agricultural products fresh for long-term storage and transportation.[2] Potassium permanganate and ozone have been proposed as oxidants for the decomposition of ethylene;[3,4] however, their high toxicity and stoichiometric reaction system fail in conventional technology for long-term ethylene removal. Physical adsorption with activated carbon[5] and zeolites[6] is also insufficient for ethylene removal due to limited adsorption capacity. In contrast, chemocatalytic ethylene decomposition with heterogeneous catalysts has recently been recognized as a sustainable method for practical applications. Several catalysts such as Co/Mordenite,[7] Au/Al_2O_3,[8] Au/Co_3O_4,[9–11] Cu/MnO_2,[12] CoO/mesoporous carbon,[13] Pt/MnO_2,[14] Ag/zeolite[15] and a UV-light responsive Pt/TiO_2 photocatalyst[16–18] have been studied for ethylene oxidation. Bimetallic alloy nanocrystals of Pt-Pd encapsulated in ZIF-8 has also been reported to show excellent synergistic photocatalytic activity in oxidation of ethylene.[19]

We have examined various supported metal catalysts for the oxidation of ethylene (0.32%) in the presence of oxygen (20%) and identified a mesoporous silica-supported Pt catalyst that affords the highest activity at 25-100 °C among various catalysts that consisted of a variety of combinations of metals (Pt, Au, Ag and Pd) and supports (SiO_2, Al_2O_3, TiO_2 and ZrO_2).[20] A mechanistic study using Fourier-transform infrared spectroscopy at 50 °C suggested that ethylene is converted to CO_2 and H_2O via formaldehyde and CO as possible intermediates. In addition, the mesoporous silica-supported Pt catalyst is able to decompose trace ethylene (50 ppm) with a very high conversion even at 0 °C. Despite the decrease in the initial activity of the supported Pt catalyst by 20-30% during the course of the reaction, the original activity was easily recovered after heat treatment of the spent catalyst under dry conditions. Water molecules formed in the reaction partly block active Pt reaction sites, which is the reason for the decrease in catalytic activity. Nonetheless, the ability of this heterogeneous catalyst to remove ethylene and evolve CO_2 at 0 °C has led to practical use for ethylene decomposition in refrigerators,[21] in which the catalyst is used under steady state conditions in the presence of water vapor.

In the present work, the author performs a comprehensive study of the oxidation of trace ethylene by silica-supported Pt catalysts at 0 °C using a fixed-bed flow reactor. The ethylene oxidation reaction is first examined in detail using a mesoporous silica-supported Pt catalyst. SBA-15,[22] which has a highly ordered mesoporous structure, was selected as a silica support in this study due to its excellent thermal and mechanical stability compared to MCM-41.[23] The time course of the ethylene conversion and the CO_2 yield over Pt/SBA-15 was monitored after the addition of water vapor to the reactor to confirm the effect of physisorbed water on the activity of the supported Pt catalyst. Several silica-supported Pt catalysts were also

prepared using aerosol silica with high surface areas to clarify their catalytic performance for ethylene oxidation.

2.2 Experimental

2.2.1 Chemicals

Tetraethoxysilane (TEOS; 99.9%) was purchased from Kojundo Chemical Laboratory. Diamminedinitroplatinum(II) ($Pt(NH_3)_2(NO_2)_2$) solution was obtained from Tanaka Kikinzoku Kogyo. Pluronic 123 (P123; $EO_{20}PO_{70}EO_{20}$, EO = ethylene oxide moiety, PO = propylene oxide moiety, average molecular weight 5800) was received from Sigma Aldrich. Hydrochloric acid (HCl; 36-38 wt%) was purchased from Wako Chemicals. All chemicals were used as-received without further purification.

2.2.2 Preparation of Mesoporous Silica, SBA-15

Mesoporous silica SBA-15 was synthesized with an amphiphilic triblock copolymer, P123, as a structure-directing agent.[22] P123 (12 g) was completely dissolved in aqueous HCl solution (1.6 M, 450 mL) at room temperature. TEOS (25.5 g) was added dropwise to the solution at 35 °C with continuous stirring, which undergoes hydrolysis and condensation reactions, resulting in the generation of silanol and siloxane groups. The resulting transparent and micellar mixture was aged at 35 °C for 24 h and then at 100 °C for an additional 24 h. The white precipitate formed in the mixture was isolated by suction filtration and washed repeatedly with water and ethanol until no precipitation occurred in the filtrate after the

addition of $AgNO_3$ solution. The dried sample was calcined at 560 °C for 16 h to remove the structure-directing agent to yield SBA-15 as a white powder.

2.2.3 Impregnation of Pt in SBA-15 and Aerosol Silicas

SBA-15 and three amorphous silicas (Aerosil 380 and 200, (hereafter A380 and A200), Evonic Industries; Cariact Q-10 (Q-10), Fuji Silysia) were used as supports. The support material (1.00 g) was shaken in an aqueous solution (50 mL) of $Pt(NH_3)_2(NO_2)_2$ (486 mM, 0.196 mL) at 30 °C for 3 h. After evaporation of H_2O at 50 °C and subsequent drying under vacuum at the same temperature for 16 h, the sample was reduced under H_2 flow (30 mL min^{-1}) at 400 °C for 2 h, which gave Pt/SBA-15 catalyst (Pt loading 1.8 wt%). The other Pt/A380, Pt/A200 and Pt/Q-10 catalysts were prepared using the same procedure.

2.2.4 Characterization

Powder X-ray diffraction (XRD) patterns were obtained with an X-ray diffractometer (Rigaku Ultima IV) using Cu Kα radiation (40 kV, 20 mA) over the 2θ range of 0.7-80°. Nitrogen adsorption-desorption isotherms were measured at -196 °C with a high precision surface area and pore size analyzer (MicrotracBEL BELSORP-Mini). Specific surface areas and pore diameters were calculated using the Brunauer-Emmett-Teller (BET) equation and non-localized density functional theory (NLDFT). Prior to N_2 adsorption, the samples were evacuated at 120 °C for 4 h to remove physisorbed water. The size of Pt nanoparticles was measured by CO chemisorption on a fully-automated catalyst analyzer (MicrotracBEL BELCAT II). The samples were reduced under a H_2 flow (30 mL min^{-1}) at 400 °C for 1.5 h,

followed by cooling to 50 °C under a He flow (50 mL min^{-1}). CO chemisorption was measured at 50 °C under a continuous flow of CO (10%) in He, and the size of the Pt nanoparticles was calculated based on the Pt dispersion assuming a 1:1 ratio of Pt:CO. Pt/SBA-15 was also studied using transmission electron microscope (TEM; JEM-2100F) with an accelerating voltage of 200 kV without metal deposition. X-ray photoelectron spectra (XPS) was acquired using a JEOL JPC-9010MC instrument at a pass energy of 20 eV using a Mg Kα line. Charge correction was based on the position of C 1s (C 284.8 eV) in the case of Pt/SBA-15

2.2.5 Ethylene Oxidation with a Fixed-Bed Flow Reactor

The catalytic oxidation of ethylene was performed in a stainless-steel tubular fixed-bed flow reactor (inner diameter 4 mm) under atmospheric pressure (Figure 2.1). Each catalyst in granular form (355-500 μm granule size, 0.40 g) was loaded in the reaction tube and pretreated at 150 °C for 2 h under a He flow (40 mL min^{-1}). A gas mixture of C_2H_4 (50 ppm), O_2 (20%), N_2 (5%) and He (balance) was fed to the catalyst bed at 0 °C in an ethanol bath using mass flow controllers under ambient pressure with a space velocity (SV) of 1500 mL h^{-1} g^{-1}. The outlet gases were collected every 10 min and analyzed using online gas chromatography (GC; Agilent 3000 A Micro GC) with a thermal conductivity detector. Molecular sieves 5A (10 m) and Plot U (8 m) were used as columns to detect C_2H_4 and CO_2, where the experimental detection limit for C_2H_4 was 0.1 ppm.

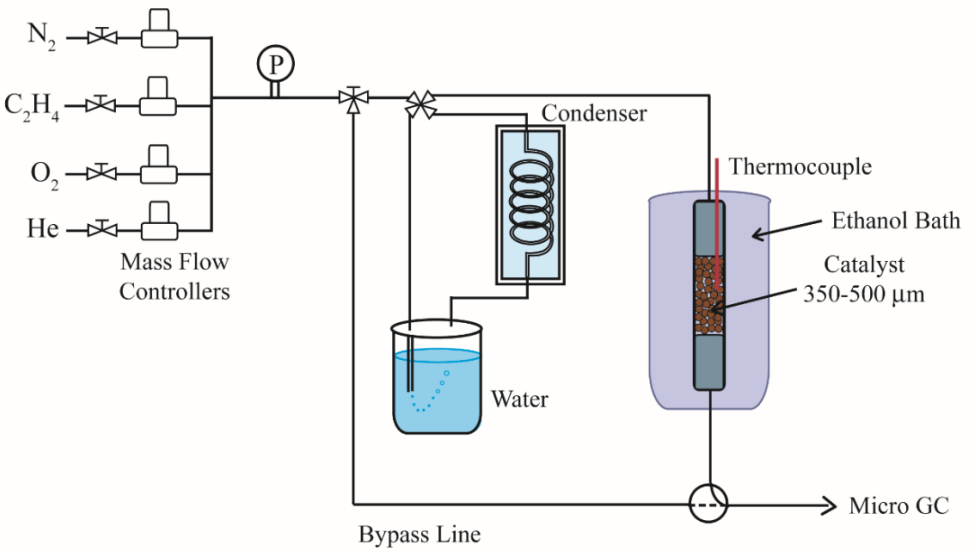

Figure 2.1. Schematic representation of the flow reactor used in low temperature ethylene oxidation.

Water vapor was added to the gas mixture (Figure 2.1) to examine the influence of water formed during the reaction. A gas mixture containing water vapor (0.86%) was supplied to the catalyst-bed (Pt/SBA-15, 0.067 g) at 28 °C with an SV of 9000 mL h^{-1} g^{-1} in order to prevent plugging the reactor with liquid water. The temperature was maintained at 5 °C to calculate the vapor pressure of water. The ethylene conversion (X_{C2H4}) and CO_2 yield (Y_{CO2}) were calculated from the following equations.

$$X_{C_2H_4} = ([C_2H_4]_{inlet} - [C_2H_4]_{outlet}) \times 100 / [C_2H_4]_{inlet}$$

$$Y_{CO_2} = [CO_2]_{outlet} \times 100 / 2[C_2H_4]_{inlet}$$

$[C_2H_4]_{inlet}$, $[C_2H_4]_{outlet}$ and $[CO_2]_{outlet}$ in the equations are the initial C_2H_4 concentration, and C_2H_4 and CO_2 concentrations at the outlet of the reactor, respectively.

2.3 Results and Discussion

2.3.1 Characterization of Pt Loaded Silica

Pristine and Pt-loaded silicas were characterized using XRD and N_2 adsorption measurements. Figure 2.2(A) shows small-angle XRD patterns for SBA-15 and Pt/SBA-15. These samples exhibited three characteristic diffraction peaks at 1.0°, 1.7° and 1.9°, which were assigned to the (100), (110) and (200) planes of a typical hexagonal (*p6mm*) mesoporous structure of one-dimensional cylindrical channels.[22–24] Change in the intensity and position of the original diffraction peaks was observed after the incorporation of Pt nanoparticles (Figures 2.2(A)). This is probably due to hydrogen reduction at high temperature (400 °C), which induces a slight change in the periodicity and ordering of the mesopores. Figure 2.2(B) shows XRD patterns for SBA-15 and supported Pt catalysts over a wide angular range. Three diffraction peaks appeared at 40°, 46° and 67° for Pt/SBA-15, and these were assigned to the (111), (200) and (220) planes of the face-centered cubic (fcc) Pt lattice. These characteristic diffraction peaks were also observed for other silica-supported Pt catalysts (Figure 2.2(B)). Therefore, impregnation of Pt ions and subsequent hydrogen reduction formed metallic Pt particles on all of the silica supports.

Figure 2.2(C) shows N_2-adsorption-desorption isotherms for SBA-15 and Pt/SBA-15. The samples had type IV isotherms according to the classification of Brunauer et al.[25] and IUPAC[26] with an H1 hysteresis loop, and these features are characteristic of SBA-15, as reported previously.[27] The lack of any apparent difference between the two isotherms indicates that the mesopores are not plugged after the formation of Pt particles. A typical transmission electron microscopy (TEM) image of Pt/SBA-15 is shown in Figure 2.2(E),

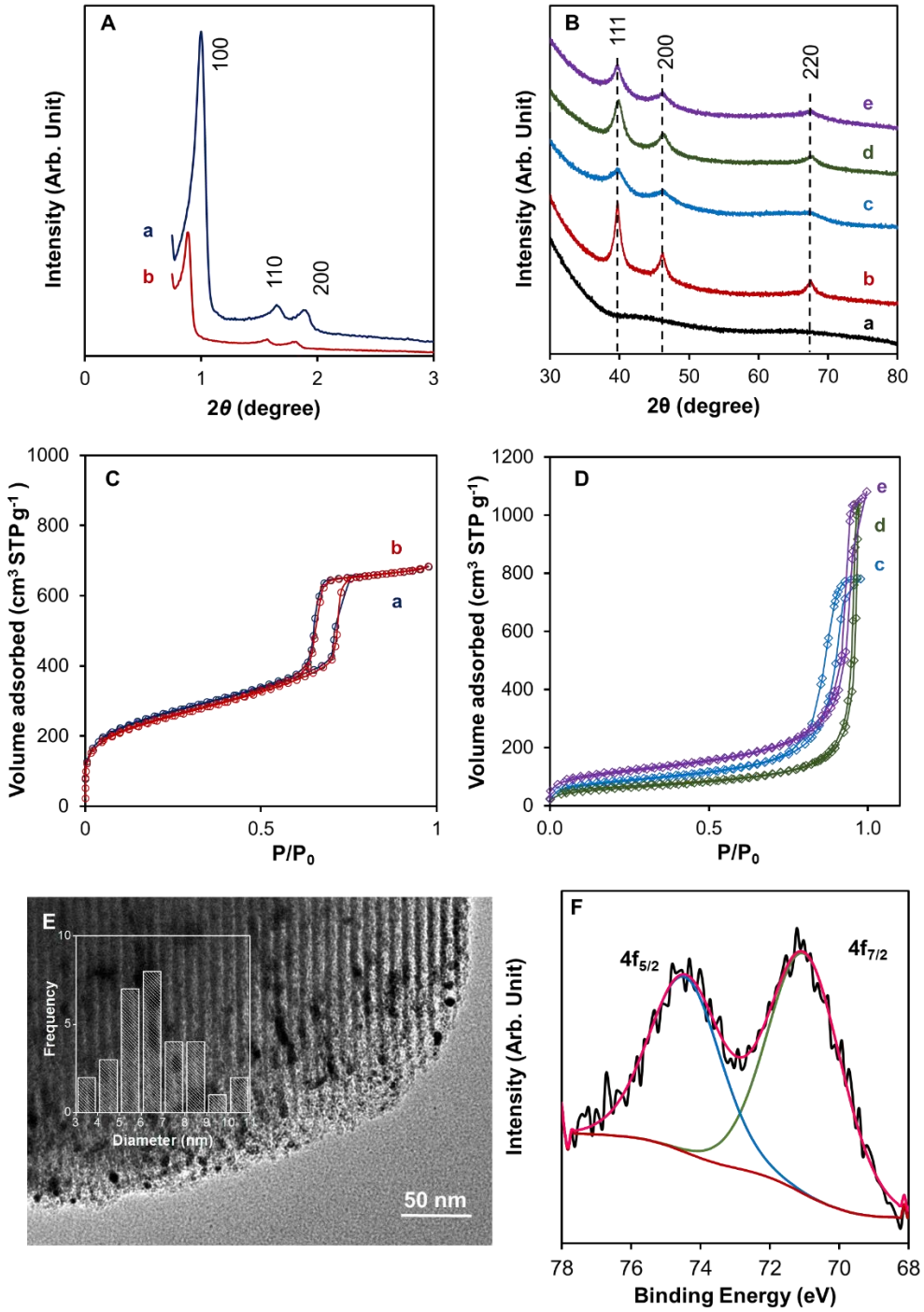

Figure 2.2. XRD patterns for SBA-15 and supported Pt catalysts in small (A) and wide angle regions (B). N_2 adsorption isotherms for mesoporous silicas (C) and Pt catalysts with aerosol silicas (D): (a) SBA-15, (b) Pt/SBA-15, (c) Pt/A380, (d) Pt/A200 and (e) Pt/Q-10. TEM image and size distribution curve of Pt/SBA-15 (E) and XPS of Pt/SBA-15 (F).

which shows a high dispersion of Pt nanoparticles mainly inside the mesopores. Three Pt catalysts using aerosil SiO_2 (Pt/A380, Pt/A200 and Pt/Q-10) exhibited type-II isotherms without a pronounced hysteresis loop[28] (Figure 2.2(D)). The structural parameters of these Pt catalysts obtained from the isotherms are summarized in Table 2.1.

The XPS spectrum of Pt/SBA-15 is shown in Figure 2.2(F). The peaks at around 71 eV and 74 eV are attributed to Pt $4f_{7/2}$ and Pt $4f_{5/2}$ of metallic Pt in the zero valent state, which is consistent with the results obtained in XRD (Figure 2.2).[29]

SBA-15 has a larger BET surface area (889 m^2 g^{-1}) and pore volume (1.1 mL g^{-1}) than the other aerosol silica supports, and these were preserved in Pt/SBA-15. In addition, the average size of Pt particles was in the range 4-7 nm, as estimated by CO chemisorption. The size of the Pt nanoparticles was smaller than that of mesopores; therefore, most Pt nanoparticles were incorporated into the mesoporous channels of SBA-15. High dispersion of Pt nanoparticles inside the channels was directly observed by the TEM image of Pt/SBA-15 in Figure 2.2(E), and the average size estimated from the size distribution histogram is 6.5 nm (Inset in Figure 2.2(E)).

Table 2.1. Structural parameters and catalytic activity for Pt supported silica catalysts[a]

	S_{BET}[b] / m^2 g^{-1}	V_{meso}[c] / mL g^{-1}	D_{meso}[d] / nm	D_{Pt}[e] / nm	Catalytic activity at 240 min	
					Conv.[f] (%)	Yield[g] (%)
SBA-15	889	1.1	13.8			
Pt/SBA-15	867	1.0	12.7	6.9	33	16
A380	377	0.40	N.D.[h]			
Pt/A380	392	0.39		4.3	32	11
A200	237	0.31	N.D.[h]			
Pt/A200	205	0.22		6.5	28	11
Q-10	280	0.31	N.D.[h]			
Pt/Q-10	284	0.29		4.5	22	8

[a] Reaction conditions: catalyst Pt/SBA-15 0.40 g (Pt 1.8 wt%); C_2H_4 50 ppm, O_2 20%, N_2 5%, He balance, SV 1500 mL h^{-1} g^{-1}. [b]BET surface area. [c]Pore volume estimated using the Barrett-Joyner-Halenda (BJH) equation. [d]Average diameter estimated using NLDFT. [e]Average size of Pt nanoparticles estimated by CO chemisorption. [f]Ethylene conversion. [g]CO_2 yield. [h]Not determined.

2.3.2 Oxidation of Trace Ethylene at 0 °C over SBA-15-Supported Pt Catalyst

Pt/SBA-15 was applied for the oxidation of ethylene (50 ppm) at 0 °C using a fixed-bed flow reactor. Figure 2.3 shows time courses for the ethylene conversion and CO_2 yield over Pt/SBA-15. While Pt/SBA-15 converted trace ethylene completely at the initial stage, the ethylene conversion decreased gradually after 90 min and reached ca. 30%. No products other than CO_2 were detected using GC during the reaction. However, the CO_2 yield was always lower than the corresponding ethylene conversion, and the ethylene conversion and CO_2 yield at 240 min were 33% and 16%, respectively. The difference between the conversion and the yield at the initial stage may be explained by the formation of

intermediates such as HCHO and CO,[20] which are probably stabilized on the catalyst surface. The formation of acetic acid may also occur, and this would remain on the catalyst surface without undergoing any reaction in the presence of O_2. It should be noted that the initial activity could be recovered after heat treatment of the spent catalyst at 150 °C for 120 min in a He flow, as shown in Figure 2.3. The re-activated Pt/SBA-15 catalyst exhibited the same time course of this reaction, which indicates that Pt/SBA-15 has no structural change in this reaction. Based on the amount of ethylene converted and the number of surface Pt atoms, the turnover number (TON) with Pt/SBA-15 was estimated to be 3.

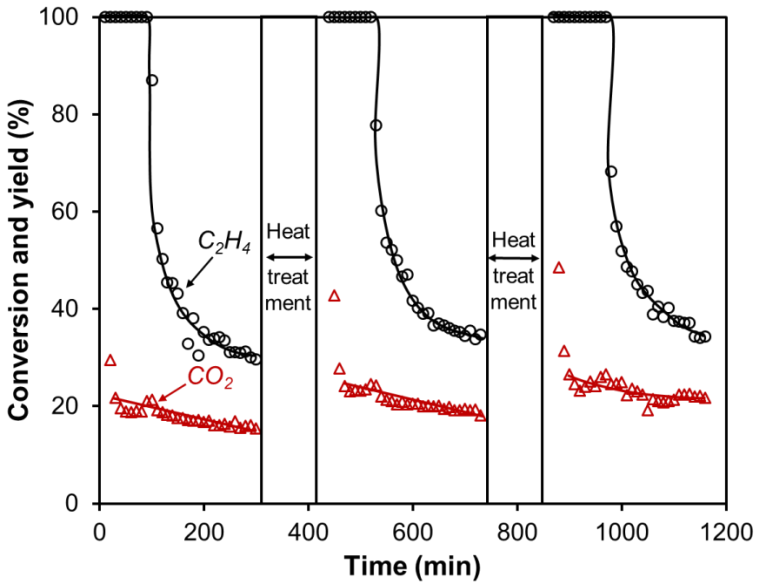

Figure 2.3. Time courses for ethylene conversion (black circles) and CO_2 yield (red triangles) over Pt/SBA-15 at 0 °C. Reaction conditions: Pt/SBA-15 0.40 g (Pt 1.8 wt%), C_2H_4 50 ppm, O_2 20%, N_2 5%, He balance, SV 1500 mL h^{-1} g^{-1}. After 310 min, the catalyst was heated at 150 °C for 2 h in a He flow (40 mL min^{-1}) and then re-used for the subsequent run.

The reaction with different SVs was carried over Pt/SBA-15 (Figure 2.4) to evaluate the effect of diffusion limitation at the steady state. Both ethylene conversion and CO_2 yield at 300 min decreased with the increase in SV, which means no mass transfer limitation under the reaction conditions.

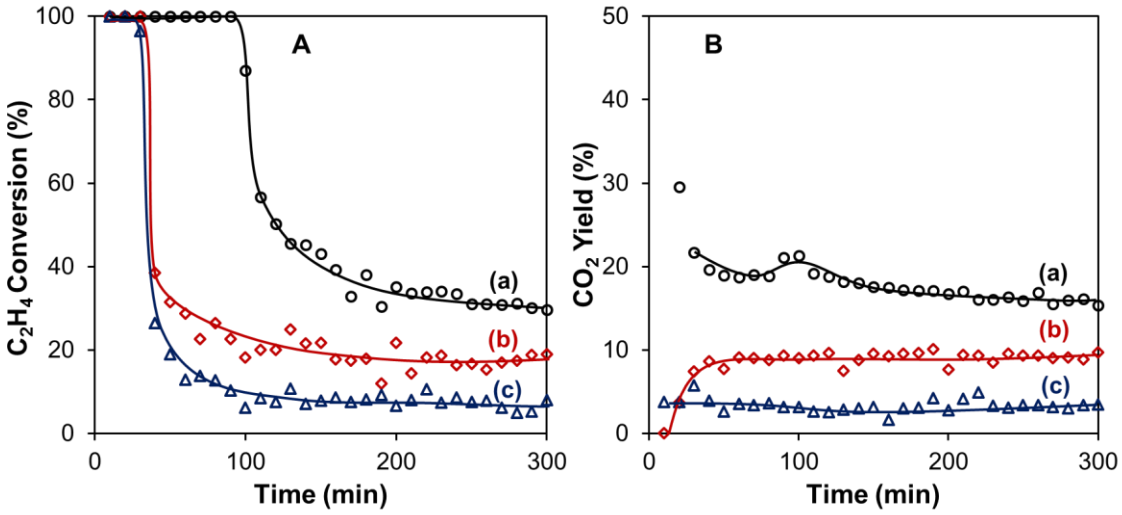

Figure 2.4. Ethylene conversion (A) and CO_2 yield (B) studied for varying space velocities, SV (a) 1500 mL h^{-1} g^{-1} (Pt/SBA-15 0.40 g), (b) 3000 mL h^{-1} g^{-1} (Pt/SBA-15 0.20 g) and (c) 6000 mL h^{-1} g^{-1} (Pt/SBA-15 0.10 g). Reaction condition: Pt/SBA-15 (Pt 1.8%), C_2H_4 200 ppm, O_2 20%, He balance, Flow rate 10 mL min^{-1}.

CO_2 formation in the re-activation step was studied to clarify the mass balance of this reaction. Figure 2.5 shows time courses of the moles of converted ethylene and CO_2 formed over a period of 300 min, and the subsequent formation of CO_2 from the spent catalyst by heat treatment in an inert atmosphere. Here the author assumed that the amount of intermediates stabilized on the catalyst surface within 300 min could be calculated by subtracting the total amounts of ethylene introduced and CO_2 evolved during the reaction. This calculation was conducted using the integrated area shown by the hatched region in

Figure 2.5, the SV (1500 mL h^{-1} g^{-1}) and the ethylene concentration (50 ppm), which gave 6.9 μmol of carbon.

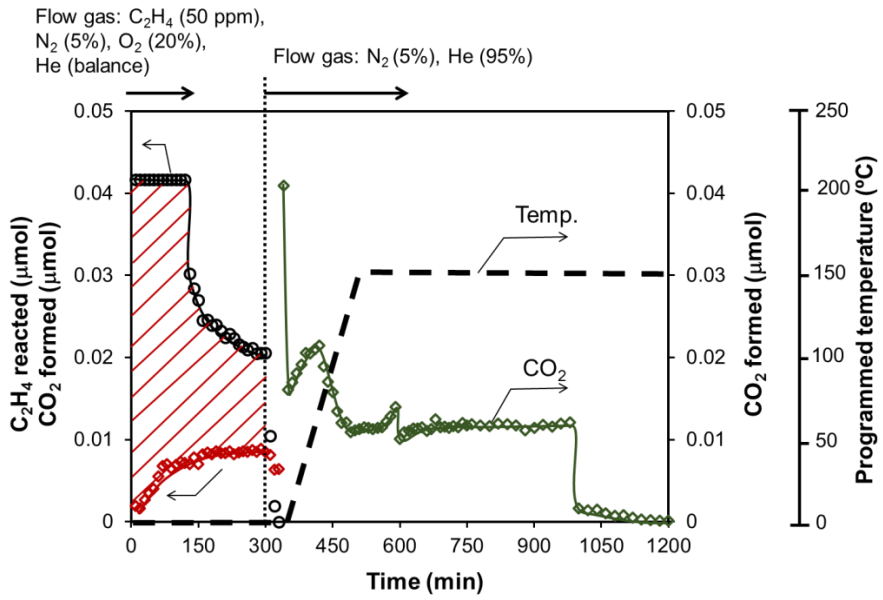

Figure 2.5. Moles of ethylene converted (black circles) and CO_2 formed (red diamonds) over Pt/SBA-15 at 0 °C, followed by CO_2 formation (green diamonds) by heat treatment at 150 °C (ramp rate, 1 °C min^{-1}) under a He/N_2 flow (95%/5%), (10 mL min^{-1}). Reaction conditions: Pt/SBA-15 0.40 g (Pt 1.8 wt%), C_2H_4 50 ppm, O_2 20%, N_2 5%, He balance, SV 1500 mL h^{-1} g^{-1}.

After ethylene oxidation at 0 °C, the spent catalyst was heated to 150 °C at a ramp rate of 1 °C min^{-1} under continuous flow of a mixed gas (He/N_2, 95%/5%), and held at 150 °C until no CO_2 was detected by GC measurements (Figure 2.5). It was obvious that CO_2 formation in the absence of O_2 is caused by thermal decomposition of oxygenated intermediates formed in the preceding 300 min. The amount of CO_2 evolved during the heat treatment was 8.3 μmol as determined by GC, which is a little higher compared to the calculated amount of intermediates (6.9 μmol). This might be due to the contribution of the carbon species decomposed to CO_2 from the catalyst support. To confirm it, a blank experiment was carried

out in the absence of C_2H_4 (O_2, He and N_2 was flown) for a period of 300 min followed by the same procedure under He/N_2 (95%/5%). This resulted in the evolution of 1.2 μmol CO_2 from the catalyst surface as shown in Figure 2.6, which might be the outcome of decomposition of carbon species already present on Pt/SBA-15. Hence it can be assumed that 6.9 μmol of the carbon species accumulated on the catalyst surface is decomposed to 7.1 μmol of CO_2 in the heat treatment.

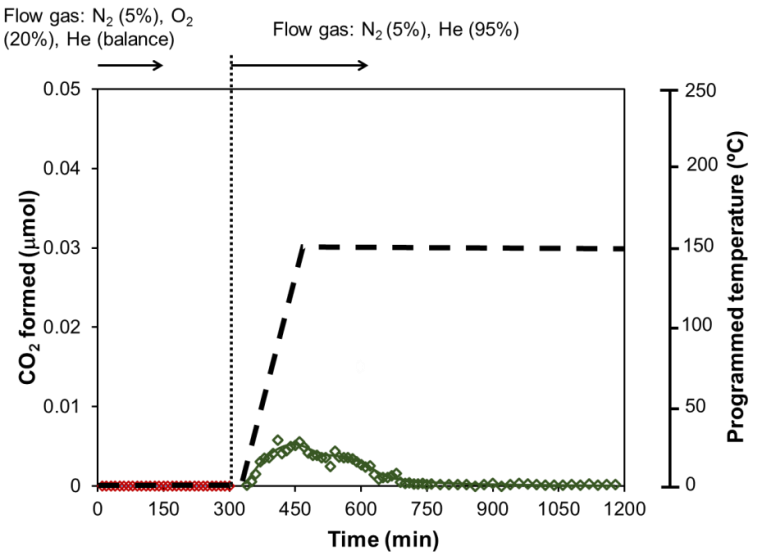

Figure 2.6. Two-step treatment of Pt/SBA-15 consisting of a mixed gas flow (O_2: 20%, N_2: 5%, He: balance) at 0 °C for 300 min, followed by heat treatment at 150 °C (ramp rate, 1 °C min^{-1}) under a He/N_2 (95%/5%) flow (10 mL min^{-1}). Green diamonds are denoted as the amounts of CO_2 formed. Reaction conditions: catalyst Pt/SBA-15 0.40 g (Pt 1.8 wt%), O_2 20%, N_2 5%, He balance, SV 1500 mL h^{-1} g^{-1}.

Instead of an inert gas flow, the oxidation of the carbon species was conducted by heat treatment of the spent catalyst in the presence of O_2 (O_2 : He : N_2 = 20% : 75% : 5%), which resulted in 6.3 μmol of CO_2 formed (Figure 2.7). This value is almost the same as that estimated from the hatched area of Figure 2.5 (6.5 μmol). There are two intense and

distinctive peaks at 40 ºC and 150 ºC during the combustion treatment (Figure 2.7), strongly suggesting the presence of two different types of intermediates and/or spectators on the surface of the spent catalyst.

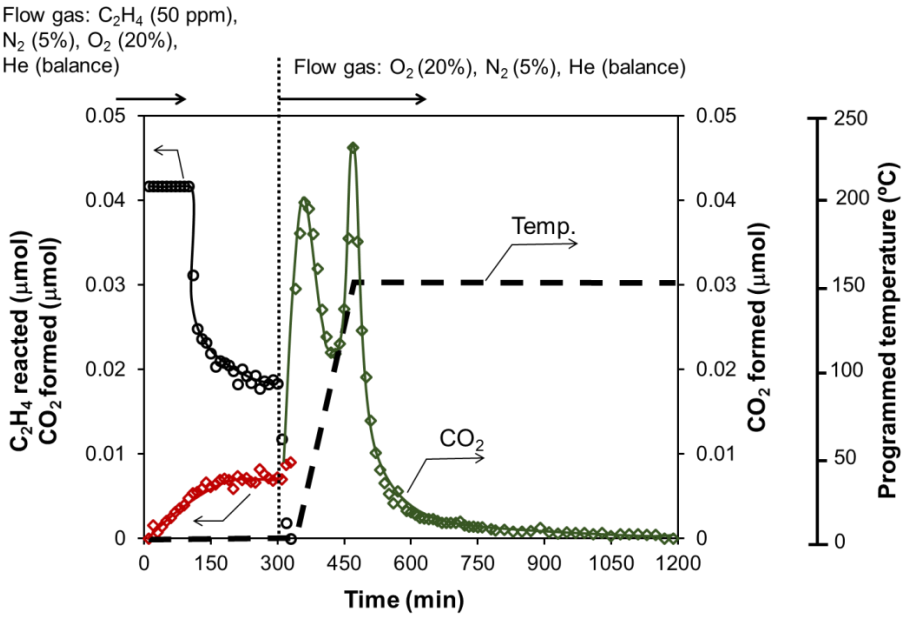

Figure 2.7. Moles of ethylene converted (black circles) and CO_2 formed (red diamonds) over Pt/SBA-15 at 0 °C for 300 min, followed by CO_2 formation (green diamonds) by heat treatment at 150 °C (ramp rate, 1 °C min^{-1}) under a O_2/He/N_2 flow (20%/75%/5%), (10 mL min^{-1}). Reaction conditions: catalyst Pt/SBA-15 0.40 g (Pt 1.8 wt%), C_2H_4 50 ppm, O_2 20%, N_2 5%, He balance, SV 1500 mL h^{-1} g^{-1}.

To evaluate the steady state activity, the reaction time was further prolonged together with an increase in the SV to 3000 mL h^{-1} g^{-1}. Figure 2.8 shows time courses for ethylene conversion and CO_2 yield over a period of 15 h. After the decrease in the initial activity, ethylene conversion and CO_2 yield gradually approached a steady state, and finally both remained constant at 8-9%. The TON for Pt/SBA-15 at 15 h was calculated to be 6, which indicates that Pt nanoparticles can function catalytically in this reaction. While the steady state activity of Pt/SBA-15 appears moderate under the conditions shown in Figures 2.2 and

2.8, a mesoporous silica-supported Pt catalyst was used for practical ethylene decomposition in refrigerators.[21] This can be explained by the low ethylene production rate under practical conditions. Ethylene produced in refrigerators is thus readily decomposed by Pt nanoparticles, so that vegetables and fruits can be stored without deterioration for long periods.

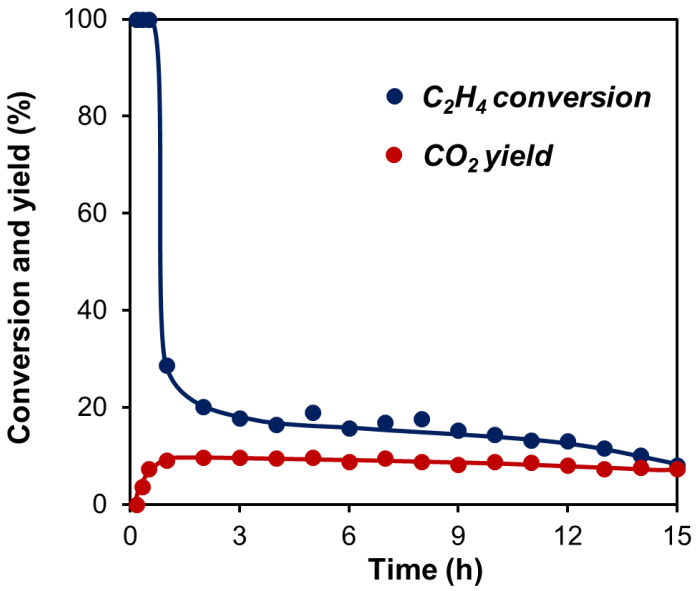

Figure 2.8. Ethylene oxidation over Pt/SBA-15 at 0 °C for 15 h. Reaction conditions: catalyst 0.20 g (Pt 1.8 wt%), C_2H_4 50 ppm, O_2 20%, N_2 5%, He balance, SV 3000 mL h^{-1} g^{-1}.

A long time reaction at 25 ºC was also conducted with Pt/SBA15 (Figure 2.9). No apparent decrease in initial activity was observed even after 25 h, and Pt/SBA15 keeps high ethylene conversion (>99%) and CO_2 yield (ca. 80%). This is due to a high reaction temperature that enhances the desorption of physisorbed H_2O and also the decomposition of intermediates. Ethylene conversion is not equal to CO_2 yield in this system, which indicates that this reaction does not yet reach a steady state at 27 h. The TON based on ethylene conversion and number of Pt surface atoms was calculated to be 5 at 27 h.

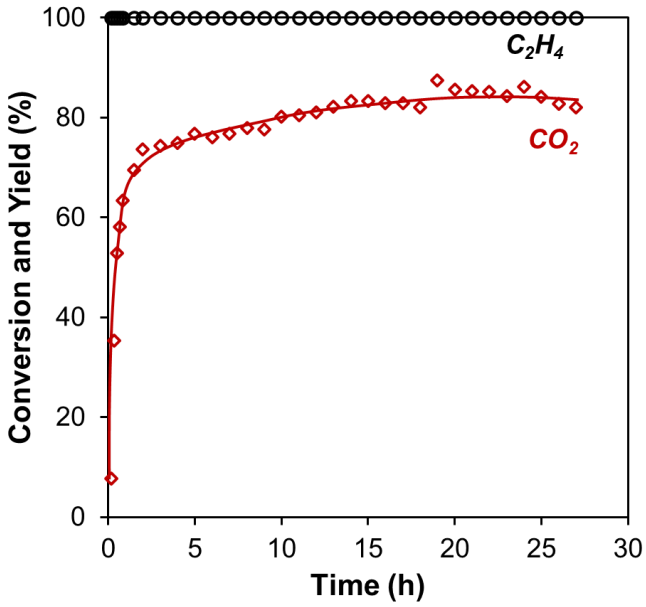

Figure 2.9. Time courses for ethylene conversion (black circles) and CO_2 yield (red diamonds) over Pt/SBA-15 at 25 °C. Reaction conditions: Pt/SBA-15 0.40 g (Pt 1.8 wt%), C_2H_4 50 ppm, O_2 20%, N_2 5 %, He balance, SV 1500 mL h^{-1} g^{-1}.

Water formed by the complete oxidation of ethylene is also expected to have a negative effect on the supported Pt catalyst because water molecules are preferably stabilized on both silica and Pt surfaces at low temperature. Therefore, heat treatment of the spent catalyst after the first run involved the removal of physisorbed water from the catalyst surfaces (Figure 2.3). Ethylene oxidation over Pt/SBA-15 was next examined in the presence of water vapor to clarify the effect of physisorbed water on the catalytic activity. Figure 2.10 shows time courses for the ethylene conversion and CO_2 yield over Pt/SBA-15. The reaction was performed at 28 °C with a relatively large SV of 9000 mL h^{-1} g^{-1} to prevent the formation of liquid water in the reactor and to maintain steady ethylene conversion at *ca*. 40-50%. Both the conversion and yield decreased gradually with time over a period of 15 h and became constant at 37% and 29%, respectively. When water vapor (0.86%) was supplied to the reactant gas mixture at 16 h, the ethylene conversion and CO_2 yield decreased drastically and

became less than 5% after 4 h. While the catalytic activity of Pt/SBA-15 was gradually recovered after the supply of water vapor was stopped, deactivation was again observed with the repeated introduction of water vapor to the reactor. This deactivation-recovery phenomenon was controlled by the adsorbed water, which revealed that physisorption of water molecules on active Pt sites results in a decrease of the original activity.

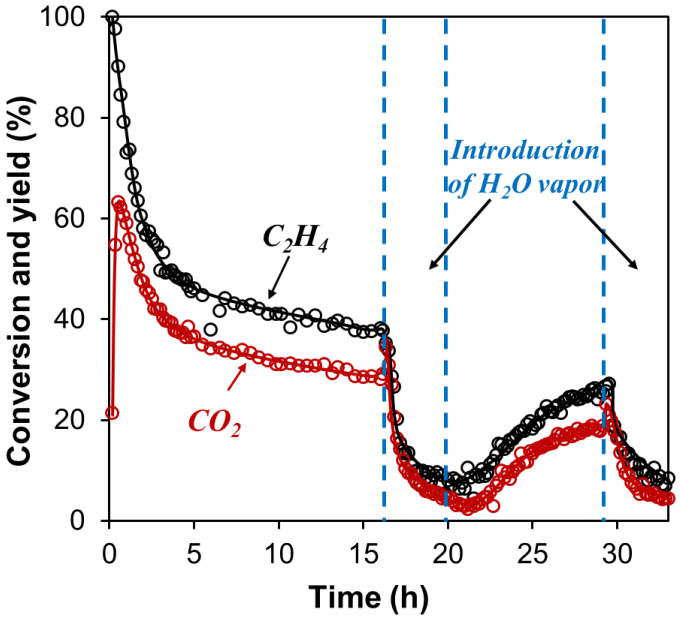

Figure 2.10. Effect of water vapor addition on the catalytic activity of Pt/SBA-15. Reaction conditions: catalyst 0.067 g (Pt 1.8 wt%), C_2H_4 50 ppm, O_2 20%, N_2 5%, water vapor 0.86%, He balance, SV 9000 mL h^{-1} g^{-1}, temperature 28 °C.

2.3.3 Ethylene Oxidation over Silica-Supported Pt Catalysts

Pt catalysts using aerosil silica supports were also tested by ethylene oxidation. Figure 2.11 shows time courses for the ethylene conversion and the CO_2 yield over these Pt catalysts. They exhibited similar reaction profiles to Pt/SBA-15, which indicates that these silicas are also useful as inorganic supports for Pt nanoparticles for ethylene oxidation. Table 2.1 compares the structural properties and catalytic activities of these catalysts at 240 min.

All of these catalysts comprised amorphous SiO_2 with highly dispersed Pt nanoparticles in sizes of 4-7 nm. While the activity of Pt/Q-10 was slightly inferior to the other three catalysts in terms of both the ethylene conversion and the CO_2 yield, the catalytic activities of Pt/A380 and Pt/A200 were comparable to that of Pt/SBA-15. These results indicate that the formation of highly dispersed Pt nanoparticles on a silica surface is essential for the development of a highly active Pt catalyst for oxidation of trace ethylene at 0 °C.

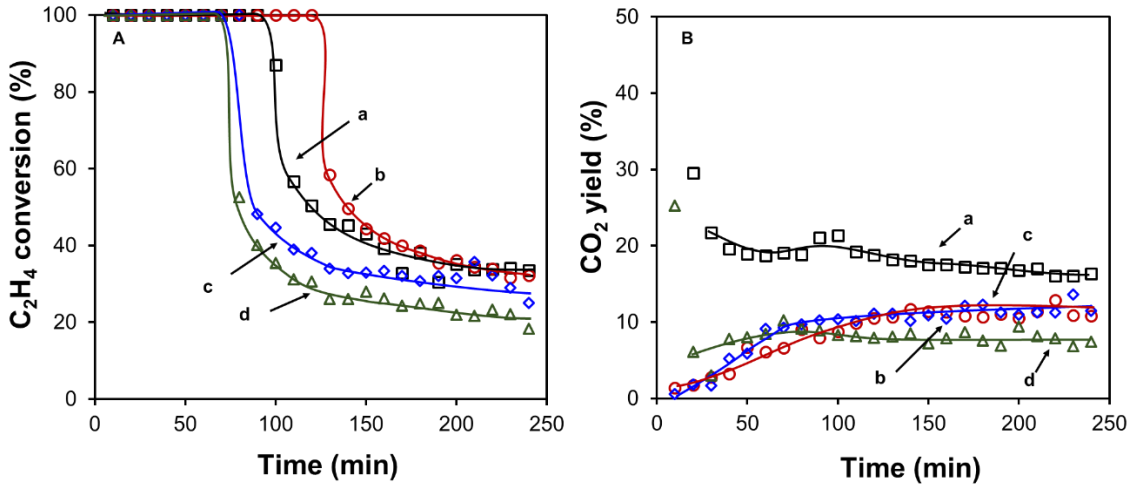

Figure 2.11. Time courses for ethylene conversion (A) and CO_2 yield (B) over silica-supported Pt catalysts at 0 °C: (a) Pt/SBA-15 (squares), (b) Pt/A380 (circles), (c) Pt/A200 (diamonds) and (d) Pt/Q-10 (triangles). Reaction conditions: catalyst 0.40 g (Pt 1.8 wt%), C_2H_4 50 ppm, O_2 20%, N_2 5%, He balance, SV 1500 mL h^{-1} g^{-1}.

2.4 Conclusions and Perspective

Silica-supported Pt catalysts effectively converted trace ethylene to CO_2 at 0 °C. Heat treatment of the spent catalyst in a He flow produced a large amount of CO_2 by thermal decomposition of oxygen-containing intermediates and regenerated the original activity for subsequent reaction. Thus, intermediates stabilized on the catalyst surface can be recovered

as CO_2 by a simple heat treatment. Water molecules evolved during the reaction block some of the surface active Pt sites and decrease the ethylene conversion and the CO_2 yield. Amorphous silicas such as Aerosil 380 and 200 were also useful as supports for highly dispersed Pt nanoparticles, and the resulting supported Pt catalysts exhibited high activities for ethylene oxidation.

References

(1) Saltveit, M. E. Effect of Ethylene on Quality of Fresh Fruits and Vegetables. *Postharvest Biol. Technol.* **1999**, *15*, 279–292.

(2) Wills, R. B. H.; McGlasson, W. B.; Graham, D.; Joyce, D. C. Postharvest: An Introduction to the Physiology and Handling of Fruit, Vegetables and Ornamentals. In Postharvest: An Introduction to the Physiology and Handling of Fruit, *Vegetables and ornamentals*. **2007**, 28–167.

(3) Illeperuma, C. K.; Jayasuriya, P. Prolonged Storage of "Karuthacolomban" Mango by Modified Atmosphere Packaging at Low Temperature. *J. Hortic. Sci. Biotechnol*. **2002**, *77*, 153–157.

(4) Salvador, A.; Abad, I.; Arnal, Mart´ inez-Javega, J. M. Effect of Ozone on Postharvest Quality of Persimmon. *J. Food Sci*. **2006**, *71*, S443–S446.

(5) Ma, X.; Ouyang, F. Adsorption Properties of Biomass-Based Activated Carbon Prepared with Spent Coffee Grounds and Pomelo Skin by Phosphoric Acid Activation. *Appl. Surf. Sci.* **2013**, *268*, 566–570.

(6) Triebe, R. W.; Tezel, F. H.; Khulbe, K. C. Adsorption of Methane, Ethane and Ethylene on Molecular Sieve Zeolites. *Gas Sep. Purif.* **1996**, *10*, 81–84.

(7) Kim, S. I.; Watabe, Y.; Aida, T.; Niiyama, H. Complete Oxidation of Ethylene by Co-Modified Mordenites under Microwave Irradiation. *J. Chem. Eng. Japan* **2005**, *38*, 828–834.

(8) Ahn, H. G.; Choi, B. M.; Lee, D. J. Complete Oxidation of Ethylene over Supported Gold Nanoparticle Catalysts. *J Nanosci Nanotechnol*. **2006**, *6*, 3599–3603.

(9) Li, J.; Ma, C.; Xu, X.; Yu, J.; Hao, Z.; Qiao, S. Efficient Elimination of Trace Ethylene over Nano-Gold Catalyst under Ambient Conditions. *Environ. Sci. Technol*. **2008**, *42*, 8947–8951.

(10) Ma, C. Y.; Mu, Z.; Li, J. J.; Jin, Y. G.; Cheng, J.; Lu, G. Q.; Hao, Z. P.; Qiao, S. Z. Mesoporous CO_3O_4 and Au/Co_3O_4 Catalysts for Low-Temperature Oxidation of Trace Ethylene. *J. Am. Chem. Soc*. **2010**, *132*, 2608–2613.

(11) Xue, W. J.; Wang, Y. F.; Li, P.; Liu, Z. T.; Hao, Z. P.; Ma, C. Y. Morphology Effects of CO_3O_4 on the Catalytic Activity of Au/CO_3O_4 Catalysts for Complete Oxidation of Trace Ethylene. *Catal. Commun.* **2011**, *12*, 1265–1268.

(12) Njagi, E. C.; Genuino, H. C.; King'Ondu, C. K.; Dharmarathna, S.; Suib, S. L. Catalytic Oxidation of Ethylene at Low Temperatures Using Porous Copper Manganese Oxides. *Appl. Catal. A Gen*. **2012**, *421–422*, 154–160.

(13) Li, W.; Zhang, Z.; Wang, J.; Qiao, W.; Long, D.; Ling, L. Low Temperature Catalytic Combustion of Ethylene over Cobalt Oxide Supported Mesoporous Carbon Spheres. *Chem. Eng. J.* **2016**, *293*, 243–251.

(14) Wang, M.; Zhang, L.; Huang, W.; Zhou, Y.; Zhao, H.; Lv, J.; Tian, J.; Kan, X.; Shi, J. Pt/MnO_2 Nanosheets: Facile Synthesis and Highly Efficient Catalyst for Ethylene Oxidation at Low Temperature. *RSC Adv.* **2017**, *7*, 14809–14815.

(15) Yang, H.; Ma, C.; Zhang, X.; Li, Y.; Cheng, J.; Hao, Z. Understanding the Active Sites of Ag/Zeolites and Deactivation Mechanism of Ethylene Catalytic Oxidation at Room-Temperature. *ACS Catal*. **2018**, *8*, 1248–1258.

(16) Fu, X.; Clark, L. A.; Zeltner, W. A.; Anderson, M. A. Effects of Reaction Temperature and Water Vapor Content on the Heterogeneous Photocatalytic Oxidation of Ethylene. J. *Photochem. Photobiol. A Chem*. **1996**, *97*, 181–186.

(17) Park, D.-R.; Zhang, J.; Ikeue, K.; Yamashita, H.; Anpo, M. Photocatalytic Oxidation of Ethylene to CO_2 and H_2O on Ultrafine Powdered TiO_2 Photocatalysts in the Presence of O_2 and H_2O. *J. Catal*. **1999**, *185*, 114–119.

(18) Pan, X.; Chen, X.; Yi, Z. Defective, Porous TiO_2 Nanosheets with Pt Decoration as an Efficient Photocatalyst for Ethylene Oxidation Synthesized by a C_3N_4 Templating Method. *ACS Appl. Mater. Interfaces* **2016**, *8*, 10104–10108.

(19) Huang, Y.; Zhang, Y.; Chen, X.; Wu, D.; Yi, Z.; Cao, R. Bimetallic Alloy Nanocrystals Encapsulated in ZIF-8 for Synergistic Catalysis of Ethylene Oxidative Degradation. *Chem. Commun.* **2014**, *50*, 10115–10117.

(20) Jiang, C.; Hara, K.; Fukuoka, A. Low-Temperature Oxidation of Ethylene over Platinum Nanoparticles Supported on Mesoporous Silica. *Angew. Chem. Int. Ed*. **2013**, *52*, 6265–6268.

(21) Https://www.hitachiconsumer.com/madeinjapanmicrosite2/refrigerator-features-02.html#1_0.

(22) Zhao, D.; Feng, J.; Huo, Q.; Melosh, N.; Fredrickson, G. H.; Chmelka, B. F.; Stucky, G. D. Tri Block Copolymer Synthesis of Mesoporous Silica with Periodic 50 to 300 Angstrom Pores. *Science* **1998**, *279*, 548–552

(23) Zhao, D.; Huo, Q.; Feng, J.; Chmelka, B. F.; Stucky, G. D. Nonionic Triblock and Star Diblock Copolymer and Oligomeric Sufactant Syntheses of Highly Ordered, Hydrothermally Stable, Mesoporous Silica Structures. *J. Am. Chem. Soc.* **1998**, *120*, 6024–6036.

(24) Khodakov, A. Y.; Zholobenko, V. L.; Impéror-Clerc, M.; Durand, D. Characterization of the Initial Stages of SBA-15 Synthesis by in Situ Time-Resolved Small-Angle X-Ray Scattering. *J. Phys. Chem. B* **2005**, *109*, 22780–22790.

(25) Brunauer, S.; Deming, L. S.; Deming, W. E.; Teller, E. On a Theory of the van Der Waals Adsorption of Gases. *J. Am. Chem. Soc*. **1940**, *62*, 1723–1732.

(26) Thommes, M.; Kaneko, K.; Neimark, A. V.; Olivier, J. P.; Rodriguez-Reinoso, F.; Rouquerol, J.; Sing, K. S. W. Physisorption of Gases, with Special Reference to the Evaluation of Surface Area and Pore Size Distribution (IUPAC Technical Report). *Pure Appl. Chem.* **2015**.

(27) Kruk, M.; Jaroniec, M.; Ko, C. H.; Ryoo, R. Characterization of the Porous Structure of SBA-15. *Chem. Mater*. **2000**, *12*, 1961–1968.

(28) Bhambhani, M. R.; Cutting, P. A.; Sing, K. S. W.; Turk, D. H. Analysis of Nitrogen Adsorption Isotherms on Porous and Nonporous Silicas by the BET and [Alpha]s Methods. *J. Colloid Interface Sci*. **1972**, *38*, 109–117.

(29) Tang, W.; Wu, X.; Chen, Y. Catalytic Removal of Gaseous Benzene over Pt / SBA-15 Catalyst : The Effect of the Preparation Method. React. *Kinet. Mech. Catal*. **2015**, *114*, 711–723.

Chapter 3: Low Temperature Ethylene Oxidation over Pt/SBA-15: Study of Effect of Hydrophobicity of Support Material

3.1 Introduction

Ethylene formed in the vegetable compartment of refrigerators promotes excessive ripening of agricultural products including fresh vegetables, fruits, and flowers, which make them difficult for a long term storage and transportation. Current cold chain system used for these fresh products requests a striking technique for the sustainable ethylene removal at low temperatures. While various strategies such as the oxidation with stoichiometric and hashed oxidant ($KMnO_4$),[1] physical adsorption with activated carbon,[2] and aerobic oxidation with some heterogeneous catalysts[3–8] have already been proposed for this purpose, most of them did not fulfill fundamental requirements in terms of complete removal of trace ethylene and long term utility at low temperature ranges. Photocatalytic decomposition of trace ethylene is one of successful examples; however, this system requires light irradiation to activate a heterogeneous photocatalyst such as WO_3 for the oxidation of ethylene to acetaldehyde.[9] Aerobic oxidation with the supported metal catalysts can function for ethylene oxidation without light irradiation. Recently, some heterogeneous catalysts such as Ag/ZSM-5 and Au/Co_3O_4 were reported to be effective for the oxidation of low concentration ethylene; however, in these cases their activities at low temperatures (0-5 ºC) have not been fully studied so far.[10–14]

Supported Pt catalysts are widely recognized as a series of highly active and stable catalysts for a variety of redox reactions and used as heterogeneous catalysts in academia and in industry. Recently mesoporous silica supported Pt catalyst was commercialized in 2015 in Japan as an oxidation catalyst for the removal of trace ethylene in the refrigerators. Mesoporous silica-supported Pt catalyst can decompose ethylene to CO_2 and H_2O at 0 ºC without loss of its original activity for a long time once the reaction reaches steady state (Chapter 2). Our group has systematically studied the oxidation of trace ethylene at 0 ºC and recently found that water formed during complete ethylene oxidation affects largely the activity of the supported Pt catalyst.[15] Our group also revealed that water gave a negative impact on the activity of the Pt catalyst: after reaching the steady state, the introduction of water vapor to the catalyst leads to the steep decrease in ethylene conversion and CO_2 yield whereas the activity is gradually recovered under the dry conditions. This phenomenon exemplified that steady-state activity depends on the amount of physisorbed water on catalyst surface.

In this chapter the author attempted precise control of hydrophobic property of mesoporous silica support to prevent water poisoning toward active Pt site of the catalyst. There are several strategies for the modification of silica surface with organosilane compounds to control hydrophobic-hydrophilic property.[16,17] However, most of organic functional groups show low thermal stability toward heat treatment, and in the present case thermal treatment in H_2 causes thermal decomposition of these organic groups. Here the author simply calcined mesoporous and aerosol silicas at various temperatures to control the amount of hydrophilic silanol, because change in silanol density of silica surface directly affects the amount of physisorbed water on Pt surface.

3.2 Experimental

3.2.1 Chemicals

Amorphous silica, Aerosil-380 (A80), Evonic industry and mesoporous SBA-15 were used as supports for Pt nanoparticle. Tetraethoxysilane (TEOS, 99.9%) was purchased from Kojundo Chemical Laboratory. Diamminedinitroplatinum(II) ($Pt(NH_3)_2(NO_2)_2$) solution was obtained from Tanaka Kikinzoku Kogyo was used as a precursor for the formation of Pt nanoparticle on silica supports. Pluronic 123 (P123, $EO_{20}PO_{70}EO_{20}$, EO = ethylene oxide moiety, PO = propylene oxide moiety, average molecular weight = 5800) was received from Sigma Aldrich. Concentrated hydrochloric acid (HCl, 36-38 wt%) was purchased from Wako Chemicals. All the chemicals were used without any purification.

3.2.2 Preparation of Mesoporous Silica SBA-15

Mesoporous silica SBA-l5, was synthesized in the similar way as explained in Section 2.2. In case of this study, the SBA-15 support was further calcined at 700, 800, and 900 °C for 16 h to control hydrophobicity of its surface. The calcined SBA-15 is denoted as SBA-15(X) where X means calcination temperature. Aerosil-380 was also calcined under the same conditions and used as a reference material for comparison.

3.2.3 Incorporation of Pt in SBA-15 and Aerosil Silica

A support material (1 g) was shaken in an aqueous solution (50 mL) containing $Pt(NH_3)_2(NO_2)_2$ (486mM, 0.1961 g) at 30 °C for 3 h. After evaporation of H_2O at 50 °C and subsequent drying under vacuum at 50 °C for 16 h, the sample was reduced under H_2 flow (30 mL min^{-1}) at 400 °C for 2 h, which gave a silica-supported Pt/SBA-15 as well as Pt/A380

catalysts (Pt loading 1.8 wt%). The other calcined catalysts were prepared using the same procedure.

3.2.4 Characterization

Powder X-ray diffraction (XRD) patterns were obtained with an X-Ray diffractometer (Ultima IV, Rigaku) using CuKα radiation (40 kV, 20 mA) over the 2θ range of 0.7-80°. Nitrogen adsorption-desorption isotherms were measured at 77 K with BELSORP-Mini (MicrotracBEL). Specific surface areas and pore diameters were calculated by the Brauner-Emmett-Teller (BET) equation and Non-localized density functional theory (NLDFT), respectively. H_2O adsorption isotherms were measured at 298 K with a surface characterization analyzer (3-Flex, Micrometrics instrument corp.). Prior to water and nitrogen adsorption, the samples were pretreated at 150 °C and 120 °C for for 1 h and 4 h respectively under vacuum to remove physisorbed water. The size of the Pt nanoparticles was measured with CO chemisorption on BELCAT II (Microtrac BEL). The samples were reduced at 400 °C for 1.5 h under H_2 flow (30 mL min^{-1}), followed by cooling to 50 °C under He flow (50 mL min^{-1}). CO chemisorption was completed at 50 °C with continuous flow of CO (10%) in He, and the size of Pt nanoparticles was then calculated on the basis of the amount of CO adsorbed and assumption of 1:1 ratio for Pt:CO. ^{29}Si solid state magic angle spinning (MAS) nuclear magnetic resonance (NMR) measurement was performed at room temperature using an ECA600 spectrometer (600 MHz, JEOL) at a Larmor frequency of 119 MHz. The spin rate used to obtain the spectra was 18 kHz. The frequency of the spectra is expressed with respect to an aqueous TSP (sodium trimethylsilyl propionate) standard solution.

3.2.5 Ethylene Oxidation with a Fixed-Bed Flow Reactor

The catalytic oxidation of ethylene was performed in a stainless steel tubular fixed-bed flow reactor (inner diameter of 4 mm) under atmospheric pressure (Figure 2.1). Each catalyst in the granular form (0.40 g, 355-500 μm) was loaded in the reaction tube and pretreated at 150 °C for 2 h under He flow (40 mL/min). A gas mixture consisting of C_2H_4 (50 ppm), O_2 (20 vol%), N_2 (5 vol %) and He (balance) was fed to a catalyst bed at 0 ºC using mass flow controllers under an ambient pressure at a space velocity (SV) of 1500 mL h^{-1} g^{-1}. The outlet gases collected at every 10 min were analyzed using an online gas chromatograph (Agilent 3000 A Micro GC) with thermal conductivity detector (TCD). The GC was equipped with two packed columns (Molecular sieves 5 A (10m) and Plot U (8m), GL Sciences) to detect C_2H_4 and CO_2 and the detection limit of C_2H_4 was 0.1 ppm. Water vapor was added to the gas mixture to examine the influence of water formed during the reaction on catalytic activity of Pt/SBA-15 (Figure 2.1). The reactant gas mixture containing water vapor (0.86%) was fed to a catalyst-bed (67 mg, Pt/SBA-15) at 28 °C with SV of 9000 mL g^{-1} h^{-1}, in order to prevent plugging the reactor with liquid water. Ethylene conversion (X_{C2H4}) and CO_2 yield (Y_{CO2}) were calculated by

$$X_{C2H4} = ([C_2H_4]_{inlet}-[C_2H_4]_{outlet}) \times 100/[C_2H_4]_{inlet}$$

$$Y_{CO2} = [CO_2]_{outlet} \times 100/2[C_2H_4]_{inlet}$$

where $[C_2H_4]_{inlet}$, $[C_2H_4]_{outlet}$, and $[CO_2]_{outlet}$ are denoted as initial C_2H_4 concentration, C_2H_4 concentration at the outlet of the reactor and CO_2 concentration at the outlet of the reactor, respectively.

3.3 Results and Discussion

3.3.1 Characterization of Supported Pt Catalysts

Hydrophobicity of silica supports SBA-15 and A380 was controlled by a simple calcination treatment in air for 16 h to decrease the amount of hydrophilic silanol group and in turn increase the hydrophobicity[18]. The small-angle X-ray diffraction (XRD) patterns of bare SBA-15 and Pt/SBA-15 in Figure 3.1(A) exhibited three characteristic diffractions assignable to (100), (110) and (200) of two-dimensional hexagonal (p6mm) structure of cylindrical mesopores.[19] A change in the intensity and position of the original diffraction peak was observed after the incorporation of Pt nanoparticles. This is probably due to hydrogen reduction at high temperature (400 °C), which induces a slight change in the periodicity and ordering of the mesopores. The presence of the three diffractions in Pt/SBA-15(700) and Pt/SBA-15(800) as shown in Figure 3.1(A) indicates that ordered mesoporous structure is preserved after calcination at 700 ºC and 800 ºC which is also shown in the TEM images in Figure 3.2. Figure 3.2(A) and 3.2(B) show the images of SBA-15 in the direction perpendicular to the pore axis and in the direction of pore axis respectively. The hexagonal symmetry of the pores, like a honeycomb is observed (Figure 3.2(B)) along with the long cylindrical rods in Figure 3.2(A).

The three diffractions in small-angle XRD are also visible for Pt/SBA-15(700) and Pt/SBA-15(800) confirming the retention of the hexagonal structure which is in concordance with the TEM image Figure 3.2(C). The high-angle shift of these diffractions compared to that of Pt/SBA-15 was also observed in these calcined samples, which is attributed to the decrease in periodic distance (lattice constant)[20] of mesoporous structure[21,22] by thermal shrinkage of siloxane network.

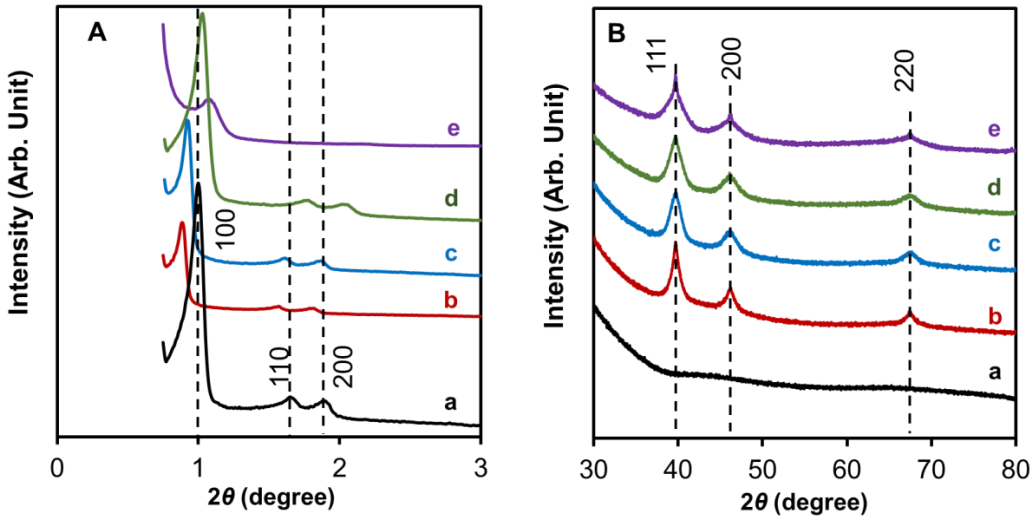

Figure 3.1. Low angle (A), high angle (B) XRD patterns of (a) SBA-15, (b) Pt/SBA-15, (c) Pt/SBA-15(700), (d) Pt/SBA-15(800) and (e) Pt/SBA-15(900).

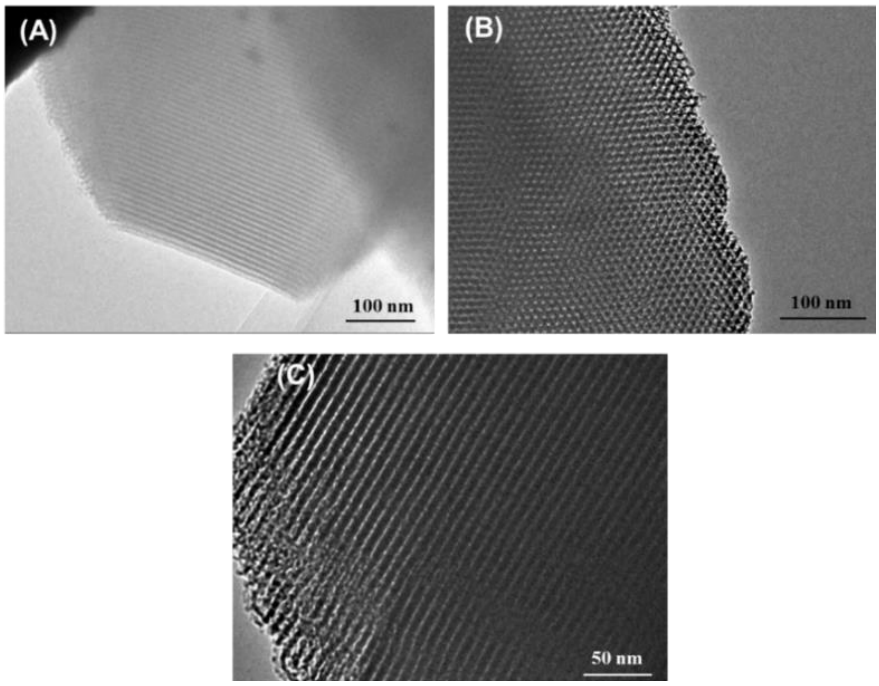

Figure 3.2. TEM images of SBA-15 in the direction perpendicular to the pore axis (A), SBA-15 in the direction of the pore axis (B) and SBA-15(800) (C).

In contrast to these samples, Pt/SBA-15(900) has no intense diffractions in this region, which suggests that degradation of original mesoporous structure takes place largely by the heat treatment.

This change was also confirmed in N_2 adsorption measurement. While Pt/SBA-15(900) has a type-IV isotherm with a H1-type hysteresis loop, the total volume of adsorbed N_2 is smaller than those of other three samples as shown in Figure 3.3(A). The pore diameter is also seen to decrease for the Pt supported mesoporous silica along with the increasing calcination temperature (Figure 3.3 (B)). The structural parameters and catalytic activities of the series of Pt/SBA-15 are summarized in Table 1. All XRD patterns in wide-angle region (Figure 3.1(B)) have three characteristic diffractions at 40º, 46º and 67º that are assignable to (111), (200) and (220) planes of metallic Pt with face-centered cubic lattice structure.[23]

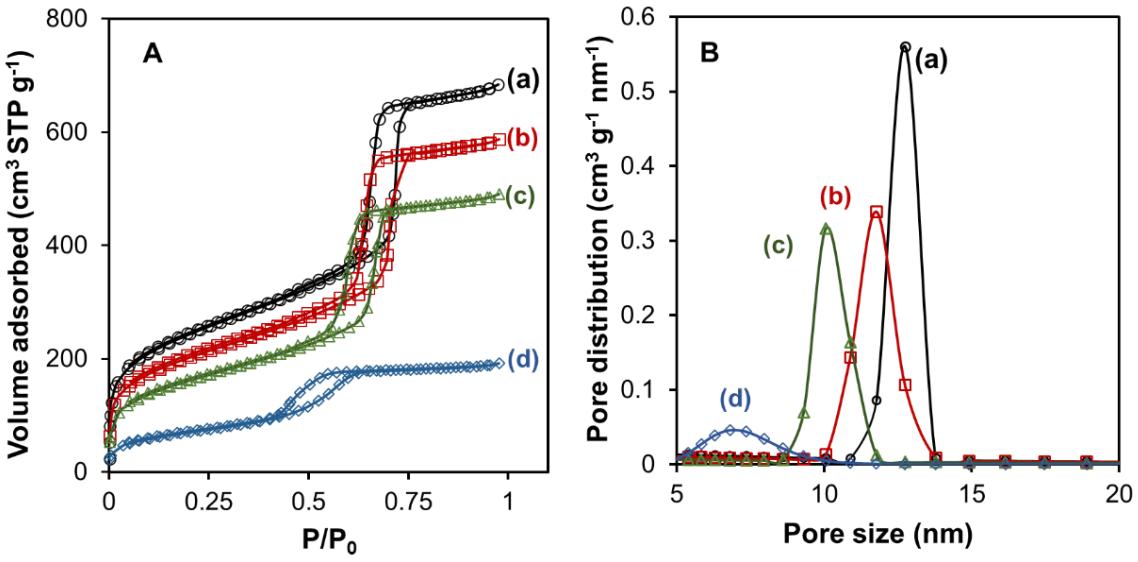

Figure 3.3. Nitrogen adsorption-desorption isotherm (A) and NLDFT plot (B) of (a) Pt/SBA-15, (b) Pt/SBA-15(700), (c) Pt/SBA-15(800) and (d) Pt/SBA-15(900).

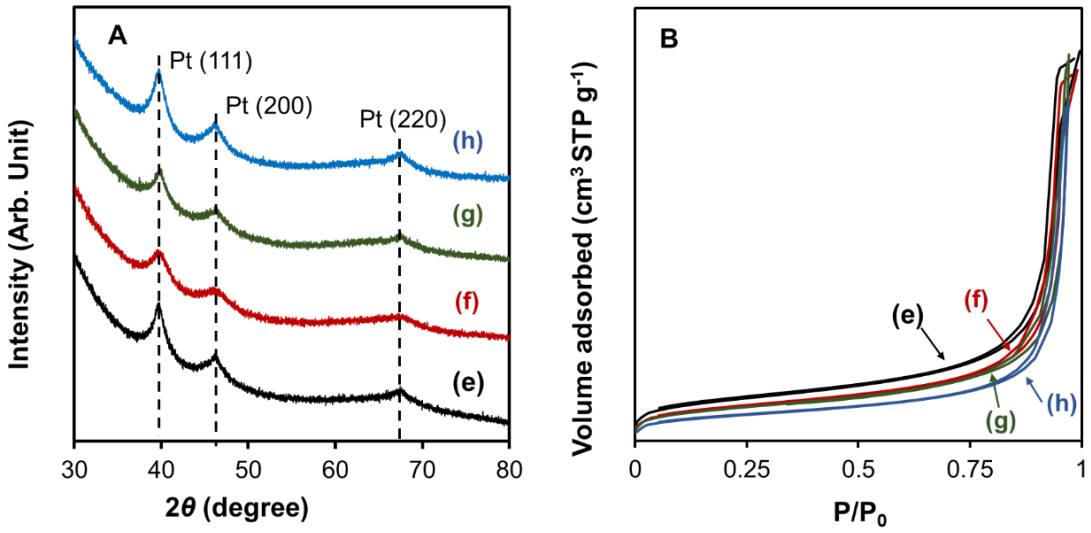

Figure 3.4. High angle XRD patterns (A) and N_2 adsorption-desorption isotherms (B) of Pt/A380 samples. (a) Pt/A380, (b) Pt/A380(700), (c) Pt/A380(800) and Pt/A380(900).

Pt/A380 calcined at different temperatures show characteristic diffraction peaks at (111), (110) and (200) assigned at 40°, 46° and 67° belonging to the face centered cubic platinum as shown in Figure 3.4(A). The N_2 adsorption isotherm of Pt/A380 calcined at varying temperature showed a type II isotherm of pronounced hysteresis loop with no significant change among each other.

Table 3.1 summarizes structural parameters of a series of Pt/SBA-15 and A380 samples. Increase in calcination temperature of pristine SBA-15 tends to decrease continuously in lattice constant of periodic mesoporous structure, BET surface area, mesopore volume, and average mesopore diameter. Although mesoporosity of original SBA-15 was preserved in Pt/SBA-15(700) and Pt/SBA-15(800), severe degradation by calcination at 900 ºC caused remarkable loss of BET surface area and mesopore volume. Therefore, Pt/SBA-15(900) can be regarded as an aerosol rather than meosporous silica, due to smaller BET surface area and mesopore volume than those of Pt/A380. In a series of A380, gradual but not marked

decrease in BET surface area was observed along with the increase in calcination temperature. This tendency is also attributed to thermal shrinkage of bulk silica particle. Average size of Pt nanoparticle was evaluated by CO chemisorption. There was little difference in average Pt size in each series of Pt/SBA-15 (6-9 nm) and Pt/A380 (4-5 nm). TEM analysis conducted for Pt/SBA-15 and Pt/SBA-15(800) revealed the average size of the Pt nanoparticles inside the mesopores to be 5.5 and 7.5 nm respectively (Figure 3.5).

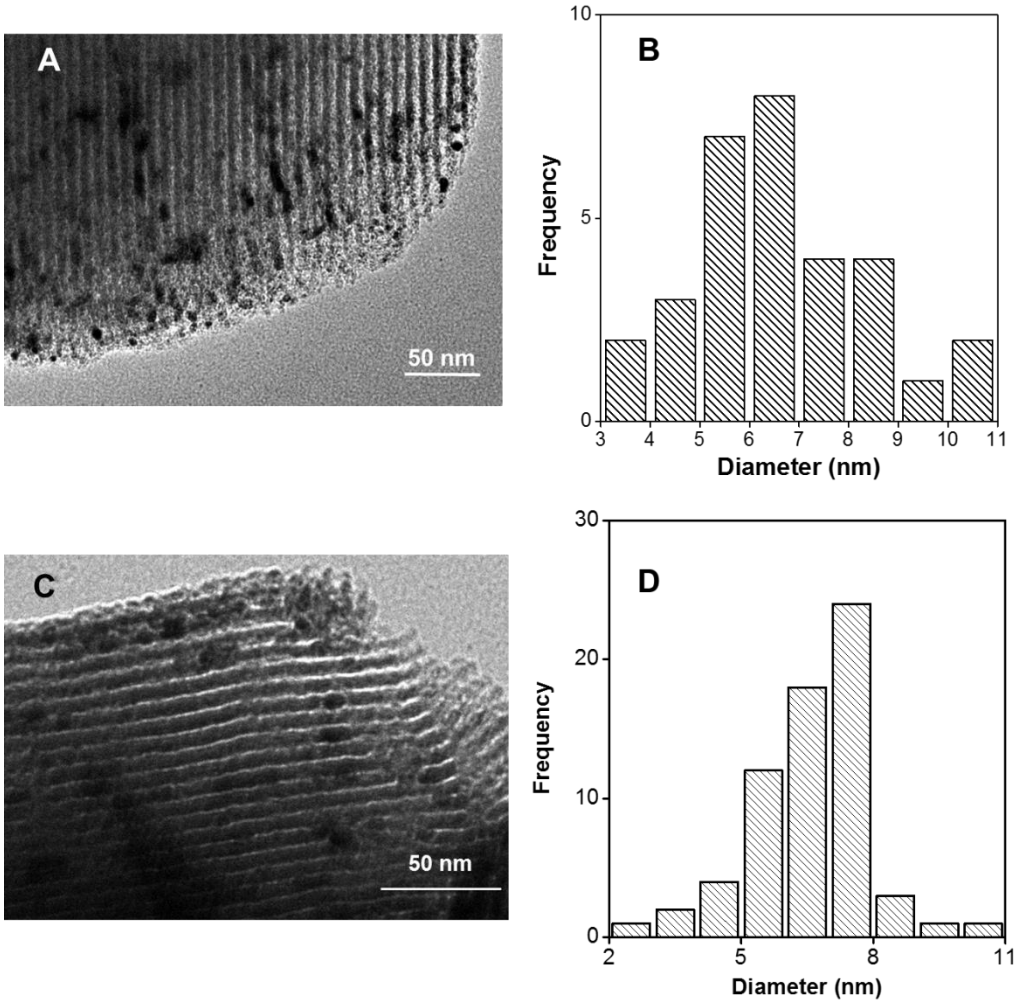

Figure 3.5. TEM image (A), (C) and particle size distribution (B), (D) of Pt/SBA-15 (A), (B) and Pt/SBA-15(800) (C), (D).

Table 3.1. Structural parameters and catalytic activity of Pt/SBA-15 and Pt/A380 samples.

	S_{BET}[a] / $m^2\ g^{-1}$	V_{meso}[b] / mL g^{-1}	D_{meso}[c] / nm	D_{Pt}[e] / nm	α[f] / nm	Catalytic activity in the steady state[g]	
						Conv.[h] (%)	Yield[i] (%)
SBA-15	889	1.10	13.8	-	-	-	-
Pt/SBA-15	867	1.0	12.7	6.9	11.4	30	16
Pt/SBA-15(700)	723	0.89	11.7	5.9	11.2	39	18
Pt/SBA-15(800)	572	0.76	10.1	9.2	10.0	45	28
Pt/SBA-15(900)	252	0.30	6.90	7.3	9.4	31	15
A380	377	0.40	N.D.[d]	-	-	-	-
Pt/A380	392	0.39	N.D.[d]	4.3	-	30	11
Pt/A380(700)	325	0.32	N.D.[d]	4.8	-	35	16
Pt/A380(800)	313	0.32	N.D.[d]	4.9	-	35	17
Pt/A380(900)	240	0.26	N.D.[d]	4.8	-	37	18

[a]BET surface area, [b]mesopore volume estimated by the BJH equation, [c]Average diameter estimated by NLDFT, [d]Not determined, [e]Average size of Pt nanoparticle estimate by CO pulse method, [f]lattice constant of periodic mesoporous structure estimated by $\alpha = (2 \times d(100))/\sqrt{3}$, [g]Reaction conditions: Pt loading, 1.8 wt%; SV, 1500 mL h^{-1} g^{-1}; Catalyst weight, 0.40 g; Reaction time, 300 min; C_2H_4, 50 ppm; O_2, 20 vol%; N_2, 5 vol%; He, balance, [h]Ethylene conversion at 300 min, [i]CO_2 yield at 300 min

3.3.2 Control in Hydrophobicity of SBA-15 for Ethylene Oxidation

Hydrophobic nature of Pt/SBA-15 and Pt/A380 samples with various calcination temperatures was evaluated by H_2O adsorption measurement at 25 °C. Figure 3.6 shows H_2O adsorption isotherms of supported Pt catalysts listed in Table 3.1. Because of large difference in BET surface area among these catalysts, the amount of adsorbed H_2O in y-axis was normalized with their surface areas. All isotherms in Figures 3.6(A) and (B) are classified into type-III where they are based on weak adsorbent (H_2O)-adsorbate (silica) interactions[24,25]. There was no large difference in the amount of H_2O adsorbed in a whole P/P_0 range (Figure 3.6(B)), which means that surface property of A380 cannot be simply controlled by calcination treatment in this temperature range.

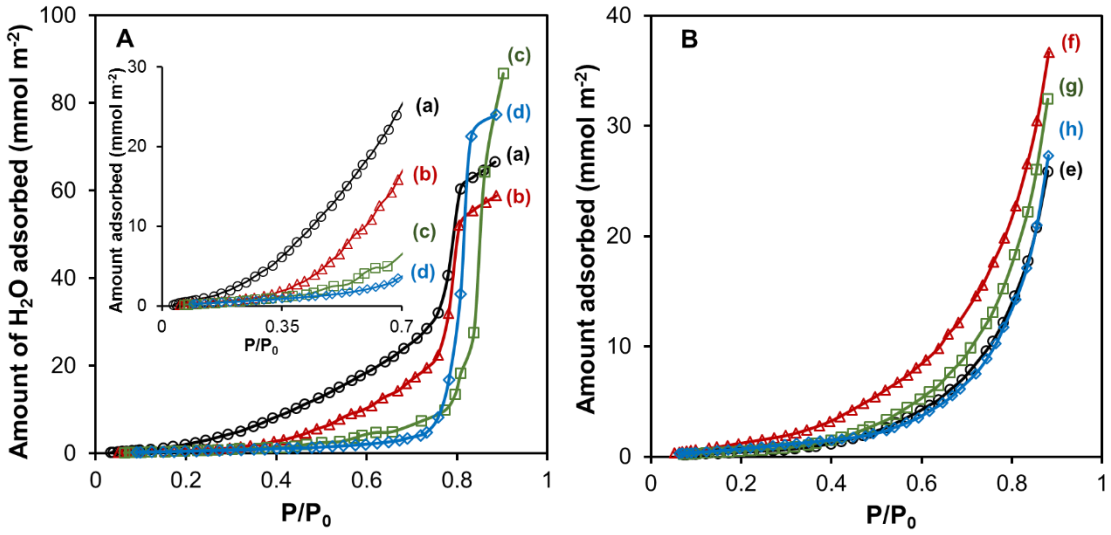

Figure 3.6. Water adsorption isotherms of Pt/SBA-15 (A) and Pt/A380 (B) samples calcined at different temperatures at 25 °C. (a) Pt/SBA-15, (b) Pt/SBA-15(700), (c) Pt/SBA-15(800), (d) Pt/SBA-15(900), (e) Pt/A380, (f) Pt/A380(700), (g) Pt/A380(800), (h) Pt/A380(900).

Due to similar hydrophilic-hydrophobic property, catalytic activities of three calcined samples Pt/A380(700), Pt/A380(800), and Pt/A380(900) were closely identical with that of Pt/A380. On the other hand, hydrophobicity of SBA-15 was greatly changed with the increase in calcination temperature (Figure 3.6(A)).

Change in hydrophobicity can be explained by two factors: one is the amount of adsorbed H_2O at P/P_0 = 0.40 (Figure 3.6(A) inset and Figure 3.7) and the uptake of adsorbed water at *ca.* P/P_0 = 0.7-0.8. Focusing on the former parameter, it is apparent that the amount of adsorbed H_2O decreases drastically with the increase in calcination temperature as shown in Figure 3.7. A sharp increase observed at relative partial pressure of 0.7-0.8 is due to the capillary condensation for all catalysts.

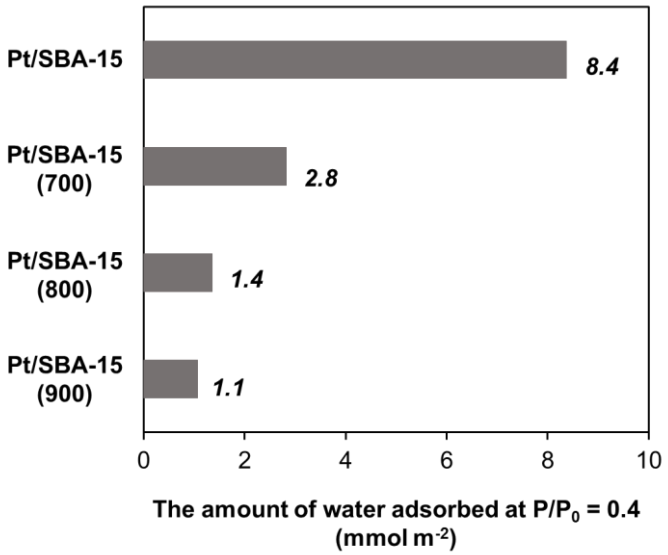

Figure 3.7. The amount of water adsorbed on Pt/SBA-15 samples calculated from corresponding H_2O adsorption isotherms at P/P_0 = 0.4.

The uptake of adsorbed H_2O due to capillary condensation was continuously shifted to large P/P_0 region with the increase in calcination temperature, which means that calcination

of SBA-15 at higher temperature leads to the formation of more hydrophobic mesopores. These two tendencies obtained from a series of Pt/SBA-15 catalysts clearly indicate that calcination treatment at high temperature creates hydrophobic silica surface that enhances desorption of physisorbed water.

3.3.3 Ethylene Oxidation over Pt/support at 0 °C

We conducted ethylene oxidation with Pt/SBA-15 and Pt/A380 calcined at varying temperatures as shown in Figure 3.8 and 3.9 respectively. 50 ppm of ethylene was introduced to the catalyst bed at 0 ºC along with N_2 (5 %), O_2 (20 %) and He (balance). The time for 100% conversion of ethylene was retained for all the Pt/SBA-15 calcined at different temperatures. At steady state, both the conversion of ethylene and yield of CO_2 were highest for Pt/SBA-15(800) whereas, the Pt/A380 (700, 800 and 900) showed no significant change in the conversion and yield. This shows high calcination temperature of mesoporous silica plays a role in increasing the catalytic activity. Owing to the high catalytic activity during steady state, ethylene oxidation of Pt/SBA-15(800) in the absence and presence of water vapor was carried out to elucidate the effect of hydrophobic property of calcined SBA-15 surface.

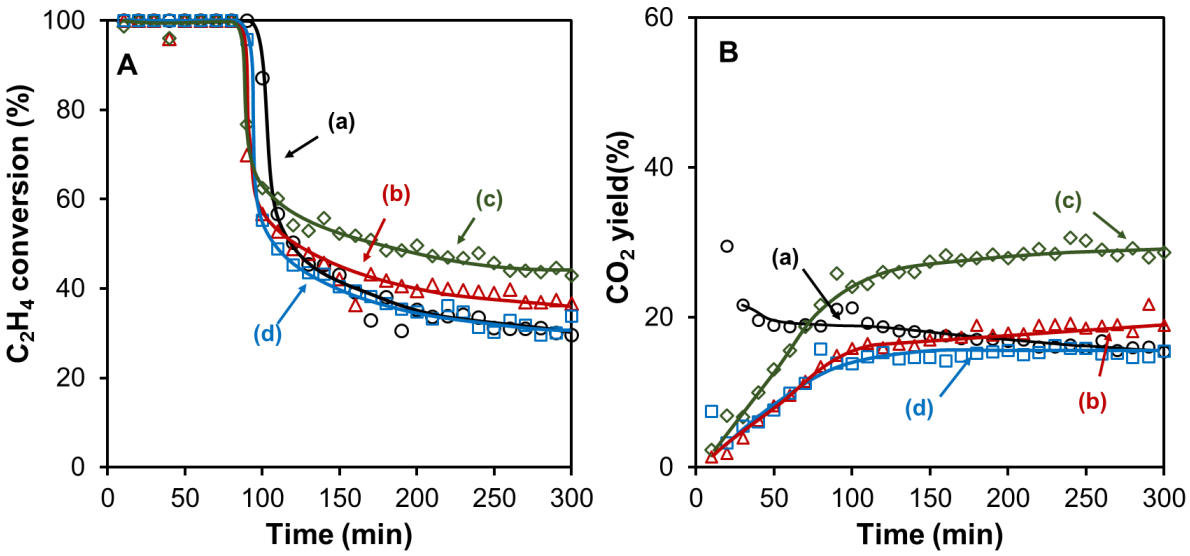

Figure 3.8. Time courses for ethylene conversion (A) and CO_2 yield (B) over Pt/SBA-15 samples calcined at different temperatures. Reaction conditions: Pt/SBA-15 0.40 g (Pt 1.8 wt%), C_2H_4 50 ppm, O_2 20%, N_2 5%, He balance, SV 1500 mL h^{-1} g^{-1}. (a) Pt/SBA-15, (b) Pt/SBA-15(700), (c) Pt/SBA-15(800), (d) Pt/SBA-15(900).

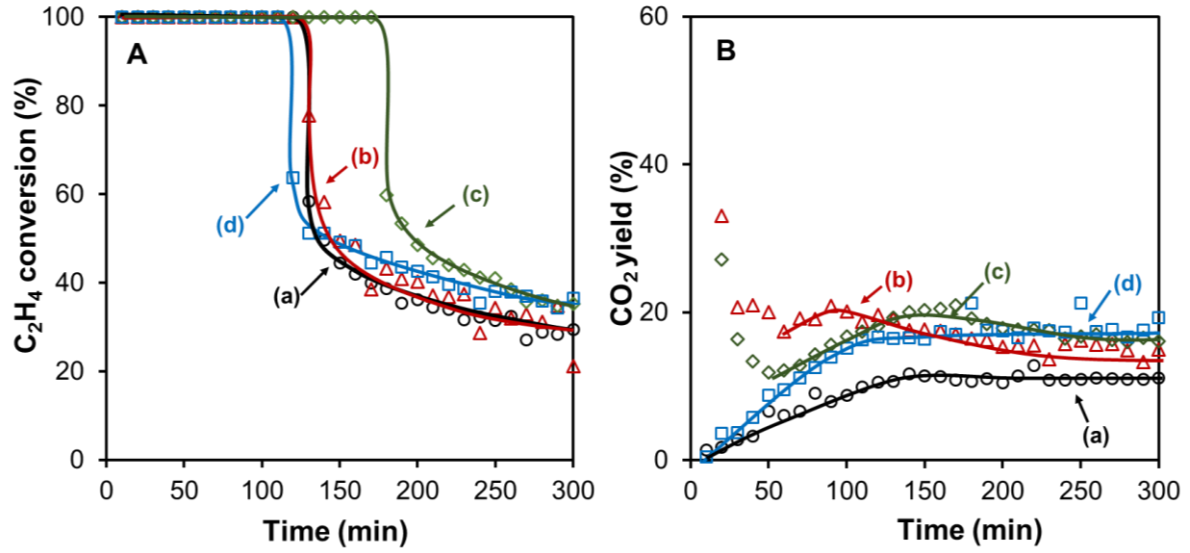

Figure 3.9. Time courses for ethylene conversion (A) and CO_2 yield (B) over Pt/A380 samples calcined at different temperatures. Reaction conditions: Pt/SBA-15 0.40 g (Pt 1.8 wt%), C_2H_4 50 ppm, O_2 20%, N_2 5%, He balance, SV 1500 mL h^{-1} g^{-1}. (a) Pt/A380, (b) Pt/A380(700), (c) Pt/A380(800), (d) Pt/A380(900).

3.3.4 Effect of H_2O Vapor on Catalytic Activity

Figure 3.10 shows time courses for ethylene conversion and CO_2 yield over Pt/SBA-15(800) at 28 °C. As observed for Pt/SBA-15, reversible deactivation-recovery phenomenon of steady-state activity was also obtained with Pt/SBA-15(800) depending upon the absence or presence of water vapor in the reaction vessel. Even though similar phenomenon happened in both catalysts, Pt/SBA-15(800) exhibited always higher catalytic activity than Pt/SBA-15 in terms of both conversion and yield. After the activity of these two catalysts became constant at 16 h, addition of water vapor (0.86%) in reactant gas mixture caused drastic decrease in their catalytic activities. Pt/SBA-15(800) is clearly superior to Pt/SBA-15 in the recovery of both conversion and yield more smoothly after stopping the supply of water vapor. This is direct evidence that hydrophobic silica surface of SBA-15 plays a decisive role for desorption of physisorbed water leading to efficient ethylene oxidation with Pt nanoparticle.

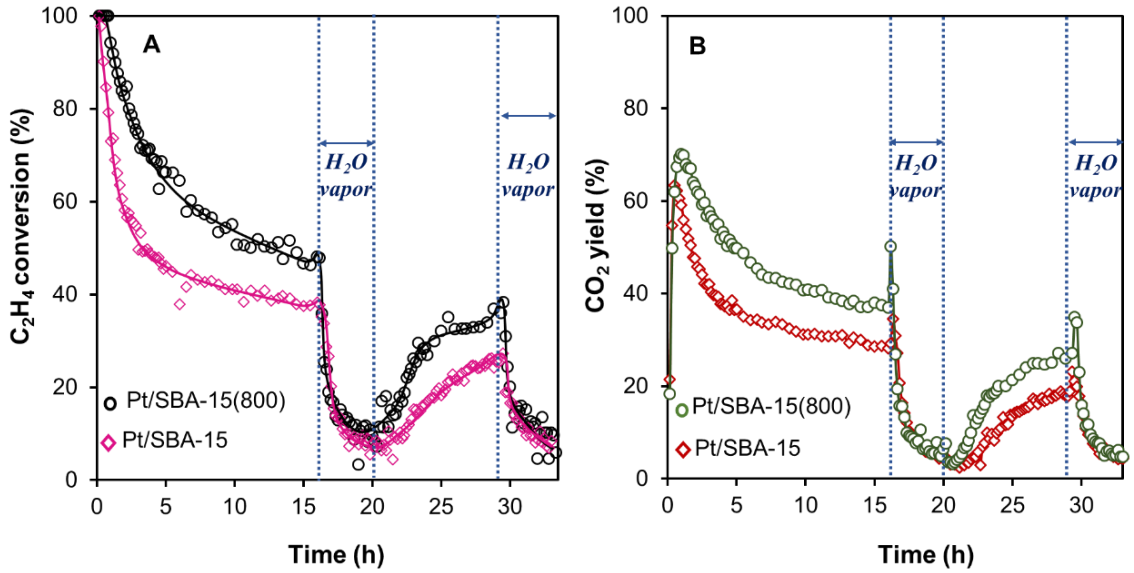

Figure 3.10. Effect of addition of water vapor on ethylene conversion (A) and CO_2 yield (B) of Pt/SBA-15 and Pt/SBA-15(800). Reaction conditions: Pt/SBA-15 0.067 g (Pt 1.8 wt%), C_2H_4 50 ppm, O_2 20%, N_2 5%, He balance, SV 9000 mL h^{-1} g^{-1}, water vapor 0.86%, reaction temperature 28 °C.

3.3.5 Study of ^{29}Si NMR Spectroscopy

Water adsorption provided direct information for water affinity to silica surface among SBA-15 and A380 samples before and after calcination. A comprehensive study on the relationship between water affinity to silica surface and condensation of silica network is required to further understand the difference in detail between SBA-15 and A380 as a silica support in ethylene oxidation. Condensation of silica network was quantitatively evaluated with the proportion of Q_4 species to the sum of all Q sites (Q_2+ Q_3+ Q_4) where Q_2 ($Si(OH)_2(OSi)_2$), Q_3 ($Si(OH)(OSi)_3$), and Q_4 ($Si(OSi)_4$) sites[26] were calculated from ^{29}Si MAS NMR spectra of the samples.

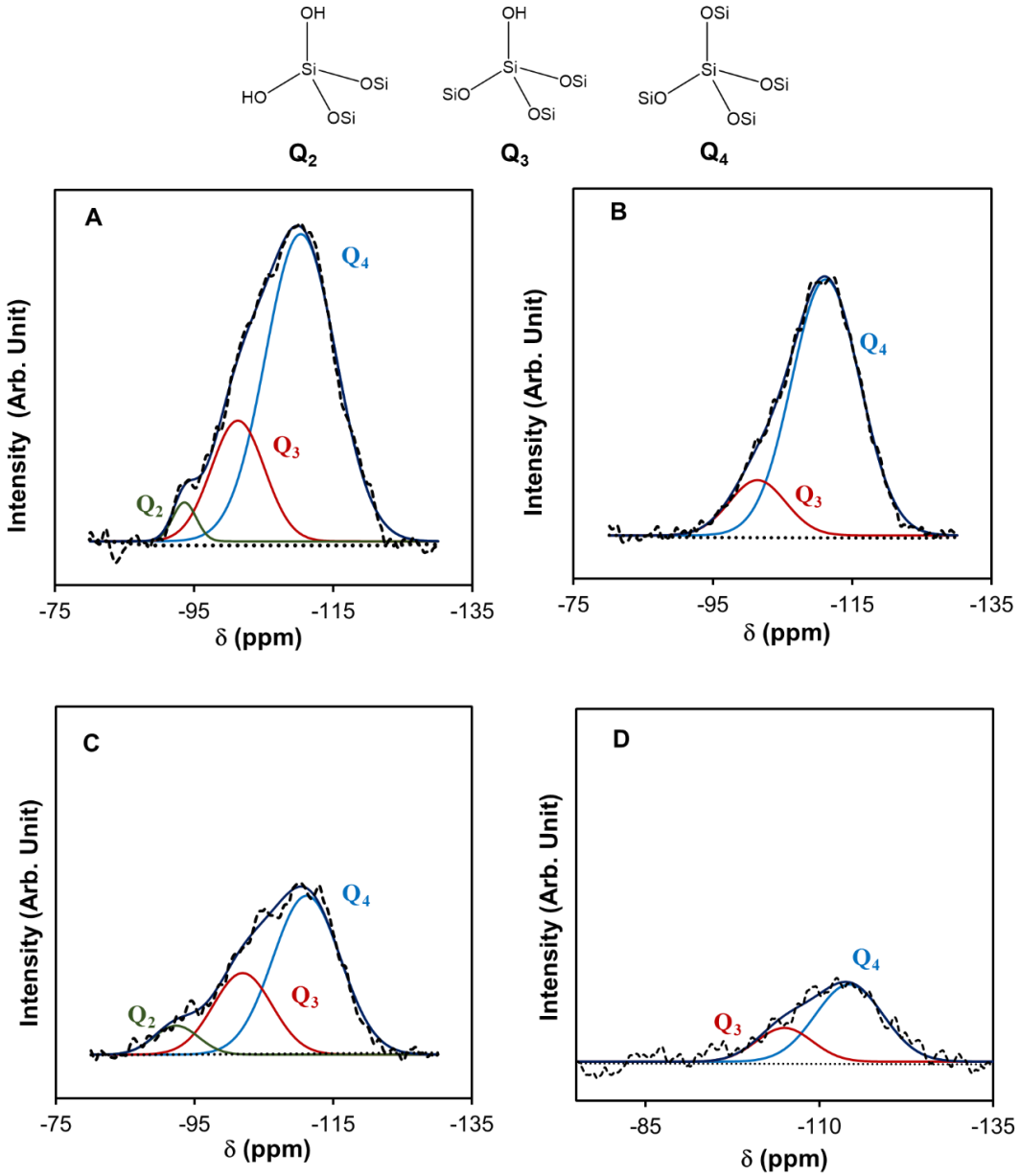

Figure 3.11. ^{29}Si MAS NMR spectra of Pt/SBA-15 (A), Pt/SBA-15(800) (B), Pt/A380 (C), and Pt/A380(800) (D). Q_2, Q_3, and Q_4 represent $Si(OH)_2(OSi)_2$, $Si(OH)(OSi)_3$ and $Si(OSi)_4$ respectively.

Table 3.2 summarizes catalytic activities and contents of Q sites for four representative samples (Pt/SBA-15, Pt/SBA-15(800), Pt/A380, and Pt/A380 (800)) and for spent and regenerated Pt/SBA-15(800). Three Q resonances can be identified in ^{29}Si MAS NMR spectra of the supported Pt catalysts by a curve fitting technique (Figures 3.11 and 3.12).

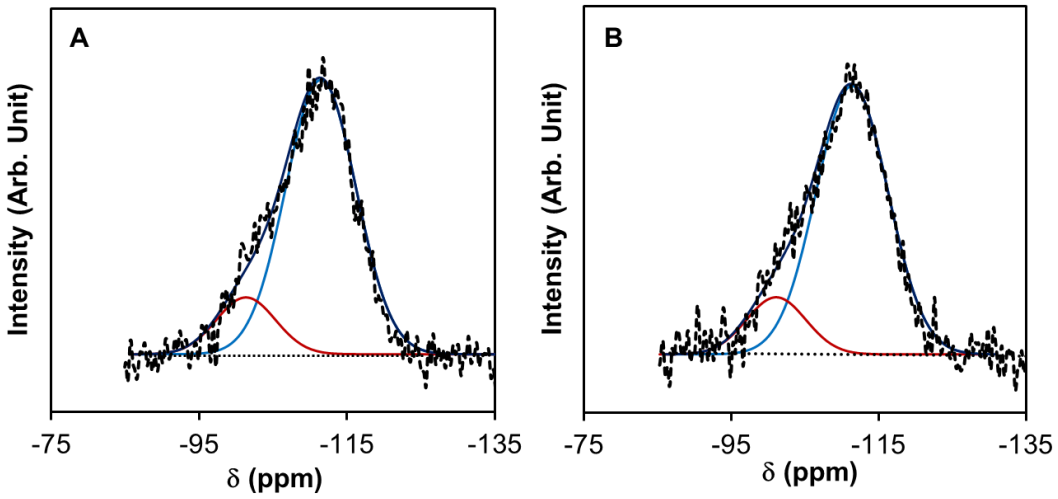

Figure 3.12. ^{29}Si MAS NMR spectra of Pt/SBA-15(800)-Spent (A) and Pt/SBA-15(800)-Regenerated (B).

Table 3.2. Surface areas, Q contents, and catalytic activities of Pt/SBA-15 and Pt/A380 samples

	S_{BET}[a] / m^2 g^{-1}	Q content[b] (%)			Catalytic activity[c]	
		Q_2	Q_3	Q_4	Conv.[d] (%)	Yield[e] (%)
Pt/SBA-15	867	3.2	22.2	74.7	30	16
Pt/SBA-15(800)	572	0.0	15.1	84.9	45	28
Pt/SBA-15(800)-Spent	-	0.0	14.8	85.2	-	-
Pt/SBA-15(800)-Regenerated	-	0.0	14.9	85.1	-	-
Pt/A380	392	7.7	28.5	63.8	30	11
Pt/A380(800)	313	0.0	26.5	73.5	35	17

[a]BET surface area, [b]mesopore Q contents of silica-supported Pt catalysts where Q_2, Q_3 and Q_4 represent $Si(OH)_2(OSi)_2$, $Si(OH)(OSi)_3$, $Si(OSi)_4$ respectively. [c]Reaction conditions: Pt/SBA-15 0.40 g (Pt 1.8 wt%), C_2H_4 50 ppm, O_2 20%, N_2 5%, He balance, SV 1500 mL h^{-1} g^{-1}. [d]Ethylene conversion at 300 min, [e]CO_2 yield at 300 min.

Q_4 site of both supports increased as a result of the decrease in Q_2 and Q_3 sites by thermal condensation at 800 °C (Scheme 3.1). High hydrophobicity of silica surface can be interpreted by the increase in Q content, because water molecules are preferably adsorbed on hydrophilic SiOH group. In the case of SBA-15, increase in both ethylene conversion and CO_2 yield is correlated with Q content, which is well consistent with the result of H_2O adsorption experiment as discussed above. Ethylene oxidation with water vapor (Figure 3.10(A)) indicated that hydrophobic environment of Pt/SBA-15(800) contribute dominantly to the increase in original activity of Pt/SBA-15. The spent and the regenerated Pt/SBA-15(800) have similar Q_2, Q_3, and Q_4 contents to fresh Pt/SBA-15(800) as shown in Figure 3.12 and Table 3.2. This confirms that in-situ formation of H_2O molecules during the reaction have no direct effect on the change in the density of hydroxyl group on the silica surface. In contrast, no large improvement was obtained for Pt/A380 samples whereas further condensation was also evidenced by the increase in Q_4 site.

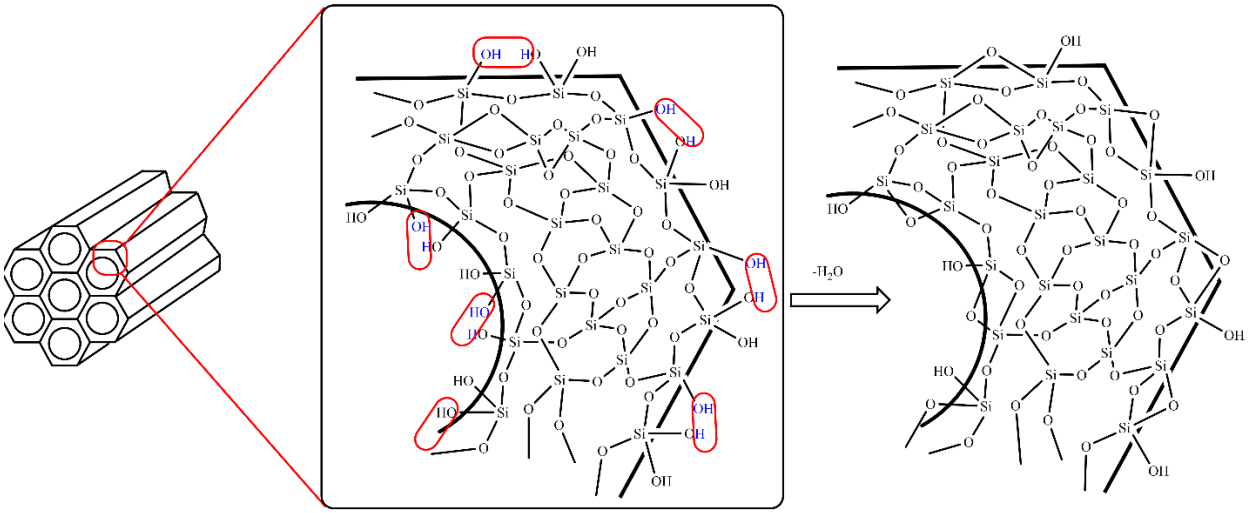

Scheme 3.1. Condensation of silanol groups of silica network of SBA-15 for the formation of siloxane groups.

Distinctive hydrophobicity of Pt/SBA-15(800) contributing to high activity for ethylene oxidation can be explained by surface area and mesoporous structure. Assuming that Q_3 sites are mainly distributed as a defect site on the surface, SiOH density of Pt/SBA-15(800) has to be much smaller than that of Pt/A380(800), due to large surface area derived from mesoporous structure and small Q_3 content (Table 3.2). Moreover, it can be reasonably speculated that most of Pt nanoparticles in average size of ca. 7.5 nm are immobilized inside mesopores (ca. 10 nm) and tightly surrounded three-dimensionally with hydrophobic silica wall, as compared to Pt/SBA-15 with hydrophilic silica wall, as shown in Schemes 3.2(A) and 3.2(B). In-situ generated water on the Pt particles is smoothly released from Pt surface and subsequently discharged to the outside of hydrophobic mesopore by such unique environment (Scheme 3.2(B)). Rapid desorption of water molecules from Pt surface then enhances overall ethylene oxidation, which affords large conversion and CO_2 yield. In contrast, Pt nanoparticles are simply dispersed on flat SiO_2 surface in the case of Pt/A380 (Pt/A380), and therefore no significant effect for water removal even if hydrophobicity of silica network slightly increases by calcination treatment (Scheme 3.2(B)). Based on these results, the combination of hydrophobic silica surface and mesoporous structure is highly beneficial for the development of a highly active Pt catalyst for this reaction.

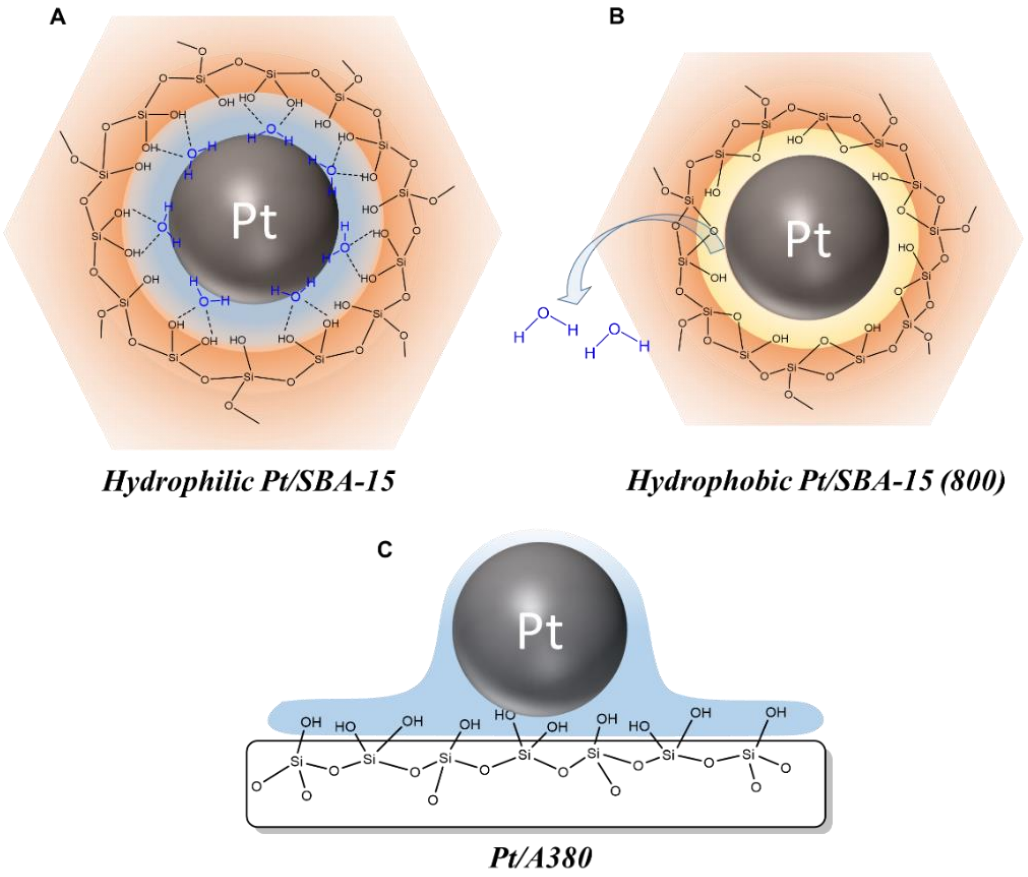

Scheme 3.2. Schematic structure of Pt/SBA-15 (A), Pt/SBA-15(800) (B) and Pt/A380(800) (C) during oxidation of trace ethylene at 0 ºC.

3.4 Conclusions

Supported Pt catalysts with hydrophobic SBA-15 supports calcined at 700 and 800 ºC showed higher ethylene conversion and CO_2 yield than original Pt/SBA-15 catalyst whereas calcination treatment was not effective for non-ordered SiO_2 support. This enhancement can be explained by hydrophobic mesopores: water molecules formed on Pt nanoparticles tightly incorporated into hydrophobic mesopores are released outside the mesopores, which prevents Pt sites from deactivation with water.

References

(1) Illeperuma, C. K.; Jayasuriya, P. Prolonged Storage of "Karuthacolomban" Mango by Modified Atmosphere Packaging at Low Temperature. *J. Hortic. Sci. Biotechnol*. **2002**, *77*, 153–157.

(2) Baumann, H. Adsorption of Ethylene and CO_2 by Activated Carbon Scrubbers. *Acta Hortic*. **1989**, *258*, 125–129.

(3) Kou, Y.; Sun, L.-B. Size Regulation of Platinum Nanoparticles by Using Confined Spaces for the Low-Temperature Oxidation of Ethylene. *Inorg. Chem*. **2018**, *57*, 1645–1650.

(4) Ahn, H. G.; Choi, B. M.; Lee, D. J. Complete Oxidation of Ethylene over Supported Gold Nanoparticle Catalysts. *J Nanosci Nanotechnol*. **2006**, *6*, 3599–3603.

(5) Isaifan, R. J.; Ntais, S.; Baranova, E. A. Particle Size Effect on Catalytic Activity of Carbon-Supported Pt Nanoparticles for Complete Ethylene Oxidation. *Appl. Catal. A Gen*. **2013**, *464–465*, 87–94.

(6) Li, W.; Zhang, Z.; Wang, J.; Qiao, W.; Long, D.; Ling, L. Low Temperature Catalytic Combustion of Ethylene over Cobalt Oxide Supported Mesoporous Carbon Spheres. *Chem. Eng. J.* **2016**, *293*, 243–251.

(7) Imanaka, N.; Masui, T.; Terada, A.; Imadzu, H. Complete Oxidation of Ethylene at Temperatures below 100 °C over a $Pt/Ce_{0.64}Zr_{0.16}Bi_{0.20}O_{1.90}$ /γ-Al_2O_3 Catalyst. *Chem. Lett.* 2**008**, *37*, 42–43.

(8) Rojluechai, S.; Chavadej, S.; Schwank, J. W.; Meeyoo, V. Catalytic Activity of Ethylene Oxidation over Au, Ag and Au-Ag Catalysts: Support Effect. *Catal. Commun*. **2007**, *8*, 57–64.

(9) Wicaksana, Y.; Liu, S.; Scott, J.; Amal, R. Tungsten Trioxide as a Visible Light Photocatalyst for Volatile Organic Carbon Removal. *Molecules* **2014**, *19*, 17747–17762.

(10) Yang, H.; Ma, C.; Zhang, X.; Li, Y.; Cheng, J.; Hao, Z. Understanding the Active Sites of Ag/Zeolites and Deactivation Mechanism of Ethylene Catalytic Oxidation at Room Temperature. *ACS Catal*. **2018**, *8*, 1248–1258.

(11) Yang, H.; Ma, C.; Li, Y.; Wang, J.; Zhang, X.; Wang, G. Synthesis, Characterization and Evaluations of the Ag/ZSM-5 for Ethylene Oxidation at Room Temperature : Investigating the Effect of Water and Deactivation. *Chem. Eng. J*. **2018**, *347*, 808–818.

(12) Li, J.; Ma, C.; Xu, X.; Yu, J.; Hao, Z.; Qiao, S. Efficient Elimination of Trace Ethylene over Nano-Gold Catalyst under Ambient Conditions. *Environ. Sci. Technol*. **2008**, *42*, 8947–8951.

(13) Xue, W. J.; Wang, Y. F.; Li, P.; Liu, Z. T.; Hao, Z. P.; Ma, C. Y. Morphology Effects of CO_3O_4 on the Catalytic Activity of Au/Co_3O_4 catalysts for Complete Oxidation of Trace Ethylene. *Catal. Commun.* **2011**, *12*, 1265–1268.

(14) Ma, C. Y.; Mu, Z.; Li, J. J.; Jin, Y. G.; Cheng, J.; Lu, G. Q.; Hao, Z. P.; Qiao, S. Z. Mesoporous CO_3O_4 and Au/CO_3O_4 Catalysts for Low-Temperature Oxidation of Trace Ethylene. *J. Am. Chem. Soc*. **2010**, *132*, 2608–2613.

(15) Jiang, C.; Hara, K.; Fukuoka, A. Low-Temperature Oxidation of Ethylene over Platinum Nanoparticles Supported on Mesoporous Silica. *Angew. Chem. Int. Ed*. **2013**, *52*, 6265–6268.

(16) Hara, K.; Akahane, S.; Wiench, J. W.; Burgin, B. R.; Ishito, N.; Lin, V. S. Y.; Fukuoka, A.; Pruski, M. Selective and Efficient Silylation of Mesoporous Silica: A Quantitative Assessment of Synthetic Strategies by Solid-State NMR. *J. Phys. Chem. C* **2012**, *116*, 7083–7090.

(17) Jaroniec, C. P.; Kruk, M.; Jaroniec, M.; Sayari, A. Tailoring Surface and Structural Properties of MCM-41 Silicas by Bonding Organosilanes. *J. Phys. Chem. B* **1998**, *102*, 5503–5510.

(18) Ojeda-López, R.; Pérez-Hermosillo, I. J.; Marcos Esparza-Schulz, J.; Cervantes-Uribe, A.; Domínguez-Ortiz, A. SBA-15 Materials: Calcination Temperature Influence on Textural Properties and Total Silanol Ratio. *Adsorption* **2015**, *21*, 659–669.

(19) Zhao, D.; Huo, Q.; Feng, J.; Chmelka, B. F.; Stucky, G. D. Tri-, Tetra-, and Octablock Copolymer and Nonionic Surfactant Syntheses of Highly Ordered, Hydrothermally Stable, Mesoporous Silica Structures. *J. Am. Chem. Soc*. **1998**, *120*, 6024–6036.

(20) Miyazawa, K.; Inagaki, S. Control of the Microporosity within the Pore Walls of Ordered Mesoporous Silica SBA-15. *Chem. Commun*. **2000**, *21*, 2121–2122.

(21) Imperor-Clerc, M.; Davidson, P.; Davidson, A. Existence of a Microporous Corona around the Mesopores of Silica-Based SBA-15 Materials Templated by Triblock Copolymers. *J. Am. Chem. Soc.* **2000**, *122*, 11925–11933.

(22) Ryan, K. M.; Coleman, N. R. B.; Lyons, D. M.; Hanrahan, J. P.; Spalding, T. R.; Morris, M. A.; Steytler, D. C.; Heenan, R. K.; Holmes, J. D. Control of Pore Morphology in Mesoporous Silicas Synthesized from Triblock Copolymer Templates. *Langmuir* **2002**, *18*, 4996–5001.

(23) Chen, C. S.; Lai, Y. T.; Chen, T. C.; Chen, C. H.; Lee, J. F.; Hsu, C. W.; Kao, H. M. Synthesis and Characterization of Pt Nanoparticles with Different Morphologies in Mesoporous Silica SBA-15 for Methanol Oxidation Reaction. *Nanoscale* **2014**, *6*, 12644–12654.

(24) Oh, J. S.; Shim, W. G.; Lee, J. W.; Kim, J. H.; Moon, H.; Seo, G. Adsorption Equilibrium of Water Vapor on Mesoporous Materials. *J. Chem. Eng. Data* **2003**, *48*, 1458–1462.

(25) Hertl, W.; Hair, M. L. Adsorption of Water on Silica. *Nature* **1969**, *223*, 1150–1151.

(26) Sindorf, D. W.; Maciel, G. E. 29Si CP/MAS NMR Studies of Methylchlorosilane Reactions on Silica Gel. *J. Am. Chem. Soc.* **1981**, *103*, 4263–4265.

Chapter 4: Kinetics and In-situ FTIR Study of Ethylene Oxidation over Platinum Supported SBA-15 Catalyst

4.1 Introduction

Platinum is recognized to be one of the active metals for the oxidation of petroleum-derived hydrocarbons in chemical industry over the years.[1,2] Ethylene oxidation with a heterogeneous catalyst is an important topic in the field of storage and transportation of fresh vegetables, fruits, and flowers, etc., because trace amount of ethylene released in a closed container promotes their undesirable ripening. Our group has reported that a heterogeneous catalyst, MCM-41-supported Pt nanoparticles, decompose trace ethylene in the ppm level to CO_2 at 0 ºC.[3] Due to a long-term activity and a high stability, the supported Pt catalyst is now commercialized in 2015 for the new refrigerators released by HITACHI appliance Co. Ltd., a household appliances manufacturer. In-situ measurement of MCM-41 supported Pt catalyst under the reaction conditions using diffuse reflectance infrared Fourier transform spectroscopy (DRIFT) proposed the presumable reaction pathway in this system: ethylene can be converted to CO_2 and H_2O via formaldehyde (HCHO) and carbon monoxide (CO) in the presence of molecular oxygen as an oxidant, and formic acid is recognized as a by-product. However, a lot of concerns still remained unresolved. For example, CO as an intermediate generally blocks active Pt surface through the formation of stable CO-Pt adduct. As mentioned in the previous chapter, physisorption of water molecules formed by complete ethylene oxidation also results in the decrease in original activity of Pt nanoparticles.

In this chapter, two useful techniques were applied to the characterization of reaction phenomenon using SBA-15 supported Pt catalyst (Pt(1.8 wt% and 10 wt%)/SBA-15). One is kinetic modeling using a fixed-bed flow reactor. The reactions were conducted systematically by changing Space Velocity (SV = 3000-7500 mL h^{-1} g^{-1}) and reaction temperature (0-40 °C), in order to evaluate ethylene conversion and CO_2 yield at the steady state. These data are useful to estimate apparent activation energy of the overall reaction with the kinetics modeling of pseudo-first order reaction. The oxidation of trace CO (100 ppm) with large SV (7500 mL h^{-1} g^{-1}) was also performed in a range of reaction temperatures (0-40 °C) to compare the difference in the reaction rate between ethylene and CO oxidation. Turnover frequency (TOF) value based on Pt loading in ethylene oxidation was compared to that in CO oxidation, which provides us with simple prediction on whether CO oxidation is the rate-determining step for ethylene oxidation or not. CO oxidation was also performed in the presence of water vapor at 0 °C to understand the effect of physisorbed water on the activity of Pt nanoparticles. Another technique is in-situ measurement of ethylene oxidation on Pt/SBA-15 by FTIR. Reaction dynamics of the ethylene oxidation can be proposed based on the change in band intensities of intermediates adsorbed on solid surface. A close circulation system and a gas-flow system equipped with an IR cell were used in FTIR measurement where the latter is a batch-type reactor. The author also observed the decomposition phenomena of some possible intermediates such as HCHO, HCOOH, and CH_3COOH on Pt/SBA-15 in the absence and presence of oxygen.

4.2 Experimental

4.2.1 Ethylene Oxidation on Pt/SBA-15

Ethylene oxidation was carried out with SBA-15 supported Pt catalyst (Pt (1.8 wt%)/SBA-15) using a fixed-bed flow type reactor as shown in Figure 4.1. The gas mixture of C_2H_4 (50 ppm), O_2 (20%), N_2 (5%) and He (balance) was fed to the catalyst bed (0.40 g). Space velocity and reaction temperature changed from 3000 to 7500 mL g^{-1} h^{-1} and from 0 – 40 °C °C, respectively. All reactions were performed for 8 h to obtain steady-state activities. The values for ethylene conversion and CO_2 yield were estimated by the following equations where $[C_2H_4]_{inlet}$, $[C_2H_4]_{outlet}$, and $[CO_2]_{outlet}$ are C_2H_4 concentration at the inlet of the reactor, C_2H_4 and CO_2 concentrations at the outlet of the reactor, respectively.

$$X_{C_2H_4} = ([C_2H_4]_{in}–[C_2H_4]_{out})\times100/[C_2H_4]_{in}$$

$$Y_{CO_2} = [CO_2]_{out} \times100/2[C_2H_4]_{in}$$

4.2.2 CO oxidation by Mesoporous Silica Supported Pt Catalyst

Similar to the ethylene oxidation, CO oxidation was carried out using a fixed-bed flow reactor as shown in Figure 4.1. The granular catalyst (0.40 g) in the reactor was pretreated at 150 °C for 2 h under continuous flow of He (40 mL/min). Reaction gas mixture of CO (100 ppm), O_2 (20%), N_2 (5%) and He (balance) was fed to the catalyst bed at 0 °C using mass flow controllers under an ambient pressure at an SV of 1500 mL h^{-1} g^{-1}. At an SV of 7500 mL h^{-1} g^{-1} the oxidation was carried out at 0 – 40 °C. The reactant and products after the reaction was also conducted by GC. The values of CO conversion and CO_2 yield were estimated after 8 h of the reaction where the reactions reached the steady state.

Water vapor was added to the gas mixture using a saturator (Figure 4.1) to examine the influence of water formed during this reaction. A gas mixture containing water vapor (0.61%) was supplied to the catalyst-bed (Pt/SBA-15, 0.40 g) at 0 °C with an SV of 1500 mL h^{-1} g^{-1}. The values for CO conversion and CO_2 yield were estimated by the following equations where $[CO]_{inlet}$, $[CO]_{outlet}$, and $[CO_2]_{outlet}$ are CO concentration at the inlet of the reactor, CO and CO_2 concentrations at the outlet of the reactor, respectively.

$$X_{CO} = ([CO]_{inlet}–[CO]_{outlet})\times100/[CO]_{inlet}$$

$$Y_{CO_2} = [CO_2]_{out} \times100/ [CO]_{in}$$

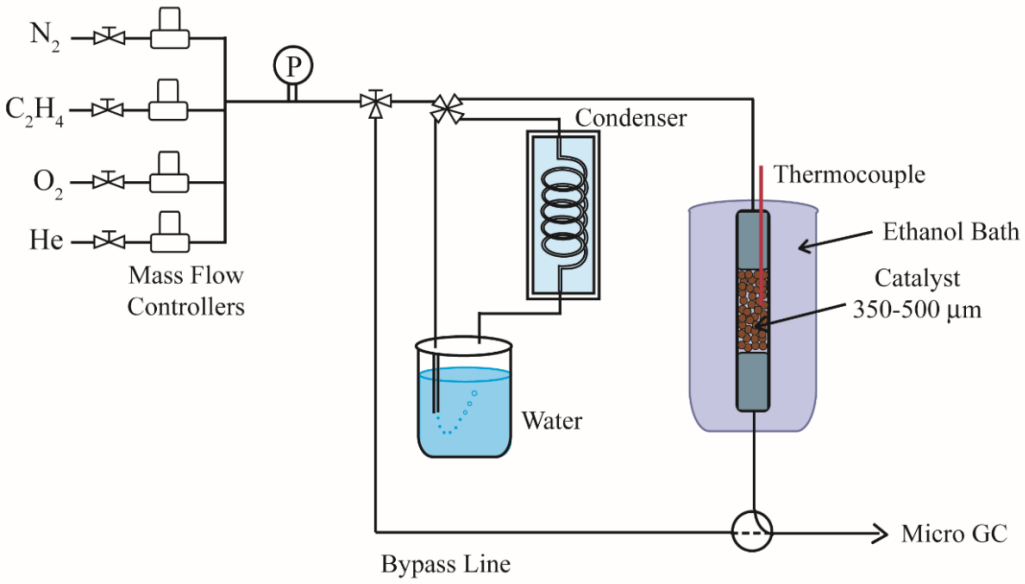

Figure 4.1. Schematic representation of the flow reactor used in low temperature ethylene oxidation.

4.2.3 HPLC and ^{1}H NMR Study

0.40 g of 1.8% Pt/SBA-15 was used in ethylene oxidation under the flow of C_2H_4 (50 ppm), O_2 (20%), N_2 (5%) and He (balance) at 0 °C and the spent catalyst was stirred in 3 mL

of water for 1.5 h to extract intermediates and spectators stabilized on catalyst surface. The filtrate was analyzed using high performance liquid chromatography (HPLC; Prominence, Shimadzu) with refractive index detector. The HPLC apparatus was equipped with an Aminex HPX-87H column (Bio-Rad Laboratories) and used at 35 °C with 5 mM H_2SO_4 as an eluent at a flow rate of 0.5 mL min^{-1}.

The same extraction was conducted with 2 mL of D_2O under Ar bubbling. The extracted solution was isolated by centrifugation at 3500 rpm, and then analyzed using ^1H nuclear magnetic resonance (NMR) (Jeol, ECX 400, 32 scans).

4.2.4 In-situ FTIR Spectroscopy Measurements

Ethylene oxidation was carried out over Pt (10 wt%)/SBA-15. 0.02 g of a catalyst in the pellet form was put in an IR cell connected with a gas-flow system, as shown in Figure 4.2. After heat treatment of the sample at 200 °C for 2 h under He flow, a gas-mixture of C_2H_4 (200 ppm), O_2 (20%) and He (balance) was introduced to the catalyst at 0 °C for 60 min. The reaction continued under He flow containing only O_2 (20%). The spectra were collected during the reaction using PerkinElmer Spectrum 100 (resolution 4 cm^{-1}, integration 64 times).

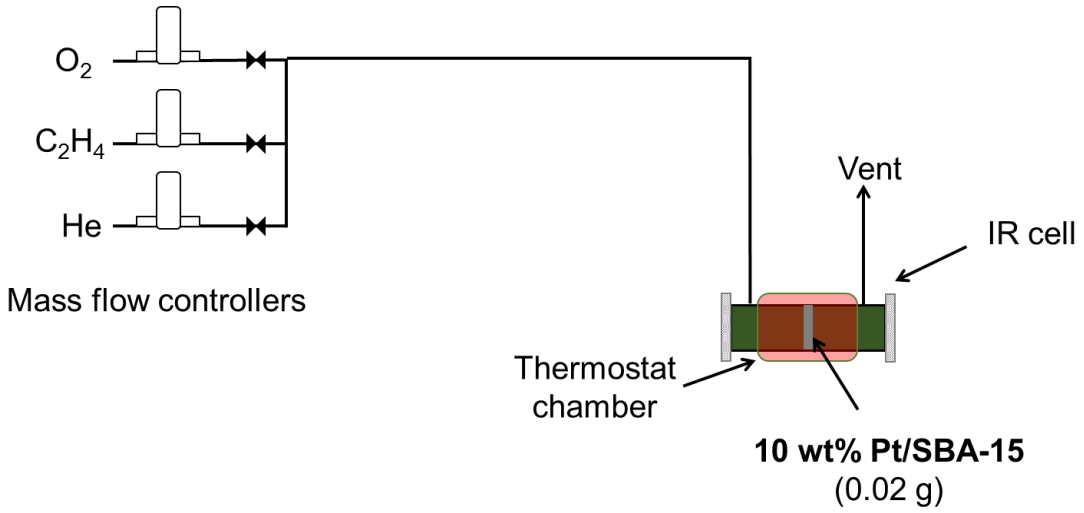

Figure 4.2. Schematic representation of the DRIFT and flow reactor used in low temperature ethylene oxidation.

In the case of FTIR study using a batch system, the pellet of Pt (10 wt%)/SBA-15 (0.02 g) was pretreated in an IR cell connected to batch reactor (Figure 4.3) at 200 °C for 2 h under vacuum. Reaction gas of C_2H_4 700 ppm, O_2 20% and He (balance) was prepared using a pressure gauge. The purity of oxygen and helium used in this experiment was 99.9999%. The pressure in the reactor was 30 kPa. The reaction in the IR-cell was performed at 30 °C. FTIR spectra during the reaction were taken using Jasco FT / IR 6600 (MCT, resolution 4 cm^{-1}, integration 64 times).

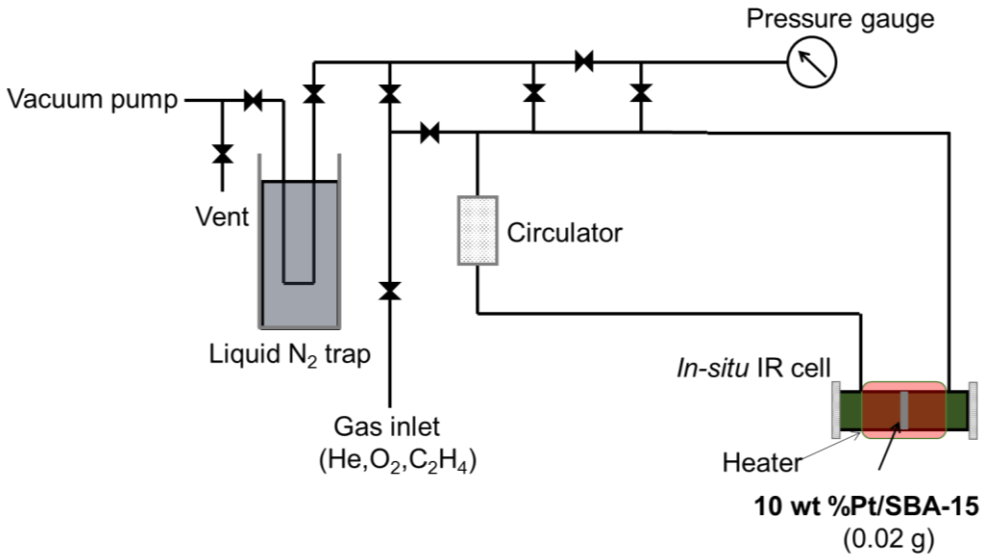

Figure 4.3. Schematic representation of a closed circulation system connected with an IR cell.

4.2.5 Decomposition and Oxidation of Formaldehyde, Formic acid and Acetic acid

The FTIR system in Figure 4.3 was also used as a batch reactor for the decomposition and oxidation of HCHO, HCOOH, and CH_3COOH with Pt (10 wt%)/SBA-15. The three compounds are regarded as intermediates and/or spectator in ethylene oxidation. The catalyst in the pellet form was placed into the IR cell and heated at 200 °C for 2 h under vacuum to remove the physisorbed water. HCHO decomposition was performed at 30 °C with He containing a tiny amount of HCHO (3200 ppm). HCHO oxidation was conducted at the same temperature with the mixture of He (80%) and O_2 (20%) in the presence of HCHO (3200 ppm). FTIR spectra during the reactions were taken using Jasco FT/IR 6600. HCHO was obtained by thermal decomposition of paraformaldehyde under vacuum in both cases. Decomposition and oxidation of HCOOH (1500 ppm) and CH_3COOH (700 ppm) were also performed under the same conditions as the case of HCHO.

4.3 Results and Discussion

4.3.1 Reaction Kinetics Study using a Fixed-Bed Flow Reactor

Reaction kinetics of Pt (1.8 wt%)/SBA-15 in the oxidation of trace ethylene was studied with a fixed-bed flow reactor. First the reaction was conducted at various temperatures (0, 10, 20, 25, 30, 35, 40 °C) and SV (3000, 4500, 6000 and 7500 mL h^{-1} g^{-1}). The reactions were continued for 8 h to obtain the steady state activities. Figures 4.4(A)-(D) shows the dependence of ethylene conversion and CO_2 on reaction temperature in various SV conditions. It is observed that the ethylene conversion and the CO_2 yield monotonically increased with reaction temperature. In all reactions a large amount of O_2 was used with respect to ethylene. When the values of ethylene conversion in the form of ln(1-*x*) were plotted against the values of contact time (W/F), a linear line can be obtained at each temperature (Figure 4.4(E)), which means that this reaction can be assumed as a pseudo-first order reaction. The reaction rate constants at all temperatures can be estimated from the following equation (4.1) and they are summarized in Table 4.1.

$$\ln(1-x) = -k' \frac{W}{F} \qquad 4.1$$

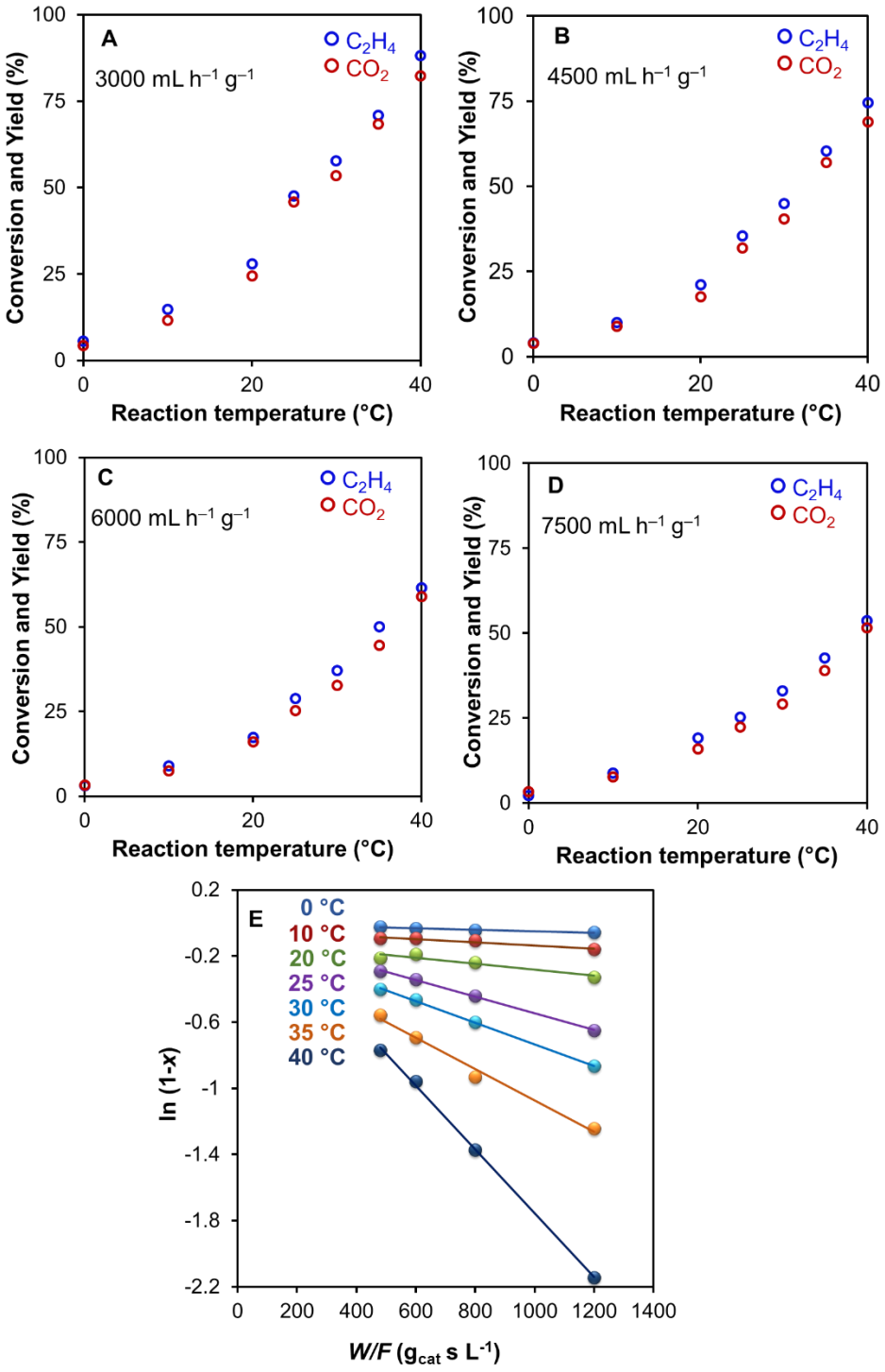

Figure 4.4. Conversion of ethylene and yield of CO_2 as a function of temperature over Pt/SBA-15 at varying space velocities: SV=3000 mL h^{-1} g^{-1} (A), SV= 4500 mL h^{-1} g^{-1} (B), SV=6000 mL h^{-1} g^{-1} (C) and SV=7500 mL h^{-1} g^{-1} (D). Dependence of ethylene conversion (ln(1-*x*), *x*: ethylene conversion) on contact time at temperatures of 0 – 40 °C (E).

Table 4.1. Rate constant, *k* of ethylene conversion

k (L g^{-1} s^{-1})	
k_0	4.61×10^{-5}
k_{10}	9.74×10^{-5}
k_{20}	1.80×10^{-4}
k_{25}	5.03×10^{-4}
k_{30}	6.54×10^{-4}
k_{35}	9.47×10^{-4}
k_{40}	1.93×10^{-3}

These values in Table 4.1 can be used for the estimation of apparent activation energy of the reaction with the Arrhenius equation (4.2),

$$k = Ae^{-E_a/RT} \qquad 4.2$$

where *A*, E_a, R, and T are the pre-exponential factor, activation energy, the gas constant, and temperature, respectively.

The apparent activation energy was calculated to be E_a = 66 kJ/mol. In the previous paper HCHO and CO are regarded as possible intermediates in the current reaction system. Since the formation of ethylene oxide (epoxidation) and acetic acid from ethylene using a supported Ag and Pt catalysts through partial oxidation gave 60.7 kJ mol^{-1} (210 – 270 °C)[4] and 75 kJ mol^{-1} (77 – 127 °C)[5] respectively. These activation energies are almost comparable to that the author estimated in this study, but reaction temperature of our study is quite low. This strongly suggests none of these two reactions taking place in the author's system.

4.3.2 Low Temperature Oxidation of CO and Effect of Water Vapor

In our previous study employing the in-situ DRIFT measurement of ethylene oxidation over Pt/silica at 50 °C, it was assumed that reaction proceeds via CO oxidation as the rate determining step of the reaction.[3] Hence CO oxidation was carried out under the similar conditions at 0 – 40 °C and an SV of 7500 mL h^{-1} g^{-1}.

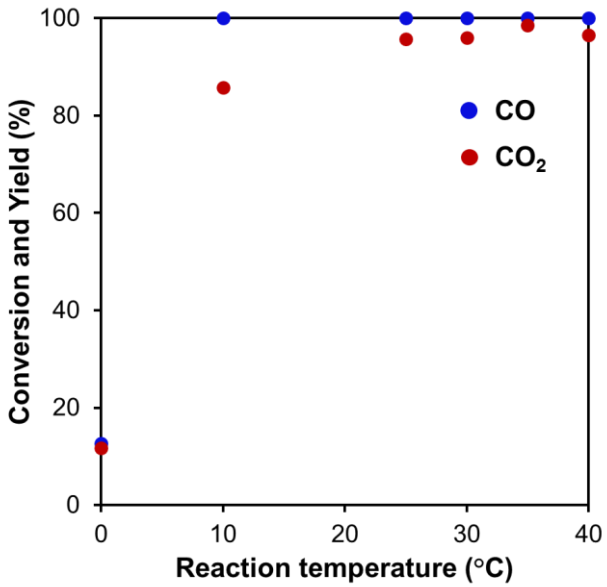

Figure 4.5. Conversion of CO and yield of CO_2 as a function of temperature over Pt/SBA-15 at SV=7500 mL h^{-1} g^{-1}. Reaction condition: Pt/SBA-15 0.40 g (Pt 1.8 wt%), CO 100 ppm, O_2 20%, N_2 5%, He balance, SV 1500 mL h^{-1} g^{-1}.

Figure 4.5 shows CO conversion and CO_2 yield at 8 h at various temperatures. Pt/SBA-15 can oxidize CO at 0 °C, and its activity (CO conversion, ca. 12%) is superior to that in ethylene conversion (see Figure 4.3(D)). CO conversion reached more than 99% at > 0 °C (Figure 4.5) whereas ethylene conversion at 40 °C was ca. 50% (Figure 4.3(D)). Therefore, the rate for CO oxidation to CO_2 is much faster than that of overall ethylene oxidation and

CO oxidation is not the rate determining step in low-temperature oxidation of trace ethylene using mesoporous silica-supported Pt catalyst.

CO oxidation was also carried out at a low SV of 1500 mL h^{-1} g^{-1} at 0 °C in the presence and absence of water vapor.

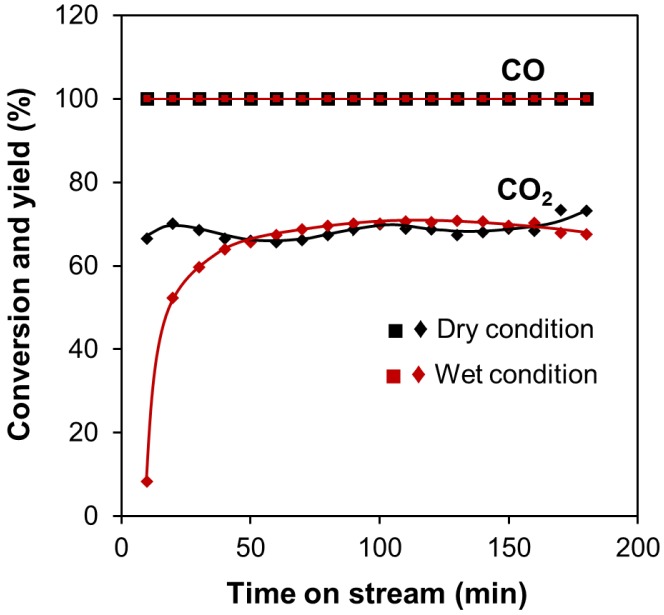

Figure 4.6. Time courses for CO conversion (square) and CO_2 yield (diagonal) over Pt/SBA15 in dry (black symbols) and wet condition (red symbols). Reaction conditions: Pt/SBA-15 0.40 g (Pt 1.8 wt%), CO 100 ppm, O_2 20%, N_2 5%, He balance, SV 1500 mL h^{-1} g^{-1}, T 0 °C, water vapor 0.86%.

Pt/SBA-15 kept complete CO conversion for 180 min in both dry and wet conditions. The difference between the conversion and yield might be due to adsorption of CO on the catalyst surface since CO oxidation does not involve any intermediates in its reaction pathway and total amount of CO introduced within 180 min is too small compared to Pt content in the catalyst bed. No significant effect of water vapor was observed in terms of CO conversion and CO_2 yield although physisorption of water vapor on catalyst surface results in the steep decrease in original activity in ethylene oxidation (Figure 3.10). CO oxidation is not affected

by water vapor, which is consistent with the previous report using a supported Pt catalyst.[6,7] The turnover frequency (TOF) for the CO oxidation at a steady state (Figure 4.6) is calculated to be 0.4 h^{-1} which is almost twice that of ethylene oxidation at the steady state (5 h) in Figure 2.3 of Chapter 2 (TOF = 0.2 h^{-1}). Metallic Pt is generally deactivated with CO; however, the oxidation of trace CO with a supported Pt catalyst proceeds smoothly without decrease in original activity even at low temperature.

In previous reports, ethylene epoxidation over Ag-Cs/α-Al_2O_3 catalyst at a range of temperature of 210-270 °C showed an apparent activation energy of 60.7 kJ/mol.[4] The apparent activation energy for ethylene oxidation over Pt/SBA-15 at a range of 0 – 40 °C was 66 kJ/mol which is in reality very low based on the reaction temperature when compared to that of epoxidation reaction. Hence, from this it can be concluded that ethylene oxidation does not proceed through the formation of epoxide on the catalyst surface. The possibility of the stabilization of formate as well acetic species at lower temperature reaction is high, so the small yield of CO_2 obtained during oxidation of 50 ppm of ethylene at 0 °C could be formed via formation of formic acid which in turn converts to CO_2. For increasing reaction temperature, other pathways are also activated which would show higher catalytic activity.

4.3.3 HPLC and ^{1}H NMR Study

In Section 2.3.2 of Chapter 2, it was described that ethylene conversion is not equal to CO_2 yield in ethylene oxidation at 0 °C over 1.8% Pt/SBA-15. This difference may be attributed to the formation of intermediates species that are adsorbed on catalyst surface. The mass balance was finally satisfied by a simple heat treatment under inert atmosphere where the stabilized intermediate species were desorbed in the form of CO_2. For clarification of the presence of carbon species on catalyst surface, surface species of spent catalyst was extracted

using water. The spent catalyst in water was stirred for 2 hours, centrifuged and filtered. The filtrate was analyzed with HPLC, which revealed the presence of acetic acid. This was also confirmed using ^{1}H NMR spectroscopy as shown in Figure 4.7.

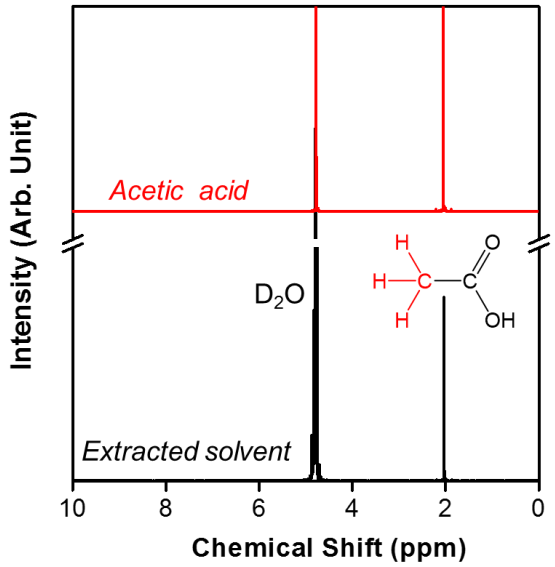

Figure 4.7. ^{1}H NMR spectra of extracted filtrate of washed catalyst and pure acetic acid as a reference.

The extracted filtrate was mixed with D_2O used as solvent and its ^{1}H NMR spectrum was recorded. The large peak at 4.8 ppm was assigned to that of D_2O which was used as a solvent. The α-Hs of the acetic acid gave rise to a singlet at 2.0 ppm which is similar to that of pure acetic acid in D_2O.[8] This showed that acetic acid was present on catalyst surface even after the reaction and it could be a potential spectator instead of intermediates. However quantification of amount of acetic acid collected from the catalyst surface is difficult since the 5 hour ethylene oxidation reaction gave rise to such low amount of acetic acid as spectator that it was way below the detection limit. Hence the reaction was carried out for longer time (24 h in this case) to collect the surface stabilized acetic acid. Hence, in-situ FTIR study is

done in the next sections to reveal the intermediate species and further confirm the presence of acetic acid on catalyst surface.

4.3.4 In-situ FTIR Study of Ethylene Oxidation over Pt/SBA-15 at 0 °C in an IR cell Equipped with a Gas-flow System

In order to preliminarily study the surface species during ethylene oxidation at 0 °C, the reaction was performed with Pt(10 wt%)/SBA-15 in an IR cell equipped with a gas-flow system, as shown in Figures 4.2. In the flow system, a mixture of ethylene (200 ppm), O_2 (20%), and He (balance) was fed to the pellet of Pt/SBA-15 placed in the IR cell at 0 °C, and FTIR spectra were taken during the course of the reaction. After 60 min of the reaction, the supply of ethylene gas was stopped and the catalyst was heated at elevated temperatures in O_2 (20%), and He (80%) flow. Figure 4.8 shows difference FTIR spectra of Pt(10 wt%)/SBA-15 during the reaction ((a)-(e)) and during the heat treatment in He(balance) and O_2(20%) flow at elevated temperatures ((f)-(h)) where bare FTIR spectrum of pretreated Pt(10 wt%)/SBA-15 (He flow, temperature: 200 °C, time: 2 h) was used as the background of these spectra. Two positive bands were visible for OH stretching (3500-3000 cm^{-1}) and OH bending (1600 cm^{-1}) modes, due to the formation of water molecules that were stabilized mainly on silica surface. There are two shoulder peaks contained in the bending mode at around 1705 and 1577 cm^{-1}. Additional two broad but weak bands were observed at ca. 2050 cm^{-1} and 1400 cm^{-1}, and their intensities are gradually increased with time during the reaction ((a)-(e)).The former band can be assigned to linear CO species on Pt surface. The latter is strongly related to two shoulder bands mentioned above and a series of the bands is due to carbonyl or carboxylic acid group in some intermediates.

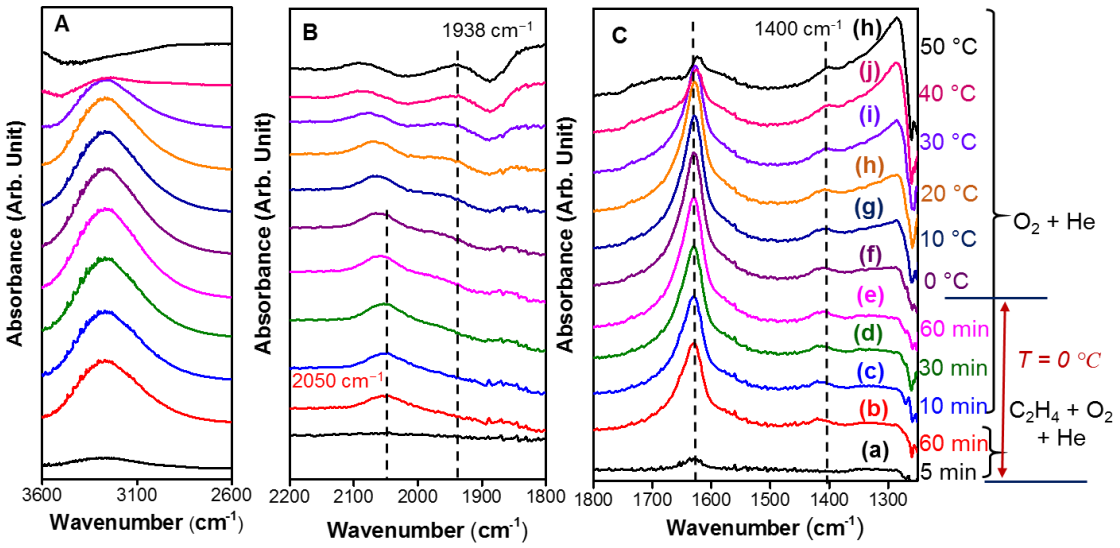

Figure 4.8. Oxidation of ethylene at 0 °C over Pt/SBA-15 followed by flow of O_2 and heating under the flow of O_2 at ranges of 3600-2600 cm^{-1} (A), 2200-1800 cm^{-1} (B) and 1800-1250 cm^{-1} (C). Reaction condition: Pt/SBA-15 0.02g (Pt 10%), C_2H_4 200 ppm, O_2 20%, He balance.

When the catalyst was heated under the flow of O_2 and He at elevated temperatures, the intensities of OH stretching and bending modes decreased due to the desorption of physisorbed water. Focusing on the behavior of Pt-CO band (2050 cm^{-1}) with time and temperature, the heat treatment accompanies the decrease in the band intensity of the linear Pt-CO band and the increase in the new band for bridged CO-Pt species at 1938 cm^{-1}. The latter band was likely formed from the pre-formed linear Pt-CO species by surface rearrangement or through the decarbonylation of some possible intermediates such as HCHO, HCOOH, and CH_3COOH.

In order to discuss the carbonyl-related compounds stabilized on catalyst surface, the intense and asymmetric band centered at 1600 cm^{-1} in spectrum (e) was fitted with four bands (Figure 4.9). The bands at 1710, and 1639 cm^{-1} are assignable to C=O stretching and asymmetric COO stretching modes of acetic acid and acetate, respectively. This assignment

can be directly supported by the previous experiment described in 4.3.3, because acetic acid (and acetate) can be identified as an intermediate or spectator by HPLC measurement. Along with this assignment, the band at 1410 cm^{-1} is successfully assignable to symmetric COO stretching mode of acetate. Aside from the OH bending mode of physisorbed water at 1629 cm^{-1}, the band at 1574 cm^{-1} can be attributed to asymmetric COO stretching mode of formate species, because the formation of formate species also gives another band for the symmetric COO stretching mode that can be also obtained at 1333 cm^{-1} in the same spectrum. HCHO can be easily oxidized to formate or CO as shown below (see 4.3.5), so that the possibility of HCHO formation can be excluded in these assignments. There are no information about C-H stretching modes generally appearing at 3000-2800 cm^{-1}. Therefore, next ethylene oxidation was performed with a concentrated gas mixture (ethylene, 700 ppm) using an IR cell connected with a batch reactor to monitor the change in the bands in this region during the reaction.

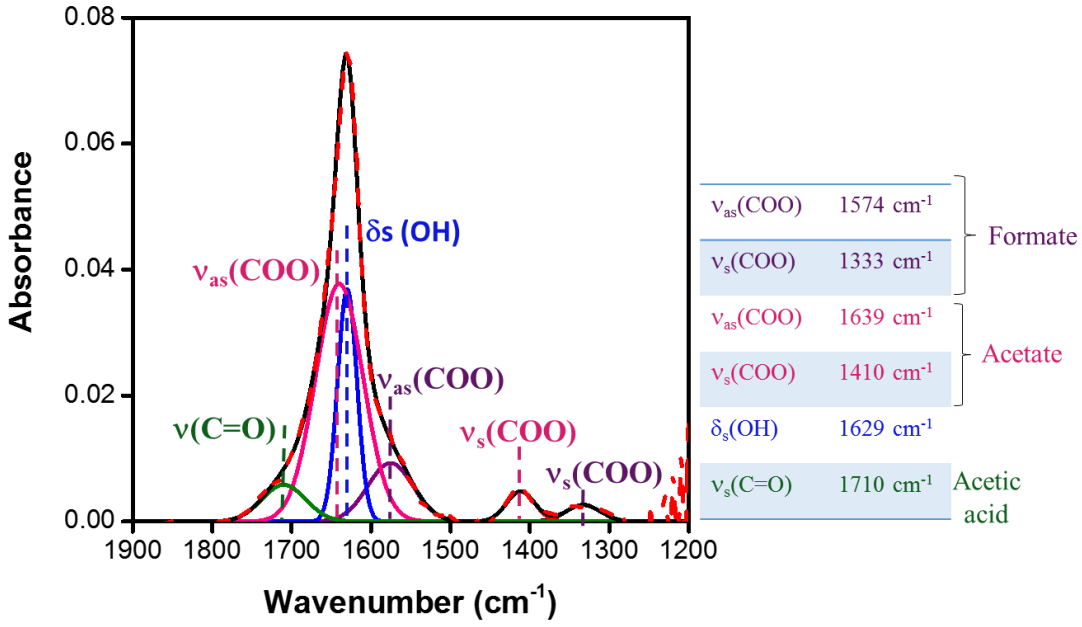

Figure 4.9. Deconvolution of Spectrum (e) of Figure 4.11(B).

4.3.5 In-Situ FTIR Study of Ethylene Oxidation over Pt/SBA-15 at 30 °C

FTIR measurement was also conducted with an IR cell connected with a close-circulating system (Figure 4.3). This system can be regarded as a batch reactor that can be useful for identifying the formation of the intermediates on the catalyst surface using a concentrated ethylene gas mixture (700 ppm). Ethylene oxidation was carried out with a mixture of ethylene (700 ppm), O_2 (20%) and He (balance) over Pt/SBA-15 at 30 °C to confirm IR bands in C-H stretching region of possible intermediates as already observed in Figure 4.10. IR spectra were taken at 5, 15, 30, 60, 90, and 120 min where the FTIR spectrum of pretreated Pt/SBA-15 was used as the background. Figure 4.10(A) shows difference FTIR spectra at each temperature. As observed in Figure 4.10(B), same phenomenon was obtained in 3800-2800 cm^{-1} (OH-stretching band), in 2100-1950 cm^{-1} (Pt-CO bands), and 1800-1300 cm^{-1} (OH-bending and CO/COO stretching modes of acetate/acetic acid/formate).

Focusing on C-H stretching region, there are several weak bands at 2997, 2944, and 2888 cm^{-1}. Based on the possible intermediates observed in Figure 4.9, the bands at 2997 and 2888 cm^{-1} can be assigned to CH stretching modes of formate species.[9-11] These species could be oxidized further to CO + H_2 or CO_2 + H_2O in the presence of O_2. A very weak band at 2944 cm^{-1} was likely due to C-H stretching mode of methyl moiety in acetic acid adsorbed on Pt/SBA-15.[12] The absence of the band in 3100-3000 cm^{-1} region predicts that HCHO as a highly reactive intermediate cannot be detected by FTIR measurement.

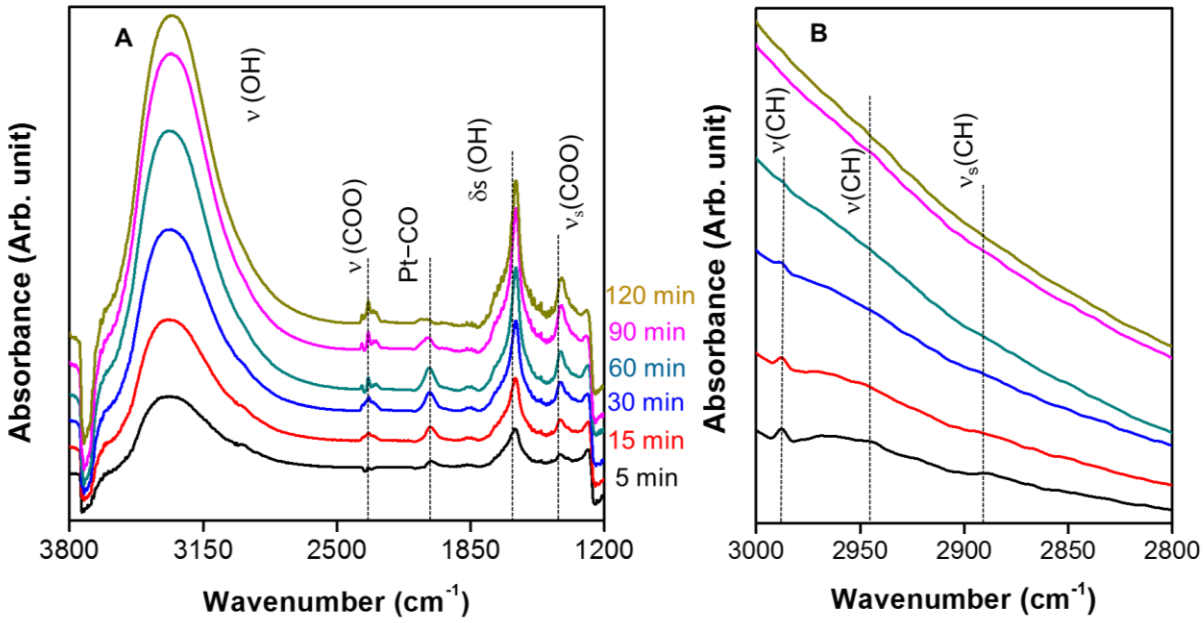

Figure 4.10. Time-dependent IR spectra for ethylene oxidation (A) and magnified FTIR spectra from 3000 to 2800 cm^{-1} (B) on 10% Pt/SBA-15 at 30 °C. C_2H_4 700 ppm, O_2 20%, He 80%.

4.3.6 In-situ FTIR Study of Formaldehyde, Formic Acid and Acetic Acid Oxidation over Pt/SBA-15

Formaldehyde was considered as an intermediate during ethylene oxidation. To confirm the presence of this intermediate, both formaldehyde adsorption and oxidation were carried out on Pt/SBA-15 surface in combination with FTIR measurement at various reaction times (Figure 4.11). After heat treatment of Pt/SBA-15 in He at 200 °C for 2 h to remove physisorbed water, the catalyst was contacted with the vapor of *p*-formaldehyde at 30 °C in pure He or in a mixture of O_2 (20%) and He (balance) under atmospheric pressure. After formaldehyde adsorption on the catalyst in He, one intense band appeared at 2074 cm^{-1} that can be due to linear Pt-CO species on Pt surface. Despite a lot of small bands present in the spectra, they are negligibly small, which means that HCHO is readily converted to CO even in the presence of oxidant (O_2) maybe through decarbonylation path. In the case of the

mixture of O_2 and He, the Pt-CO band disappeared completely within 30 min, and only intense band for OH bending mode was observed at 1600 cm^{-1}. Therefore, HCHO can be smoothly oxidized to CO_2 via the formation of CO in the presence of O_2. No specific bands for formate species indicate that formate/formic acid formed in ethylene oxidation is formed from HCHO.

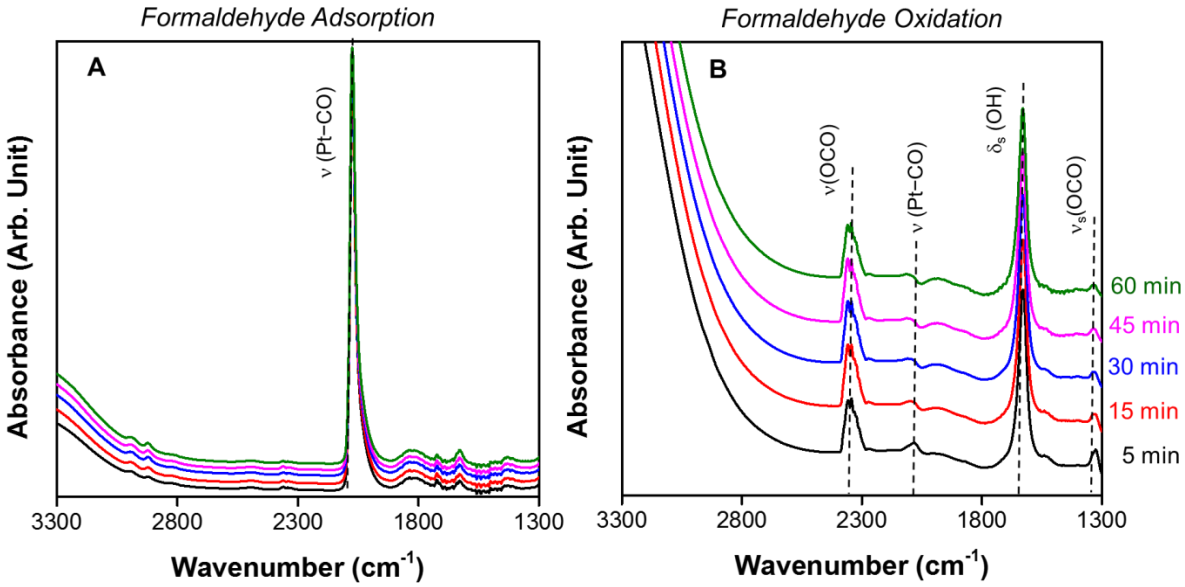

Figure 4.11. Time dependent FTIR spectra of formaldehyde adsorption in pure He (A) and in a mixture of O_2 (20%) and He (B) over Pt/SBA-15.

Next, same experiments were conducted using formic acid as a reactant. Figures 4.12(A) and 4.12(B) show difference FTIR spectra of Pt/SBA-15 after adsorption of formic acid in pure He and in a mixture of O_2 (20%) and He (balance). Formic acid adsorption in pure He results in the formation of new bands for free formic acid and formate species (C-H stretching mode of formate at 2945 cm^{-1}, two C=O stretching modes for formic acid at 1801 and 1723 cm^{-1}, and two COO stretching modes for formate at 1456 and 1358 cm^{-1}). The presence of two intense band for Pt-CO (2071 cm^{-1}) and physisorbed water (1630 cm^{-1}) indicates that CO can be formed from HCOOH through decarbonylation even in the absence

of oxygen, in parallel with a simple oxidation of HCOOH to CO_2 and H_2O. The apparent band intensity of H_2O remained unchanged after 30 min, meaning that HCOOH oxidation stopped after consumption of any oxidants (maybe O_2 and H_2O) in this system. In contrast, most of HCOOH is immediately involved in complete oxidation to form CO_2 and H_2O in the presence of O_2 (Figure 4.12(B)), due to only small bands for Pt-CO at 2076 cm^{-1}. These results indicate that formic acid formed in ethylene oxidation is not a spectator and directly and easily converted to CO_2 and H_2O under the current reaction conditions.

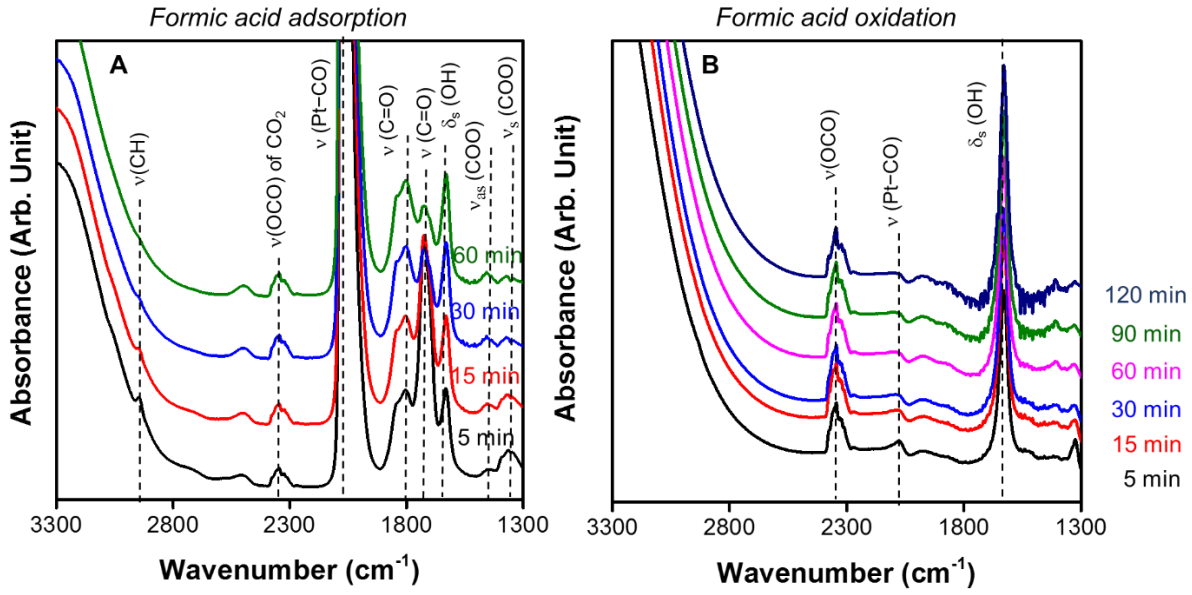

Figure 4.12. Time dependent FTIR spectra of formic acid adsorption (A) and oxidation (B) over Pt/SBA-15.

Finally acetic acid adsorption was conducted with Pt/SBA-15 in a mixture of O_2 (20%) and H_2. While HCHO and HCOOH are easily oxidized with O_2 to form CO_2 and H_2O, no significant change in the intensities of all bands was observed within 120 min (Figure 4.13). These bands are assignable to acetic acid (C-H stretching mode at 2944 cm^{-1}, C=O stretching at 1710 cm^{-1} and C–O stretching at 1279 cm^{-1}) and acetate (COO stretching modes for acetate at 1637 and 1407 cm^{-1}), as shown in Figure 4.14. A small band for Pt-CO in Figure 4.13

suggests partial decomposition of these surface species via decarbonylation, but this reaction is not preferable. Therefore, decomposition of acetic acid on Pt/SBA-15 is a very slow reaction compared to other possible intermediates (CO, HCHO. And HCOOH), and acetic acid itself can be considered as a spectator in ethylene oxidation.

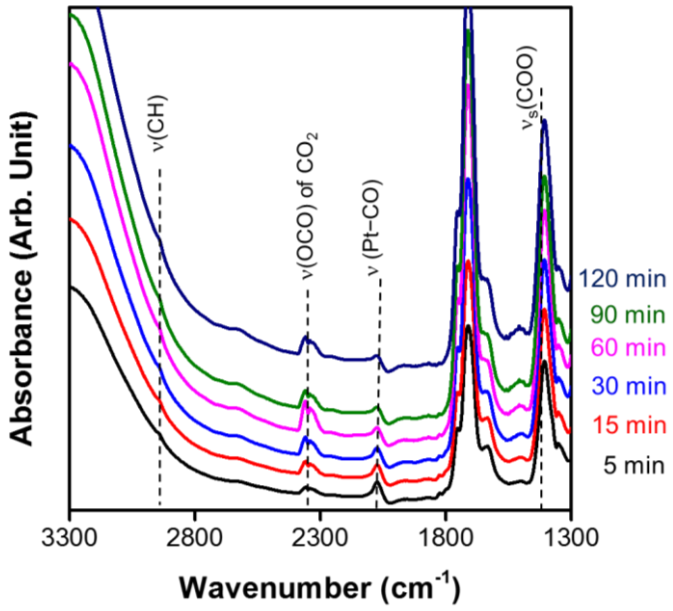

Figure 4.13. In-situ FTIR spectra of oxidation of acetic acid over Pt/SBA-15.

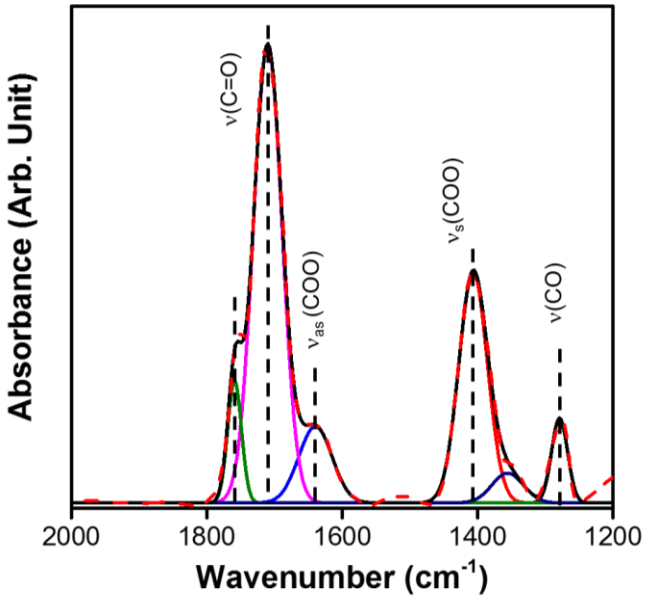

Figure 4.14. Deconvolution of spectrum recorded at 120min from Figure 4.13 between range of 2000-1200 cm^{-1}.

4.3.7 Possible Mechanism

Based on all observations in this chapter, a possible pathway in the previous paper can be successfully modified as shown in Scheme 4.1. Ethylene is adsorbed on metallic Pt nanoparticles supported over meosporous SBA-15 and reacts with the atomic oxygen to form CO_2 and water via the formation of formaldehyde as a major route. Despite no direct evidence for the formation of HCHO as an intermediate, HCHO undergoes oxidation to CO_2 and H_2O readily. HCOOH formation was only confirmed by FTIR measurement (Figure 4.12), but, it is also easily oxidized to CO_2 and H_2O. Due to smooth oxidation phenomenon, partial oxidation or decarbonylation of HCHO to give the pair of CO and H_2O are a minor reaction path in the presence of O_2. Therefore, ethylene oxidation has two pathways: the complete ethylene oxidation to CO_2 and water via the formation of HCHO, CO, and HCOOH (major path) and the partial ethylene oxidation to acetic acid that is the spectator (minor path). Formaldehyde, formic acid and formate could be assigned as the intermediates in ethylene oxidation. In contrast, CH_3COOH is the only compound that can be directly detected by HPLC. Due to high stability toward aerobic oxidation with Pt/SBA-15, CH_3COOH can be regarded as a spectator in this system.

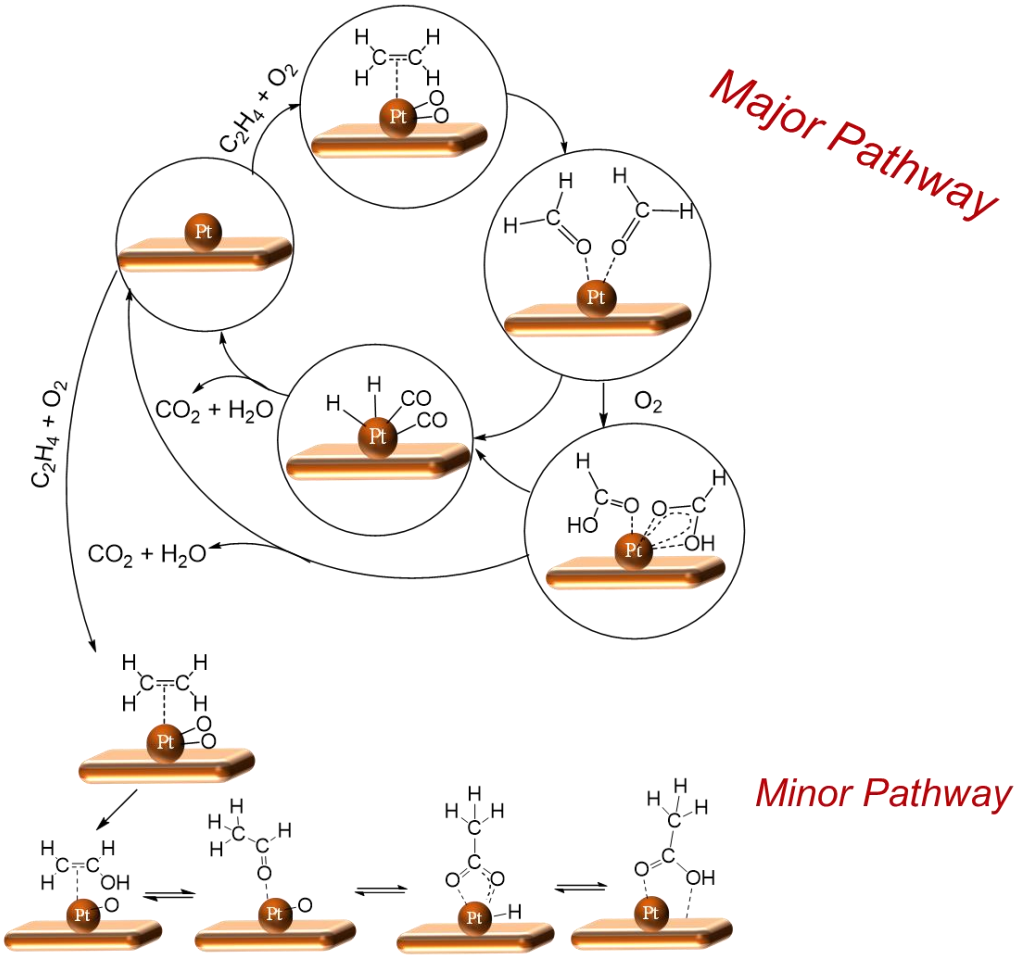

Scheme 4.1. Possible pathways for ethylene oxidation on Pt/SBA-15.

4.4 Conclusions

Kinetic study using the flow system revealed the apparent activation energy of ethylene over Pt/SBA-15 at a range of 0 – 40 °C was 66 kJ mol^{-1} which was lower compared to oxidation of ethylene to epoxide or acetic acid, showing that the current reaction is favorable in such condition. CO oxidation over Pt/SBA-15 occurs readily compared to that of ethylene oxidation showing that CO cannot be involved in the rate determining step during ethylene oxidation at 0 °C. In addition to it, HPLC and ^{1}H NMR study provided evidence for existence of acetic acid on catalyst surface. The FTIR study for ethylene oxidation at 0 °C and 30 °C

revealed presence of formate, acetate and acetic acid which were proved by in-situ FTIR of oxidation reaction of formaldehyde, formic acid and acetic acid as model reactions. HCHO, HCOOH and HCOO formed in the system can be considered as possible intermediates which oxidizes to CO_2 and H_2O. Oxidation of CH_3COOH at 30 °C proved the stabilization of the species on the catalyst surface.

References

(1) Hicks, R. F.; Qi, H.; Young, M. L.; Lee, R. G. Structure Sensitivity of Methane Oxidation over Platinum and Palladium. *J. Catal.* **1990**, *122*, 280–294.

(2) Yao, Y F. Y. The Oxidation of CO and Hydrocarbons over Noble Metal Catalysts. *J. Catal*. **1984**, *87*, 152–162.

(3) Jiang, C.; Hara, K.; Fukuoka, A. Low-Temperature Oxidation of Ethylene over Platinum Nanoparticles Supported on Mesoporous Silica. *Angew. Chem. Int. Ed*. **2013**, *52*, 6265–6268.

(4) Lafarga, D.; Al-Juaied, M. A.; Bondy, C. M.; Varma, A. Ethylene Epoxidation on Ag-Cs/α-Al_2O_3 Catalyst: Experimental Results and Strategy for Kinetic Parameter Determination. *Ind. Eng. Chem. Res.*, **2000**, *39*, 2148–2156.

(5) Cant, N.; Hall, W. K. Catalytic Oxidation II. Silica Supported Noble Metals for the Oxidation of Ethylene and Propylene. *J. Catal.* **1970**, *16*, 220–231.

(6) Gong, X.-Q.; Hu, P.; Raval, R. The Catalytic Role of Water in CO Oxidation. *J. Chem. Phys*. **2003**, *119*, 6324–6334.

(7) Jinnouchi, R.; Nagoya, A.; Kodama, K.; Morimoto, Y. Solvation Effects on OH Adsorbates on Stepped Pt Surfaces. *J. Phys. Chem. C* **2015**, *119*, 16743–16753.

(8) Fulmer, G. R.; Miller, A. J. M.; Sherden, N. H.; Gottlieb, H. E.; Nudelman, A.; Stoltz, B. M.; Bercaw, J. E.; Goldberg, K. I. NMR Chemical Shifts of Trace Impurities: Common Laboratory Solvents, Organics, and Gases in Deuterated Solvents Relevant to the Organometallic Chemist. *Organometallics* **2010**, *29*, 2176–2179.

(9) Zhang, C.; He, H.; Tanaka, K. Catalytic Performance and Mechanism of a Pt/TiO_2 catalyst for the Oxidation of Formaldehyde at Room Temperature. *Appl. Catal. B Environ*. **2006**, *65*, 37–43.

(10) Wu, H. C.; Chen, T. C.; Chen, Y. C.; Lee, J. F.; Chen, C. S. Formaldehyde Oxidation on Silica-Supported Pt Catalysts: The Influence of Thermal Pretreatments on Particle Formation and on Oxidation Mechanism. *J. Catal.* **2017**, *355*, 87–100.

(11) Raskó, J.; Kecskés, T.; Kiss, J. Formaldehyde Formation in the Interaction of HCOOH with Pt Supported on TiO_2. *J. Catal.* **2004**, *224*, 261–268.

(12) Rachmady, W.; Vannice, M. A. Acetic Acid Reduction by H_2 over Supported Pt Catalysts: A DRIFTS and TPD/TPR Study. *J. Catal.* **2002**, *207*, 317–330.

Chapter *5*: General Conclusions

In this thesis work, the author has given a detailed description on the catalytic study of ethylene oxidation at low temperature utilizing heterogeneous catalyst. In Chapter 1, the recent ordeals of the world with food loss and conventional ways of dealing with the problem has been discussed in detail. The role of ethylene in food loss and the utilization of different types of heterogeneous catalyst has been brought to light. Use of metallic Pt supported mesoporous silica and the synthesis procedures of the catalyst has also been described.

The important finding in Chapter 2 is accounting for the carbon mass imbalance rising during the oxidation reaction. The phenomenon of ethylene (50 ppm) oxidation at 0 °C, has been described in detail by employing heterogeneous catalyst, Pt supported mesoporous silica, SBA-15 (Figure 5.1) accounting for both ethylene conversion and CO_2 yield. Heat treatment of the spent catalyst under He flow resulted in formation of CO_2 due to the thermal decomposition of the oxygen containing carbon species stabilized on catalyst surface. The amount stabilized on catalyst surface was almost equal to the amount of CO_2 desorbed. Water molecules produced during the course of reaction also played a role in blocking the active sites resulting in decrease in ethylene conversion and yield. Other aerosil silicas with Pt dispersed on its surface also exhibited high activities for ethylene oxidation.

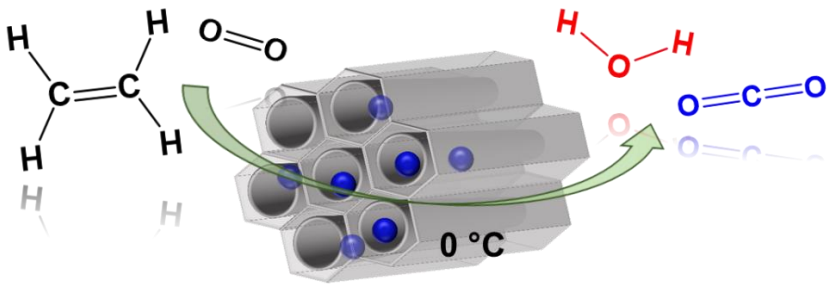

Figure 5.1. Ethylene oxidation over Pt/SBA-15 at 0 °C.

Owing to one of the conclusions of Chapter 2, where water molecule have shown to inhibit catalytic activity, Chapter 3 deals with an alternative methodology of increasing the catalytic activity up to some extent. In this chapter, the surface of the mesoporous silica was made hydrophobic in nature by simple calcination temperature followed by Pt impregnation. Extensive characterization followed by ethylene oxidation at same conditions showed improvement in catalytic activity unlike the aerosil silica used as a control experiment. The Pt supported hydrophobic SBA-15 also showed faster recovery in activity after being deactivated by water. This enhancement is due to the smooth desorption of water molecules from the surface of Pt nanoparticles tightly incorporated in the hydrophobic mesopores of SBA-15 (Figure 5.2).

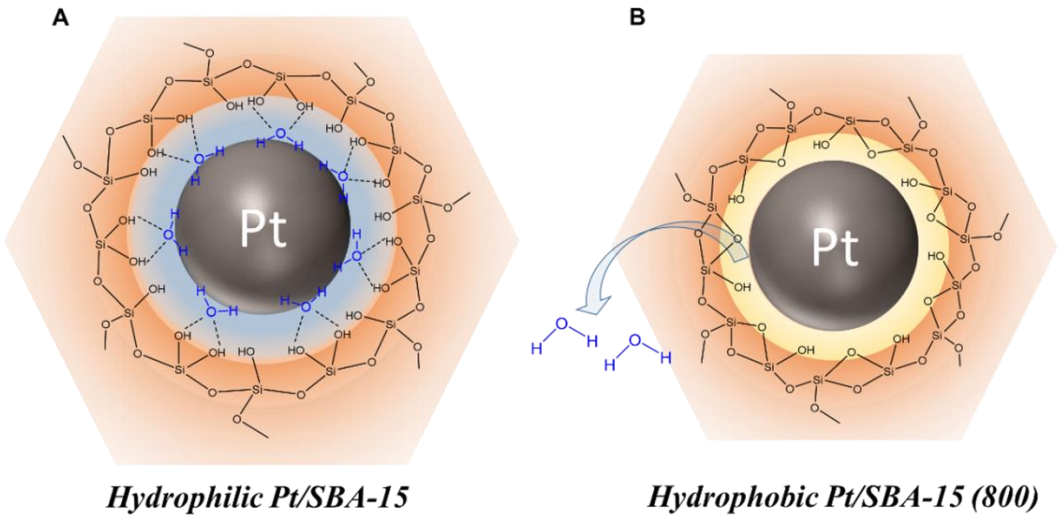

Figure 5.2. Schematic structure of Pt/SBA-15 (A), Pt/SBA-15(800) (B) oxidation of trace ethylene at 0 ºC.

In Chapter 4, using the concept of kinetics study, activation energy of the oxidation reaction over Pt/SBA-15 was calculated to be 66 kJ mol^{-1} which is less compared to epoxidation reaction over Ag-Cs/α-Al_2O_3 showing that the author's reaction does not proceed through epoxide formation. One of the carbon species speculated to be remaining on catalyst surface in Chapter 2, was confirmed to be acetic acid by ^{1}H NMR and HPLC study. Increased rate of CO oxidation compared to that of ethylene oxidation proved CO not to be involved in the rate determining step. In-situ FTIR study confirmed the presence of formate, acetate and acetic acid species on the catalyst surface. It is assumed oxidation of ethylene results in the complete oxidation to CO_2 and H_2O via the formation of HCHO, CO and HCOOH, which is considered to be the major pathway. Acetic acid is the only species proved to have been stabilized on catalyst surface even after its oxidation at 30 °C.

Appendix

In this study, the compete oxidation reaction of ethylene is expressed as follows:

$$C_2H_4 + 3O_2 \rightarrow 2CO_2 + 2H_2O$$

The rate of reaction in case of this reaction is based on the decrease in the ethylene concentration as shown in the equation below:

$$r = -\frac{d[C_2H_4]}{dt}$$

In general, the rate equation of oxidation of ethylene is:

$$r = -k[C_2H_4]^m[O_2]^n$$

If the stoichiometry of the complete oxidation of ethylene is followed, theoretically the values of *m* is 1 and *n* is 3. However, presence of a number of elementary steps results in variation of the order of the reaction. Also, the presence of catalyst, concentration of reactants, and temperature will also bring about a change in the order of the reaction. If the concentration of the catalyst is included, the rate equation is

$$r = -k[Cat]^l[C_2H_4]^m[O_2]^n$$

However, since the concentration of the catalyst remains the same, the term can be excluded from the above equation.

$$r_a = -k[C_2H_4]^m[O_2]^n \qquad (5.1)$$

In gas phase reaction, the partial pressure of the reactants is equal to the concentration of the gas. Therefore, equation (1) can be written as,

$$r_a = -kP_{C_2H_4}{}^m P_{O_2}{}^n \qquad (5.2)$$

Due to presence of excess oxygen in the reaction, equation (5.2) is expressed as:

$$r_a = -k' P_{C_2H_4}{}^m \qquad (5.3) \quad [P_{O_2}{}^n \simeq \text{constant}]$$

In a fixed-bed reactor (Figure 2.1), the partial pressure of the reactant material will vary continuously from point to point along the flow path. Consequently, in order to account for material balance, a minute space needs to be assumed in the catalyst layer, which is made for differential element of volume, d*V*. Thus for the reactant, ethylene,

Partial pressure of ethylene at the inlet = $P_{C_2H_4}$,

Partial pressure of ethylene at the oulet, $P_{C_2H_4} - \mathrm{d}P_{C_2H_4}$

Disappearance of ethylene by reaction = $(-r_A)\,\mathrm{d}V = (-r_A)\,A\mathrm{d}L$

Also denoting flow rate as *F*, flow rate at the outlet as *F* + d*F*, cross-sectional area of the differential area as *A* and differential length as d*L*.

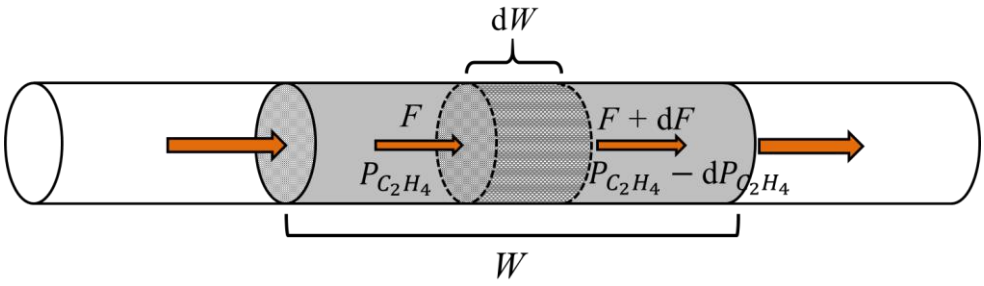

Figure 5.3. Notation for a fixed-bed flow reactor.

For ethylene, the material balance is established as such:

Input – Output – Disappearance by reaction = 0 (5.4)

Introducing the terms mentioned above in Eq (5.4)

$$FP_{C_2H_4} - (F + \mathrm{d}F)\left(P_{C_2H_4} - \mathrm{d}P_{C_2H_4}\right) - r_A\mathrm{d}V = 0$$

Assuming no change in flow rate of the reactants at the entrance and exit of the catalyst.

Therefore, $\mathrm{d}F = 0$

$$F\mathrm{d}P_{C_2H_4} - r_A\mathrm{d}V = 0$$

$$r = F\frac{\mathrm{d}P_{C_2H_4}}{\mathrm{d}V}$$

Considering the dimensions of *F*/d*V* is the reciprocal of that of T^{-1}

Since d*V* is proportional to the weight of the catalyst, *W* and density, ρ, the above equation of rate is espressed on the basis of weight as follows:

$$r_a = F\frac{\mathrm{d}P_{C_2H_4}}{\mathrm{d}W} \qquad (5.5)$$

Substituting Eq (5.3) in Eq (5.5)

$$-k^{'}{P_{C_2H_4}}^{m} = F\frac{\mathrm{d}P_{C_2H_4}}{\mathrm{d}W}$$

$$\frac{1}{F}\mathrm{d}W = -\frac{1}{k^{'}}\frac{\mathrm{d}P_{C_2H_4}}{{P_{C_2H_4}}^{m}}$$

Integrating the above equation (mass balance made over a differential element of volume) across the whole reactor:

$$\frac{1}{F}\int_0^W \mathrm{d}W = -\frac{1}{k^{'}}\int_{P_{C_2H_4{}_0}}^{P_{C_2H_4}}\frac{\mathrm{d}P_{C_2H_4}}{{P_{C_2H_4}}^{m}}$$

m ≠ 1

$$\frac{W}{F} = -\frac{1}{k^{'}(1-m)}\left({P_{C_2H_4}}^{1-m} - {P_{C_2H_4{}_0}}^{1-m}\right)$$

$$\frac{1}{(1-m)}\left({P_{C_2H_4}}^{1-m} - {P_{C_2H_4{}_0}}^{1-m}\right) = -k^{'}\frac{W}{F} \qquad (5.6)$$

If a good linearity is obtained by substituting an arbitrary order of reaction in the above equation and plotting space time, *W/F* and the ethylene concentration based on experimental data, then the order of reaction and rate constant can be determined. The following equation is used only when the reaction is considered to be a pseudo-first order reaction

$$\frac{W}{F} = -\frac{1}{k^{'}}\ln\frac{P_{C_2H_4}}{P_{C_2H_4{}_0}}$$

$$\ln(1-x) = -k^{'}\frac{W}{F} \qquad (5.7)$$

According to Eq (5.5), a graph of ln(1-*x*) versus *W/F* shows a linear relationship and rate constant can be determined from its slope.

Experimentally, it is found experimentally, that plot of log of rate constant versus 1/T gives a straight line with an intercept, which is depicted by the formula:

$$\ln k = \ln A - \frac{E_a}{RT} \qquad (5.8)$$

Where slope of the line gives $-\frac{E_a}{R}$ where E_a is the activation energy and ln A is the intercept where A is the pre-exponential factor.

The above equation can be interpreted as: $k = Ae^{-E_a/RT}$

List of Publications

1. Papers (related to this thesis)

1. Shazia Sharmin Satter, Jun Hirayama, Kiyotaka Nakajima, Atsushi Fukuoka, "Low Temperature Oxidation of Trace Ethylene over Pt Nanoparticles Supported on Hydrophobic Mesoporous Silica" *Chem. Lett*. **2018**, *47*, 1000–1002.
2. Shazia Sharmin Satter, Takuro Yokoya, Jun Hirayama, Kiyotaka Nakajima, Atsushi Fukuoka, "Oxidation of Trace Ethylene at 0 °C over Platinum Nanoparticles Supported on Silica" *ACS Sustainable Chem. Eng.* **2018**, *just accepted*.

2. Other papers and book chapter (not related to this thesis)

1. Shazia Sharmin Satter, Mahfuzul Hoque, M. Muhibur Rahman, M. Yousuf A. Mollah, Md. Abu Bin Hasan Susan, "An Approach towards Synthesis and Characterization of ZnO@Ag Core@Shell Nanoparticles in Water-in-Oil Microemulsion" *RSC Advances*, **2014**, *4*, 20612–20615.
2. Mousumi Akter, Shazia Sharmin Satter, Ajaya Kumar Singh, M. Muhibur Rahman, M. Yousuf A. Mollah, Md. Abu Bin Hasan Susan, "Hydrophilic Ionic Liquid-Assisted Control of the Size and Morphology of ZnO Nanoparticles Prepared by a Chemical Precipitation Method" *RSC Advances*, **2016**, *6*, 92040–92047.
3. Shazia Sharmin Satter, Mahfuzul Hoque, M. Muhibur Rahman, M. Yousuf A. Mollah, Md. Abu Bin Hasan Susan, "Microemulsions as Template for Synthesizing Nanoparticles with Tunable Antibacterial and Optical Properties: Current Trends and Future Perspective" in "Innovations in Nanomaterials", Editor, Al-Nakib Chowdhury, Joe Shapter, Abu Bin Imran, Nova Science Publishers, Inc. USA, 2014.

3. International Conferences

3.1 Oral Presentations

1. Shazia Sharmin Satter, Kiyotaka Nakajima, Atsushi Fukuoka, "Calcination Temperature Effect on Silica Supported Pt Catalyst for Low Temperature Ethylene Oxidation", *16th Korea-Japan Symposium on Catalysis and 3rd International Symposium of Institute for Catalysis*, Oral, May 15-17, 2017 Sapporo, Japan.

3.2 Poster Presentations

1. Shazia Sharmin Satter, Kiyotaka Nakajima, Atsushi Fukuoka, "Aerobic Oxidation of Trace Ethylene at Low Temperature over Platinum Nanoparticle on Hydrophobic Mesoporous Silica Support", *The 8th Tokyo Conference on Advanced Catalytic Science and Technology, TOCAT-8*, Poster, August 7, 2018, Yokohama, Japan.
2. Shazia Sharmin Satter, Kiyotaka Nakajima, Atsushi Fukuoka, "Oxidation of Trace Ethylene at 0 °C over Platinum Nanoparticles Supported on Silica", *Pre-Conference of TOCAT8 and the 5th International Symposium of Institute for Catalysis*, Poster, August 3, 2018, Sapporo, Japan.
3. Shazia Sharmin Satter, Kiyotaka Nakajima, Atsushi Fukuoka, "Effect of Pt Supported Hydrophobic Mesoporous Silica on Oxidation of Ethylene at Low Temperature", *Symposium on Nanomaterials for Environmental Purification and Energy Conversion (SNEPEC)*, Poster, February 20, 2018, Sapporo, Japan.

3.3 As a Co-author

1. Jun Hirayama, Takuro Yokoya, Shazia Sharmin Satter, Chuanxia Jiang, Kiyotaka Nakajima, Atsushi Fukuoka, "Low Temperature Ethylene Oxidation over Pt Supported on Mesoporous Silica", *TU/e -ICAT Joint International Symposium on Catalysis for Sustainable Society*, Poster, November 3, 2017, TU/e, Eindhoven, Netherlands.
2. Jun Hirayama, Shazia Sharmin Satter, Nobuhiro Ishito, Kiyotaka Nakajima, Atsushi Fukuoka, "Low Temperature Ethylene Oxidation over Platinum Based Bimetallic Catalyst Supported on Mesoporous Silica", *Pre-Conference of TOCAT8 and the 5th International Symposium of Institute for Catalysis*, Poster, August 3, 2018, Sapporo, Japan.
3. Jun Hirayama, Shazia Sharmin Satter, Nobuhiro Ishito, Kiyotaka Nakajima, Atsushi Fukuoka, "Low Temperature Ethylene Oxidation over Platinum Based Bimetallic Catalyst Supported on Mesoporous Silica", *The 8th Tokyo Conference on Advanced Catalytic Science and Technology, TOCAT-8*, Poster, August 7, 2018, Yokohama, Japan.

4. Domestic Conferences

4.1 Oral Presentations

1. Shazia Sharmin Satter, Kiyotaka Nakajima, Atsushi Fukuoka, "Low Temperature Oxidation of Ethylene over Pt Supported on Mesoporous Silica Calcined at Various Temperatures" *120th Annual Meeting of Catalysis Society of Japan*, Oral, September 14, 2017, Ehime, Japan.

4.2 Poster Presentations

1. Shazia Sharmin Satter, Kiyotaka Nakajima, Atsushi Fukuoka, "Low Temperature Oxidation of Trace Ethylene with a Hydrophobic SBA-15 Supported Pt Catalyst", *The 3rd National Symposium "New Trend of Chemistry Creation Chemistry", Integrated Materials Chemistry Research Promotion Organization*, October 30, 2017, Kyoto, Japan.
2. Shazia Sharmin Satter, Kiyotaka Nakajima, Atsushi Fukuoka, "Effect of Calcination Temperature on Silica Supported Pt Catalysts for Ethylene Oxidation at Low Temperature", *119th Annual Meeting of Catalysis Society of Japan*, March, 2017, Tokyo, Japan.

.

Acknowledgements

Rabindaranath Tagore once said ‘You can’t cross the sea merely by standing and staring at the water’. Staring at the water and wondering ‘what if’- was not an option as I decided to start swimming. The journey of my PhD study on ‘Low Temperature Oxidation of Ethylene by Silica-Supported Platinum Catalysts’ carried out from October 2015 to September 2018 was a challenge I gleefully accepted. This thesis is a milestone made possible in one way or another by remarkable individuals whom, I have met during my time in Hokkaido University and the ones already present in my life.

First and foremost, Prof. Atsushi Fukuoka, my humble gratitude and respect to him for providing me with the platform to pursue this PhD degree. He has taught me how a goal can be achieved with decent critical reasoning in research. His knowledge, invaluable suggestions and his joy to small findings have always inspired me and allowed me to carry out my research in joyous harmony. Without his strident thinking regarding my publications, his patience to go through my thesis, his invaluable support and motivation during my demoralizing times, it would have been impossible to successfully finish my dissertation.

Dr. Kiyotaka Nakajima, I have to thank him deeply for dealing with me and my bizarre writings. Every discussion with him, be it minutes or hours, have always turned out to be fruitful. His support, advices and guidance throughout the entire time have been a blessing. I am grateful for always guiding me towards free thinking and enlightening me with the knowledge of writing manuscripts with a new direction.

My sincere appreciation goes to Dr. Hirokazu Kobayashi for all the productive advices at precise times. I also acknowledge Dr. Abhijit Shortri individually for putting up with my occasional never ending discussions.

I would like to express my gratitude to Prof. Kei Murakoshi, Prof. Shin Mukai and Prof Kazuki Sada for reviewing this work and giving valuable suggestions. I am grateful to Ministry of Education, Culture, Sports, Science and Technology (MEXT) for providing me with the support during these three years of my PhD.

Special thanks to one of the biggest forces behind this success, former and the present members of my laboratory. Without their help, professionally and emotionally, where I stand today would not have been possible. I thank Dr. Mizhuo Yabushita for his advices every now

and then and making me feel confident. The only member of the 'Ethylene Group', Dr. Jun Hirayama; work became more fun with every discussion involved with him.

To the friends in Sapporo: Minjune and Duhita (the Dr.'s) thank you so much for enduring my craziness during the entire thesis time. Lina, Zakia, Tamanna, (more Dr's) Papry, Anika, (the future Dr's) it has been one hell of a journey in Sapporo full of color, even during the white winter; hope to cherish the memories forever. Natsumi and Miyuki, thank you for the awesome trips and the parties filled with laughter. Touchy Apu and Hakim Bhai, the duo, thank you for being there for me during my stay in Sapporo. To my friend in Yokohama; Mayeesha, we started our journey in Japan together to follow our dreams. Sorry for bailing out and graduating six months earlier. I will be waiting for you at the end of the tunnel, I promise. Naeema, words fail to explain the part she has played in my life during this entire journey.

Lastly, I would like to acknowledge my family in Bangladesh, the place where my root belongs. It was because of my amazing parents, Prof. Md. Abdus Satter, Nurun Nahar and brother, Sakin, who have always supported me, sacrificed, broke the stereotype and kept on inspiring me to go beyond the horizons. Hope we can be a family with a lot of Dr. Satters in it! I finish this by dedicating this thesis to Prof. Muzammil Haq and Hamida Haq, (my late grandparents) who would have been the most happiest on my achievement.